LIGHT ADJUSTABLE MACROMER-DOPED ELASTOMERS: THE THERMODYNAMICS, TRANSPORT, AND PHOTOCHEMISTRY OF SILICONES

Thesis by

Eric A. Pape

In Partial Fulfillment of the Requirements

for the Degree of

Doctor of Philosophy

CALIFORNIA INSTITUTE OF TECHNOLOGY

Pasadena, California

2006

(Defended November 28, 2005)

Ackowledgements

I would first like to thank Professor Julie Kornfield for being my advisor during my graduate studies at Caltech. Her enthusiasm for research and robust knowledge of polymers gave me new appreciation for the depths into which science can be explored. I would also like to thank Dr. Chris Sandstedt and Professors Robert Grubbs and David Tirrell both for reviewing my thesis and sitting on my defense committee.

I greatly appreciate the opportunity to have worked with many past and present members of the Kornfield research group. In no particular order, I would like to thank Maria Lujann Auad, Rob Lammertink, Erica Thompson, Weijun Zhou, Giyoong Tae, Wei Shen, Mike Kempe, Charles Nickerson, Lucia Fernandez-Ballester, Matt Mattson, Mike Mackel, Ameri David, Rafael Verduzco, Chris Sandstedt, Jagdish Jethmalani, Hee Hyun Lee, Neal Scruggs, and Derek Thurman. I would also like to thank Anne Hormann for taking care of paperwork, scheduling, and providing a breath of sanity and organization in the turmoil of academic research. I would particularly like to thank Rob Lammertink for many discussion on networks, gels, and microfluidics; Jagdish Jethmalani and Chris Sandstedt for helping me enter the fields of optics and polymer synthesis; Derek Thurman and Neal Scruggs for daily discussions on science, both erudite and nescient; Mike Mackel for discussions and experimental help on surface energies and morphologies; and Ameri David for fruitful discussions on polymer physics.

I would also like to thank Dr. Gerald Delker for help with Photo DSC and GPC-LS experiments and Drs. Shiao Chang and Tom Shiao for discussions relating to my research.

Finally, and most importantly, I would like to thank my parents and family for the help and support they have given me through the years. I would especially like to thank Christopher for the tremendous insight into life that only young eyes can give.

Abstract

We have designed and synthesized photo elastomer systems that exhibit macroscopic optical and mechanical changes when polymerized heterogeneously. These elastomers consist of a well-defined polydimethylsiloxane matrix, a UV absorbing photoiniator, and a reactive macromer with methacrylate endgroups and either a polydimethylsiloxane or polyphenylmethylsiloxane miblock. No previous studies have been performed to elucidate the overall effect that the combination of reaction kinetics, macromer diffusion rate, and thermodynamics have on the ultimate state and properties of a photopolymerized system. In this thesis, we synthesize model elastomer matrices, swell them with macromer, and examine mechanical, transport, and thermodynamic behaviors of the resulting photoelastomers.

We synthesized model polydimethylsiloxane (PDMS) networks using well-defined and low polydispersity (PDI) vinyl-functionalized PDMS precursors catalytically crosslinked with tetrafunctional silanes. The ratio of crosslinker to midblock endgroup functionality was optimized for each molecular weight system, was shown to be greater than a 1:1 ratio, and exhibited an increase based on increasing precursor molecular weight. Networks polymerized in a theta solvent followed theoeretical scaling predictions for modulus and preparation polymer volume fraction. This behavior shows that melt polymerization incorporates significant numbers of entrapped entanglements.

Sequential interpenetrating networks (IPNs) were formed by polymerizing different molecular weights of reactive macromer in a cured PDMS matrix. The IPNs exhibited a 50 to 150% increase in modulus after cure which was independent of network structure but highly dependent on macromer loading and macromer molecular weight. Although theories for both bicontinuous and dispersed phase IPNs predict modulus increases for low macromer loading, they underpredict modulus increases for high weight percent of macromer. Unexpectedly, mechanical

properties were also independent of photopolymerization conditions; increased photoinitiator content and irradiation intensity did not alter the material modulus. Contrary to previous work with PDMS IPNs, we did not find a single size scale of heterogeneities in our systems with light scattering measurements. However, greater scattering intensity is seen with higher macromer content, increased extent of macromer conversion, and decreased network crosslink density.

Equilibrium and intermediate swelling behaviors for both model networks and model networks with photopolymerized macromer were also measured. The extent of equilibrium swelling was found to be independent of the network precursor molecular weight for equivalent modulus networks and, in the range we examine, polymer volume fraction at network preparation. Using four different molecular weights of methacrylate endcapped PDMS macromer, we show that as molecular weight increases, experimental scaling behavior approaches the theoretical value of $G \cong Q^{-8/3}$, where G is the shear modulus and Q is the swelling ratio. However, absolute equilibrium swelling does not monotonically follow a molecular weight trend. Using a form of the Flory-Rehner equation, we show that this trend is created by the interplay in interaction parameter and entropic considerations due to macromer molecular weight. Intermediate swelling scaling behavior was also examined for the first time in well-defined networks and was shown to coincide rather poorly with Flory-Rehner theory. For photopolymerized IPNs, equilibrium swelling behavior indicated that macromer was a poorer solvent than in model networks. Poor solvent behavior is indicated both through decreases in absolute swelling and power law exponents for modulus against equilibrium swelling ratio behavior. Reactive macromers with phenyl incorporation also showed significant decreases in solubility.

Diffusion rates of different molecular weights of macromer are measured in model networks with different crosslink densities. Diffusivity values show dependence both on

molecular weight of the penetrant species and the modulus of the host network. In particular, we find that the scaling exponent α between diffusivity and macromer molecular weight ($D \cong M_d^{-\alpha}$) is significantly lower than expected for Rouse-like diffusion. The scaling exponent α is also dependent on the host modulus; higher network moduli show greater deviation from predicted behavior. Diffusivities were also measured for macromer containing up to 10% phenyl and did not change as compared to PDMS based penetrants. Diffusivity of a series of different molecular weight macromers was also measured in photopolymerized intercalated networks. As with adding phenyl content to macromer, we found that penetrant molecular weight and host network modulus are the only two important variables in diffusivities. Bimodal molecular weight distributions were similarly swollen in a series of different modulus host networks and exhibit significant molecular sieving when diffusing in tightly crosslinked networks.

We have also examined the kinetics of polymerization for methacrylate endcapped monomers. Unlike polymerization in multifunctional methacrylate or acrylate monomers, we are able to attain complete endgroup conversion even in neat macromer. We also find that, for a specific macromer molecular weight, the reaction rate scales linearly with macromer concentration. Surprisingly, we find that the scaling behavior for irradiation intensity and photoinitiator concentration are strongly dependent on reaction conditions. As irradiation intensity and photoinitiator concentration increase, reaction rate eventually reaches 0th order. This result indicates that, no matter how high photoinitiator concentrations and irradiation intensities are, there is some minimum reaction time required to attain a specific conversion. Even though macromer polymerization follows a first order rate law in endgroup concentration within a single molecular weight, scaling analysis is not adequate to describe reaction trajectories for different macromer molecular weights. Not only are maximum reaction rates not well quantified, but the extent of reaction at which they occur is also poorly predicted. It is also very surprising

that, although 500 and 1000 g/mol macromers do not support a pseudo-steady state assumption, 3000 and 5000 g/mol are well-described. Finally, we have shown the effect of chain length dependent termination in describing reaction rate trajectories.

TABLE OF CONTENTS

List of Tables

List of Figures

Chapter I: Introduction

1.1. Introduction

1.1.1. History and background of photopolymers

Photoreactive polymers, or photopolymers, consist of three important elements: an inert polymer "binder" to provide mechanical stability, a reactive monomer to effect optical changes, and a photoiniator.[1, 2] When irradiated, the materials exhibit significant changes in optical properties; refractive indices and densities are permanently altered when polymerized. With appropriate spatially-resolved irradiation, optical properties can also be modulated on a submicron size scale.

By the 1960s, these properties led to initial development of photoreactive polymer films for use as holographic recording materials.[3-6] Advances in photopolymer chemistries and formulations have allowed faster polymerization and more efficient optical diffraction. These improved attributes have been instrumental in applying photopolymers to uses such as heads-up displays,[7] optical waveguides,[8] and holographic data storage.[9, 10] However, all of these applications have been limited to optical changes on the microscale because of relatively slow read/write dynamics and large volume/density changes during sample photopolymerization.

The time scale on which optical information can be written in photopolymers is intimately linked to polymerization and diffusion kinetics of reactive monomer in the polymeric

binder. Polymerization is initiated by irradiating the photopolymer. Photonitiator molecules cleave into reactive radicals, which begin to polymerize photoreactive monomer (figure 1.1). If spatially resolved irradiation is incident on a photopolymer, such as in dark and bright stripes, polymerization in bright regions will locally deplete monomer concentrations and create a concentration gradient between dark and bright regions of the sample. Free, or unpolymerized, monomer then diffuses down the chemical gradient to replenish the bright regions. As the monomer reacts, it also contracts in volume up to 20% and the photopolymer density and refractive index increase in the polymerized region. The refractive index contrast between polymerized and unpolymerized regions is used to create optical phase gratings for holography or data storage. Density increase often leads to vitrification, impedes some free monomer from reacting, and leads to incomplete conversions.[11]

Depending on the relative rates of monomer photopolymerization and diffusion, several distinct profiles of optical heterogeneity can be formed within a photopolymer using the same irradiation profile. A simple irradiation profile, such as a sinusoidal pattern, is common for holographic gratings. When monomer diffusion rates are much faster than photopolymerization kinetics, the reacted monomer in the bright regions will be quickly replenished, leading to a profile in monomer concentration that is similar to the irradiation profile (Figure 2A). If diffusion rates are slow compared to photopolymerization kinetics, monomer species will react as soon as they enter bright regions, resulting in a complex refractive index waveform within the sample (Figure 2B).[12, 13] Since monomer diffusion rates in most photopolymer systems are between 10^{-14} and 10^{-19} m^2/sec,[14-17] photopolymerization with a spatial frequency of 1 μm must take place over the course of minutes to obtain sinusoidal write patterns and changes over 1 mm would take days.

1.1.2. Use of elastomers as photopolymers

At Caltech, Grubbs and Kornfield have designed elastomer photopolymer systems to overcome traditional problems in photopolymers such as volume shrinkage, incomplete monomer conversion, and slow diffusion rates.[18] In this new material, the polymer binder is replaced by an elastomer that confers high mobility due to low crosslink density and a glass transition temperature, T_g, that is well below ambient temperature. The reactive monomer is replaced by a "macromer" with an elastomeric midblock and photoreactive endcaps. Because of the relatively low volume of reactive endcaps, samples exhibit less than 1% shrinkage even at full cure. This lack of density change also prevents sample vitrification,[19-21] allows full conversion of reactive macromer, and exhibits diffusivity values for reactive species that are one thousand to ten million times greater than in previous photopolymers. These fast diffusivities indicate that changes on the order of 1 μm can be performed on the order of seconds and changes on the order of 1 mm can be performed in tens of minutes.

Refractive index modulation in prior systems was primarily due to volume contraction as monomer polymerized. Since elastomeric photopolymers do not shrink significantly, observed optical changes must originate from a combination of swelling and refractive index difference between macromer and matrix. As their name implies, elastomers stretch when in the presence of a solvent. When bulk photoelastomer is irradiated in a spatially heterogeneous manner, macromer is polymerized in the bright regions (figure 1.1). Due to a concentration gradient, free macromer diffuses from dark to bright regions, swelling the photopolymer. The extent of swelling is intimately linked to the thermodynamic interaction of macromer between non- and photopolymerized regions. If the macromer and matrix have different refractive indices, the swollen and polymerized region of the photopolymer will also have a different refractive index from the surrounding material. A combination of shape and refractive index changes allows for considerable spatially resolved adjustment of optical properties in photoelastomers.

Photoreactive elastomer systems can also exhibit significant increases in mechanical strength after polymerization. From the literature on interpenetrating networks (IPNs), it is known that when a polymer B is sequentially polymerized in a previously crosslinked network, the resulting polymer begins to microphase separate.[22-24] Even at low levels of macromer doping, these B-rich regions remain interconnected. Thus, the original elastomer matrix is strengthened by an additional interconnected and bicontinuous network formed by the macromer.

Because of their ability to macroscopically change shape, refractive index, and modulus on reasonable time scales, elastomer-based photopolymers show tremendous promise for use in a variety of applications. These materials could potentially be used in place of traditional photopolymer systems as high speed holographic storage materials, optical Bragg gratings, or wave guides.[25, 26] Appropriate choice of materials could also allow incorporation of elastomer photopolymers into polydimethylsiloxane (PDMS) microfluidic devices. Presently, most optical and mechanical features in microfluidic devices are formed through a complex and time-consuming multi-step photolithographic process; use of photopolymer could provide a simple single-step process for sculpting features into a device scaffold. For example, shape change could be used to change a smooth channel into a chaotic mixer for microfluidics,[27] a combination of refractive index and shape change could be used to create microlens arrays for cell counters,[28] changes in modulus would allow easier fabrication of PDMS microactuators,[29-31] or Bragg gratings could be written for use as pressure transducers[32]. With the appropriate choice of biocompatible materials, elastomeric photopolymers can also be used in biological applications such as intraocular lenses as has been demonstrated in collaboration with Dr. Daniel Schwartz, Associate Professor of Opthalmology at UCSF.[18]

1.1.3. Motivation and objectives

Light adjustment of photoelastomers is governed by diffusion rates, reaction kinetics, polymerization induced modulus change and microphase separation, and equilibrium swelling properties. The lack of literature on similar materials precludes *a priori* prediction of ultimate properties or composition distribution of materials after spatially resolved polymerization, much less the time course of these changes. Individual elements of the process such as diffusion,[12, 15, 33-46] structure of IPNs[47-53], or equilibrium swelling[43, 54-67] have been studied for a variety of different materials. However, many of these studies are material-specific and the majority use materials that are poorly characterized. Additionally, significant gaps remain both in theory and experiment for explaining reaction kinetics, microphase separation, and modulus increases for reactive, network-forming macromers embedded in an elastomer matrix.

Simplified theoretical considerations of a differential element in a three dimensional system help determine appropriate experimental measurements for *a priori* analysis of the dynamics of spatially resolved photopolymerization. In any specific element (x_1, y_1, z_1), relative concentrations of host matrix (part *A*), free macromer (part *B*) and polymerized macromer (part B_{poly}) are increasing or decreasing depending on relative rates of diffusion into the volume element and the local rate of consumption due to polymerization. For free macromer, this equates to:

$$\frac{d[M]}{dt} = \nabla \bullet \vec{q} - R_p \tag{1.1}$$

where the flux $\boldsymbol{q}$ depends on the local concentration gradient ($\nabla[M]$) and diffusivity of macromer, t is time, and R_p is the local reaction rate. Macromer diffusivity is dependent on molecular length, degree of crosslinking in the host network, and changes in system properties due to macromer polymerization as reaction time progresses. Local reaction rates are a function of instantaneous light flux, macromer reactive group concentration, and reaction history. Radical concentration

and radical size, both of which alter the reaction rate, change over the time-course of the reaction. Material fluxes will also affected by the local degree of swelling and interactions between free macromer and the combined system of host matrix and polymerized macromer.

In contrast to dry holographic materials, elastomeric photopolymers have nearly constant density during polymerization. As an element gains or loses macromer, its volume will change proportionally and with no constraints, the volume element would expand isotropically. Since the element is mechanically connected to surrounding material elements, local swelling will be dictated by stresses coupled between large numbers of individual elements. Assuming a free volume element, total swelling can be expressed by minimizing the free energy, ΔF, which is a sum of elastic stretching and mixing terms:

$$\frac{\Delta F}{n_B kT} = \frac{1}{2}\left[\lambda_x{}^2 + \lambda_y{}^2 + \lambda_z{}^2 - 3 - \ln(\lambda_x\lambda_y\lambda_z)\right] + \frac{V}{\nu}\left(\frac{\phi_A}{n_B N_A}\ln\phi_A + \frac{\phi_B}{n_B N_B}\ln\phi_B\right)$$

$$+ \frac{\chi}{n_B kT}\phi_A\phi_B \qquad (1.2)$$

where n is the number of chains, k is Boltzmann's constant, T is absolute temperature, λ is normalized change in length on stretching, V is system volume, ν is monomer volume, ϕ is volume fraction, and χ is the binary interaction parameter. Local stresses can then be approximated with appropriate use of constitutive equations incorporating these free energy terms. Due to the complexity of this problem, appropriate theoretical work is still in progress in our laboratory.[68]

The goal of this research is to create model photoreactive elastomer systems and use them

to elucidate each of the fundamental processes that determine the rate and magnitude of changes in material properties. Ultimately, this experimental knowledge provides the foundation to predict, based on materials and irradiation parameters, the macroscopic and microscopic structure of photopolymerized elastomers. To accomplish this goal, we have: (1) Synthesized and characterized an array of model elastomer networks (Chapter II). (2) Synthesized an array of reactive macromers with different molecular weight and refractive index, swollen them into networks, measured the change in modulus on photopolymerization, and determined the microstructure of phase separated IPNs (Chapter III). (3) Examined the thermodynamic interactions and swelling effects of macromer in model and interpenetrated networks (Chapter IV). (4) Measured diffusivity of different molecular weight macromer in an array of different modulus PDMS networks (Chapter V). (5) Characterized the distinctive photopolymerization kinetics of macromer-matrix systems as function of material parameters and irradiation conditions (Chapter VI).

1.2. Figures

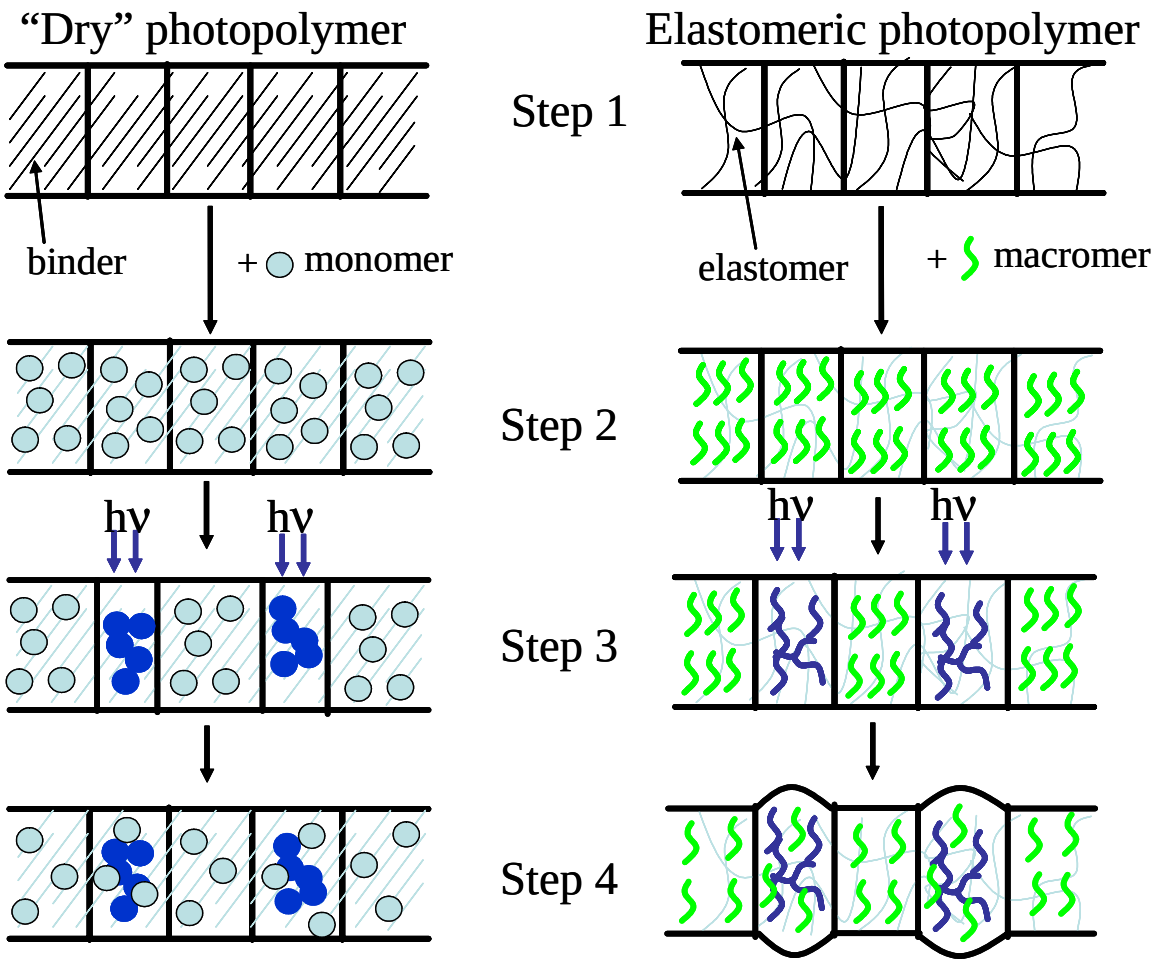

Figure 1.1. Spatially resolved photopolymerization for traditional and elastomeric photopolymers. For both systems, step 1 shows only the binder. In step 2, monomer or macromer is added to the system. In step 3, the materials are irradiated. For the traditional photopolymer, monomer polymerization in bright regions leads to density increase and shrinkage. Step 4 show diffusion and redistribution of monomer and macromer into polymerized regions. The elastomeric photopolymer swells to accommodate this redistribution.

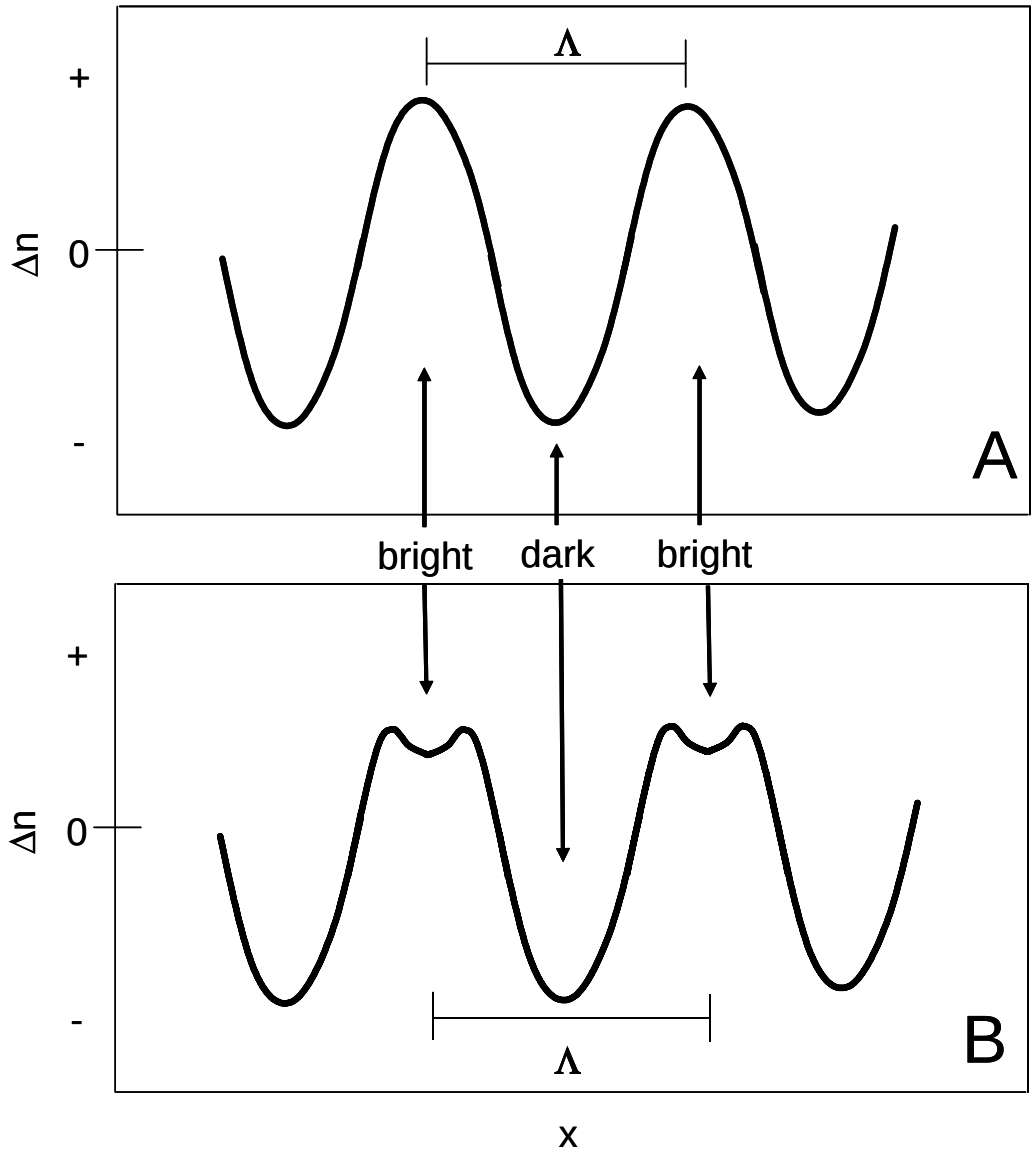

Figure 1.2. Spatial profile of the refractive index deviation from the average after exposure to a sinusoidal modulation of irradiation in a traditional photopolymer. Part A shows a refractive index profile when monomer diffusion rates are much greater than monomer reaction rates. Part B shows a complex refractive index waveform created when reaction rates are faster than monomer diffusion.

1.3. References

1. Joo, W. J., N. J. Kim, H. Chun, I. K. Moon, and N. Kim, Polymeric photorefractive composite for holographic applications. *Polymer,* 2001. **42**(24): p. 9863-9866.
2. Tomlinson, W. J., Multicomponent photopolymer systems for volume phase holograms and grating devices. *Applied Optics,* 1976. **15**(2): p. 534-541.
3. Jenney, J. A., Holographic Recording with Photopolymers. *Journal of the Optical Society of America,* 1970. **60**(9): p. 1155.
4. Booth, B. L., Photopolymer Material for Holography. *Applied Optics,* 1975. **14**(3): p. 593-601.
5. Close, D. H., A. D. Jacobson, J. D. Margerum, R. G. Brault, and F. J. McClung, Hologram Recording on Photopolymer Materials. *Applied Physics Letters,* 1969. **14**(5): p. 159.
6. Colburn, W. S., Volume Hologram Formation in Photopolymer Materials. *Applied Optics,* 1971. **10**(7): p. 1636-1641.
7. Chao, W. C. and S. Chi, Diffraction properties of windshield laminated photopolymer holograms. *Journal of Optics-Nouvelle Revue D Optique,* 1998. **29**(2): p. 95-103.
8. Trout, T. J., J. J. Schmieg, W. J. Gambogi, and A. M. Weber, Optical photopolymers: Design and applications. *Advanced Materials,* 1998. **10**(15): p. 1219.
9. Pu, A., Exposure Schedule for multiplexing holograms in photopolymer films. *Optical Engineering,* 1996. **35**(10): p. 2824-2829.
10. Pu, A. and D. Psaltis, High-density recording in photopolymer-based holographic three-dimensional disks. *Applied Optics,* 1996. **35**(14): p. 2389-2398.
11. Gallego, S., C. Neipp, M. Ortuno, A. Belendez, and I. Pascual, Stabilization of volume gratings recorded in polyvinyl alcohol-acrylamide photopolymers with diffraction

efficiencies higher than 90%. *Journal of Modern Optics,* 2004. **51**(4): p. 491-503.

12. Zhao, G., Diffusion Model of hologram formation in dry photopolymer materials. *Journal of Modern Optics,* 1994. **41**(10): p. 1929-1939.
13. Zhao, G., Second order grating formation in dry holographic photopolymers. *Optics Communications,* 1995. **115**: p. 528-532.
14. Moreau, V., Y. Renotte, and Y. Lion, Characterization of DuPont photopolymer: determination of kinetic parameters in a diffusion model. *Applied Optics,* 2002. **41**(17): p. 3427-3435.
15. Lawrence, J. R., F. T. O'Neill, and J. T. Sheridan, Adjusted intensity nonlocal diffusion model of photopolymer grating formation. *Journal of the Optical Society of America B-Optical Physics,* 2002. **19**(4): p. 621-629.
16. Wu, S. D. and E. N. Glytsis, Holographic grating formation in photopolymers: analysis and experimental results based on a nonlocal diffusion model and rigorous coupled-wave analysis. *Journal of the Optical Society of America B-Optical Physics,* 2003. **20**(6): p. 1177-1188.
17. Gallego, S., M. Ortuno, C. Neipp, A. Marquez, A. Belendez, and I. Pascual, Characterization of polyvinyl alcohol/acrylamide holographic memories with a first-harmonic diffusion model. *Applied Optics,* 2005. **44**(29): p. 6205-6210.
18. Jethmalani, J. M., R. Grubbs, J. Kornfield, D. Schwartz, C. Sandstedt, and E. Pape, Lenses capable of post-fabrication modulus change. 2002, California Institute of Technology and The Regents of the University of California.US. Patent # 6,813,097.
19. Anseth, K. S., L. M. Kline, T. A. Walker, K. J. Anderson, and C. N. Bowman, Reaction-Kinetics and Volume Relaxation During Polymerizations of Multiethylene Glycol Dimethacrylates. *Macromolecules,* 1995. **28**(7): p. 2491-2499.

20. Berchtold, K. A., T. W. Randolph, and C. N. Bowman, Propagation and termination kinetics of cross-linking photopolymerizations studied using electron paramagnetic resonance spectroscopy in conjunction with near IR spectroscopy. *Macromolecules,* 2005. **38**(16): p. 6954-6964.

21. Lovestead, T. M., K. A. Berchtold, and C. N. Bowman, An investigation of chain length dependent termination and reaction diffusion controlled termination during the free radical photopolymerization of multivinyl monomers. *Macromolecules,* 2005. **38**(15): p. 6374-6381.

22. Klempner, D., L. H. Sperling, and L. A. Utracki, eds. *Interpenetrating Polymer Networks*. Advances in Chemistry Series. Vol. 239. 1994. American Chemical Society: Washington, D.C.

23. Sperling, L. H., C. S. Heck, and J. H. An, Ternary Phase-Diagrams for Interpenetrating Polymer Networks Determined During Polymerization of Monomer-Ii. *ACS Symposium Series,* 1989. **395**: p. 230-244.

24. Lipatov, Y. S., O. P. Grigoryeva, G. P. Kovernik, V. V. Shilov, and L. M. Sergeyeva, Kinetics and Peculiarities of Phase-Separation in the Formation of Semi-Interpenetrating Polymer Networks. *Makromolekulare Chemie-Macromolecular Chemistry and Physics,* 1985. **186**(7): p. 1401-1409.

25. Bachelot, R., C. Ecoffet, D. Deloeil, P. Royer, and D. J. Lougnot, Integration of micrometer-sized polymer elements at the end of optical fibers by free-radical photopolymerization. *Applied Optics,* 2001. **40**(32): p. 5860-5871.

26. Zhang, Q., D. A. Brown, L. Reinhart, and T. F. Morse, Simple Prism-Based Scheme for Fabricating Bragg Gratings in Optical Fibers. *Optics Letters,* 1994. **19**(23): p. 2030-2032.

27. Stroock, A. D., S. K. W. Dertinger, A. Ajdari, I. Mezic, H. A. Stone, and G. M.

Whitesides, Chaotic mixer for microchannels. *Science*, 2002. **295**(5555): p. 647-651.

28. Croutxe-Barghorn, C., Fabrication of microlenses by direct photo-induced crosslinking polymerization. *Applied Surface Science*, 2000. **168**: p. 89-91.
29. Duffy, D. C., J. C. McDonald, O. J. A. Schueller, and G. M. Whitesides, Rapid prototyping of microfluidic systems in poly(dimethylsiloxane). *Analytical Chemistry*, 1998. **70**(23): p. 4974-4984.
30. Duffy, D. C., O. J. A. Schueller, S. T. Brittain, and G. M. Whitesides, Rapid prototyping of microfluidic switches in poly(dimethyl siloxane) and their actuation by electro-osmotic flow. *Journal of Micromechanics and Microengineering*, 1999. **9**(3): p. 211-217.
31. Khoo, M., Micro magnetic silicone elasomer membrane actuator. *Sensors and Actuators A*, 2001. **89**: p. 259-266.
32. Hosokawa, K., K. Hanada, and R. Maeda, A polydimethylsiloxane (PDMS) deformable diffraction grating for monitoring of local pressure in microfluidic devices. *Journal of Micromechanics and Microengineering*, 2002. **12**(1): p. 1-6.
33. Garrido, L., Studies of Self-diffusion of Poly(dimethylsiloxane) Chains in PDMS Model Networks by Pulsed Field Gradient NMR. *Journal of Polymer Science, Part B: Polymer Physics*, 1988. **26**: p. 2367-2377.
34. Gent, A. N., Diffusion of Linear Polyisoprene Molecules into Polyisoprene Networks. *Journal of Polymer Science: Part B: Polymer Physics*, 1989. **27**: p. 893-911.
35. Gent, A. N., Diffusion of Polymer Molecules into Polymer Networks: Effect of Stresses and Constraints. *Journal of Polymer Science: Part B: Polymer Physics*, 1991. **29**: p. 1313-1319.
36. Kohler, W., Polymer Analysis by Thermal-Diffusion Forced Rayleigh Scattering. *Advances in Polymer Science*, 2000. **151**: p. 1-59.

37. Kubo, T., Diffusion of Single Chains in Polymer Matrices as Measured by Pulsed-Field-Gradient NMR: Crossover from Zimm to Rouse-Type Diffusion. *Polymer Journal,* 1992. **24**(12): p. 1351-1361.

38. Sheridan, J. T., Nonlocal-Response diffusion model of holographic recording in photopolymer. *Journal of the Optical Society of America A,* 2000. **17**(6): p. 1108-1114.

39. Spiegel, D. R., Measurement of mass diffusion coefficients using nonexponential forced Rayleigh scattering signals. *Journal of Chemical Physics,* 1998. **109**(1): p. 267-274.

40. Tanner, J. E., Diffusion in a polymer Matrix. *Macromolecules,* 1971. **4**: p. 748-750.

41. O'Neill, F. T., J. R. Lawrence, and J. T. Sheridan, Comparison of holographic photopolymer materials by use of analytic nonlocal diffusion models. *Applied Optics,* 2002. **41**(5): p. 845-852.

42. Mazan, J., Diffusion of Free polydimethylsiloxane chains in polydimethylsiloxane elastomer networks. *European Polymer Journal,* 1995. **31**(8): p. 803-807.

43. Gent, A. N., Diffusion and Equilibrium swelling of macromolecular networks by their linear homologs. *Journal of Polymer Science : Polymer Physics Edition,* 1982. **20**: p. 2317-2327.

44. Tirrel, M., Polymer Self-Diffusion in Entangled Systems. *Rubber Chemistry and Technology,* 1984. **57**: p. 523-556.

45. Antonietti, M., J. Coutandin, and H. Sillescu, Diffusion of Linear Polystyrene Molecules in Matrices of Different Molecular-Weights. *Macromolecules,* 1986. **19**(3): p. 793-798.

46. Cosgrove, T., C. Roberts, G. V. Gordon, and R. G. Schmidt, Diffusion of polydimethylsiloxane mixtures with silicate nanoparticles. *Abstracts of Papers of the American Chemical Society,* 2001. **221**: p. U323-U323.

47. Turner, J. S. and Y. L. Cheng, Morphology of PDMS-PMAA IPN membranes.

Macromolecules, 2003. **36**(6): p. 1962-1966.

48. Vancaeyzeele, C., O. Fichet, S. Boileau, and D. Teyssie, Polyisobutene-poly(methylmethacrylate) interpenetrating polymer networks: synthesis and characterization. *Polymer,* 2005. **46**(18): p. 6888-6896.

49. Dong, J., Z. L. Liu, N. F. Han, Q. Wang, and Y. R. Xia, Preparation, morphology, and mechanical properties of elastomers based on alpha,omega-dihydroxy-polydimethylsiloxane/polystyrene blends. *Journal of Applied Polymer Science,* 2004. **92**(6): p. 3542-3548.

50. Turner, J. S. and Y. L. Cheng, Preparation of PDMS-PMAA interpenetrating polymer network membranes using the monomer immersion method. *Macromolecules,* 2000. **33**(10): p. 3714-3718.

51. Termonia, Y., Molecular-Model for the Mechanical-Properties of Elastomers .4. Interpenetrating Networks. *Macromolecules,* 1991. **24**(6): p. 1392-1396.

52. Harmon, M. E., W. Schrof, and C. W. Frank, Fast-responsive semi-interpenetrating hydrogel networks imaged with confocal fluorescence microscopy. *Polymer,* 2003. **44**(22): p. 6927-6936.

53. Abbasi, F., H. Mirzadeh, and A. A. Katbab, Modification of polysiloxane polymers for biomedical applications: a review. *Polymer International,* 2001. **50**(12): p. 1279-1287.

54. Escobedo, F. A., Molecular simulation of polymeric networks and gels: phase behavior and swelling. *Physics Reports,* 1999. **318**: p. 65-112.

55. Flory, P. J., Statistical Mechanics of Cross-linked polymer networks: II. Swelling. *Journal of Chemical Physics,* 1943. **11**(11): p. 521-526.

56. Hedden, R. C., Effects of Phenyl Substituents on the Mechanical and Swelling Properties of Poly(dimethylsiloxane). *Macromolecules,* 1999. **32**: p. 5154-5158.

57. Sivisailam, K., Scaling Behavior: Effect of Precursor concentration and precursor molecular weight on the modulus and swelling of polymeric networks. *Journal of Rheology,* 2000. **44**(4): p. 897-915.

58. Mark, J. E., Model Networks of end-linked polydimethylsiloxane chains. I. Comparisons between experimental and theoretical values of the elastic modulus and the equilibrium degree of swelling. *Journal of Chemical Physics,* 1977. **66**(3): p. 1006-1011.

59. Kawamura, T., K. Urayama, and S. Kohjiya, Equilibrium swelling and elastic modulus of end-linked poly(dimethylsiloxane) networks in theta solvent. *Nihon Reoroji Gakkaishi,* 1997. **25**(4): p. 195-196.

60. Lu, Z. Y. and R. Hentschke, Swelling of model polymer networks with different cross-link densities: A computer simulation study. *Physical Review E,* 2002. **66**(4).

61. Hedden, R. C., H. Saxena, and C. Cohen, Mechanical properties and swelling behavior of end-linked poly(diethylsiloxane) networks. *Macromolecules,* 2000. **33**(23): p. 8676-8684.

62. Fernandez-Nieves, A., A. Fernandez-Barbero, B. Vincent, and F. J. de las Nieves, Charge controlled swelling of microgel particles. *Macromolecules,* 2000. **33**(6): p. 2114-2118.

63. Urayama, K. and S. Kohjiya, Crossover of the concentration dependence of swelling and elastic properties for polysiloxane networks crosslinked in solution. *Journal of Chemical Physics,* 1996. **104**(9): p. 3352-3359.

64. Falcao, A. N., J. S. Pedersen, K. Mortensen, and F. Boue, Polydimethylsiloxane networks at equilibrium swelling: Extracted and nonextracted networks. *Macromolecules,* 1996. **29**(3): p. 809-818.

65. Urayama, K., T. Kawamura, and S. Kohjiya, Elastic modulus and equilibrium swelling of networks crosslinked by end-linking oligodimethylsiloxane at solution state. *Journal of Chemical Physics,* 1996. **105**(11): p. 4833-4840.

66. Clarson, S. J., An investigation of the properties of bimodal poly(dimethylsiloxane) elastomers upon swelling with a linear oligomeric phenylmethylsiloxane. *Polymer Communications,* 1986. **27**: p. 260-261.

67. Patel, S. K., S. Malone, C. Cohen, J. R. Gillmor, and R. H. Colby, Elastic-Modulus and Equilibrium Swelling of Poly(Dimethylsiloxane) Networks. *Macromolecules,* 1992. **25**(20): p. 5241-5251.

68. Turner, R., Personal communication, *Constitutive equation derivations,* 2005.

Chapter II: Synthesis and Mechanical Characterization of Model PDMS Networks

2.1. Introduction

A comprehensive set of model polymer networks is needed to examine the matrix effects for photopolymerizable sol gel systems. In particular, we achieve high extents of reaction with well-defined crosslink functionality and strand molecular weights. Extensive work exists on both the experimental and theoretical level for both elastomeric systems in general and for polydimethylsiloxane (PDMS) in particular. Much of the literature examined the effect of network entanglements for systems cured both in the melt and in solution. Competing theories suggested that either entanglements act equivalently to chemical cross-links[1-4] or that they act merely to limit chemical junction fluctuations.[5-7] However, later work examining the relationship between network modulus and preparation polymer volume fraction gives significant credence to entanglements functioning as chemical crosslinks.[3, 8, 9] In these studies, networks were formed from precursors with molecular weights both significantly above and below the entanglement molecular weight. Reported values of entanglement molecular weight, M_e, are reported to be between 8,100 and 16,600 g/mol.[10-12] These experimental results have been compared with two

mutually exlusive theories.

The c* theory, proposed by de Gennes, states that regardless of dilution state, polymerization functionally occurs at the overlap concentration, or c*.[13] Thus, at fully swollen conditions, network chains would be completely disinterpenetrated. The scaling prediction between elastic modulus and polymer volume fraction during network preparation was corroborated by several groups.[13-16] However, as Urayama, et al., note, this correspondence is a cancellation of several theoretical assumptions and not necessarily confirmation of the c* theorem.[8] Contrary to the c* theory, Panyukov *et al.* and Obukhov *et al.* have proposed scaling behaviors for good and theta solvents based on a preparation state free energy approach that uses affine deformation on swelling.[17, 18] Derivation of these scaling behaviors begins with the Flory-Rehner approach of free energy equivalencies; free energy due to osmotic pressure of swelling is balanced by the free energy of elasticity of network strands. Although a relatively thorough examination of the approach is given in the introduction of Chapter IV that is pertinent to equilibrium swelling, we will here address portions of the derivation for theta solvents that are significant to our network preparation and characterization. Assuming an affine network where each network strand acts as a simple Hookean spring, we can derive the following result.

$$G \cong \frac{kT}{N}\phi_0^{2/3}\phi^{1/3} \tag{2.1}$$

In this equation, G is the shear modulus, k is Boltzmann's constant, T is the absolute temperature, N is average degree of polymerization, ϕ_0 is polymer volume fraction at preparation, and ϕ is polymer volume fraction at measurement. If entanglements do not play a significant role in network modulus, Equation 2.1 should predict network scaling behavior. However, since we study network strands significantly longer than the entanglement molecular weight, we need to determine appropriate scaling behavior for entanglement dominated networks. If the

entanglement strand is a standard excluded volume random walk of Kuhn length blobs,[13, 19] we get:

$$N_e(\phi_0) \cong g\left(\frac{a}{\zeta}\right)^2 \cong \left(\frac{a_1}{b}\right)^2 \phi_0^{-4/3} \tag{2.2}$$

where N_e is length of the entanglement strand, g is the number of monomers in a blob ($g \cong \phi_0^{-2}$ in a θ solvent), a is the tube diameter for reptation ($a \cong a_1 \phi_0^{-2/3}$), and a_1 is the tube diameter in the melt. If we then combine Equations 2.1 and 2.2, we obtain the result:

$$G \cong kT\left(\frac{b}{a_1}\right)^2 \phi_0^{\,2} \phi^{1/3} \tag{2.3}$$

which is applicable scaling behavior if entanglements are the dominant crosslinking effect to determine elastic modulus.

Although several recent papers establish scaling behavior that seems to corroborate this theoretical proposition,[3, 8, 9] there have been several problems in network formation that are difficult to overcome. The chemistry of reaction is important when trying to establish model networks. For all high molecular weight systems, similar vinyl-silane crosslinking chemistry is used. Cross-linking molecules with four silane moieties are catalytically cross-linked with α–ω vinyl end-capped PDMS. In this reaction system, a stiochiometric ratio of reactive groups will lead to imperfect networks with relatively large soluble fractions.[20-23] Urayama, et al., do not map out optimal reactive group ratios.[9] High polymer polydispersity (PDI) will also potentially lead to scaling behavior not in accord with theory, and several literature results did not use highly fractionated materials.[3, 9]

To effectively analyze photoreactive sol gel systems, we have formed model networks

using very low PDI ($M_w / M_n < 1.25$) network precursors. These networks are shown to be fully cured by several different methodologies and have low soluble fractions. We also examine the effect of preparation state polymer volume fraction by polymerizing different molecular weight network precursors in several levels of theta solvent diluents. We compare the results of these networks to affine network theories and examine the effects of entanglements on network modulus.

2.2. Experimental section

2.2.1. Materials

Networks were formed by catalytically reacting α–ω vinyl endcapped siloxane precursors with a tetrafunctional silane. Multiple molecular weights of α–ω vinyl endcapped siloxanes were purchased from Gelest Chemicals. Initial polydispersities as measured by GPC were relatively high (1.6); cosolvent fractionation and purification were used to remove low molecular weight siloxanes and other impurities with toluene as a good solvent and methanol as a poor solvent. [24, 25] A platinum catalyst, cis-dichlorobis(diethylsulfide) platinum(II) was purchased from Strem Chemicals and diluted in anhydrous toluene. Tetrakis (dimethylsiloxy)silane was purchased from Gelest chemicals. Both the catalyst and crosslinker were used without further preparation.

2.2.2. Analysis of molecular weight for precursor molecules

Gel permeation chromatography / light scattering (GPC-LS) was used to determine absolute macromer molecular weights and polydispersity. The light scattering detector used was a Wyatt Dawn EOS 18 angle system with toluene as a solvent. The ratio of methyl to vinyl hydrogen peaks from ^{1}H NMR spectra were used to calculate number average molecular weight

(M_n) for siloxane precursors. By comparing molecular weight results between these methods, we can determine vinyl functionality. Network precursors had number average molecular weight (M_n) of 15200, 22300, and 41200 with PDIs of and 1.11, 1.18, and 1.24 as seen in table 2.1.

2.2.3. Matrix preparation

Network crosslinking was examined at concentrations ranging from neat to 50% with short chain PDMS as theta solvent. An optimum ratio, R_{opt}, of silane crosslinker to vinyl endgroups was determined for each level of diluent during network cure by determining maximum equilibrium swelling and maximum modulus. R_{opt} was also measured for different network precursor molecular weights. The components are well mixed, degassed under vacuum, and cured in 1 mm thick optical quality $\lambda/5$ quartz molds. Cure is performed at 35 °C to minimize excess crosslinking behavior.[26, 27] Although at higher temperatures there can be significant inter-chain side reactions of siloxanes, at this relatively low temperature we eliminate all but a small amount of silane-silane linking reaction between crosslinker molecules.[20, 22] IR measurements were also performed to determine completeness of cure. The vinyl absorption band centered at 1596 cm^{-1} was examined before and after cure.

Cured samples are extracted using a multistep toluene / methanol cosolvent extraction process. Toluene is used in > 50x excess volume and is replaced at 24 hour intervals. Methanol at different dilution ratios in toluene is subsequently used to extract toluene from the samples. This multistep cosolvent extraction of toluene from the sample is necessary; direct immersion of a toluene swollen network into pure methanol will cause the sample to fracture. After toluene is extracted, the sample is dried in vacuum for at least 24 hours. Control samples that have been extracted by this procedure are then left in toluene for several weeks. The solvent is then highly concentrated and examined for PDMS residue with GPC. No elution peak is observed. Since

these networks have chains that are less than 5 times the entanglement molecular weight, complete removal of unreacted chains for short extraction times is quite reasonable.

2.2.4. Swelling and modulus measurements

After exhaustive extraction of PDMS diluent and unincorporated vinyl endcapped PDMS precursors, samples were reswollen in short chain PDMS materials at 10%, 20%, 30%, and equilibrium swelling. Equilibrium swelling was determined gravimetrically and established when no further weight changes occurred over a 48 hour period. Samples swollen from 10-30% macromer concentration were allowed to equilibrate for the same length of time.

The increased cure modulus was measured using a Rheometric Scientific ARES with 25 mm parallel plate geometry. Dynamic moduli of fully cured samples were measured at a controlled temperature of 25 °C. Time cure measurements were run at 1% strain and 1 Hz under oscillatory shear. These parameters were shown, at full cure, to be in the linear viscoelastic regime. Cure experiments were run for 24 hours; no subsequent modulus change was measured. Due to plate slippage for samples prepared *ex situ*, precured samples could not be used. Frequency sweeps from *in situ* cured samples were also performed to analyze network imperfections.

Ex situ rheological measurements were performed on a Rheometric Scientific RSA III in a simple tension geometry under oscillatory mode at 25 °C with <1% strain and at 1Hz. Strain sweeps showed that even with high modulus samples, the linear viscoelastic regime extended to >2% strain. Since the storage modulus of these model networks exhibits a relatively large plateau with frequency, 1Hz oscillations were chosen for convenience. Samples were 1 cm x 3 cm x 1 mm in size; since relatively small strains (< 1%) were used, changes in cross-sectional area were neglected. This approximation is validated by the close concurrence (< 3% deviation) between

shear modulus and Young's modulus. Young's modulus data can been converted to shear modulus using the relationship $E'=3G'$ based on a Poisson ratio of 1/2.

2.3. Results and discussion

2.3.1. Polydispersity of precursor molecules

Three different molecular weights (M_n = 15200, 22300, 41200 g/mol) of α–ω vinyl endcapped PDMS precursors were used in network formation. Before fractionation, polydispersity (PDI=M_n/M_w) values were between 1.4 and 1.6 as measured with GPC; after fractionation, these values were significantly decreased. Table 2.1 shows post-fractionation molecular weight obtained with GPC-MALS, molecular weight measured with NMR, and polydispersity values. Comparison of M_n (number average molecular weight) for NMR and GPC-MALS (multi-angle light scattering) data shows a slightly lower value from light scattering. Since light scattering gives absolute molecular weight numbers, this value should be relatively accurate. Relative differences in values between these two measurement methods match well with polydispersity numbers. This shows there is very close to a 2:1 stoichiometric ratio of vinyl endgroups to chains.

2.3.2. Completeness of cure

Although our precursor molecules are well-defined with few non-functional chains, we also need to ensure that our networks have completely cured. We can do this using two different methods. Before polymerization, a vinyl absorption band is present at 1596 cm^{-1}. 24 hours after the reaction has commenced, we remeasure the absorption peak. In all cases, this has depleted to non-measurable values. All samples were cured at 35 °C; several *in situ* time sweep modulus

measurements were also used to track fractional endgroup conversion. Figure 2.1 shows three different molecular weight precursors (M_n = 15200, 22300, 41200) cured in the melt and one molecular weight, M_n = 22300, cured with polymer volume fraction, ϕ_0 = 0.5. In all cases, there is less than 1% change in modulus after 11 hours. However, samples were still cured for 24 hours at 35 °C before being used. Samples are also extracted to determine the unreacted amount of precursor chains. Table 2.2 shows that extractable mass, ω_{sol}, is less than 2% for all systems, including ones cured in diluent. Kinetic models of reaction predict similar soluble fractions.[22, 26, 28] For these networks, figure 2.2 shows *G''* values are several orders of magnitude lower than *G'* values. The low viscous loss component of the network modulus indicates that most chains are elastically effective within the network.

2.3.3. Curing moduli for different crosslinker : endgroup ratios

Altering the ratio of cross-linker silane functionalities to strand vinyl functionalities should significantly affect network properties. In figure 2.4A, we see that for each network precursor molecular weight, there is a maximum modulus exhibited when *G'* is plotted against *R*. Also, this peak is reached at greater than stoichiometric ratios of crosslinker to strand chain ends, suggesting that there are either kinetic entrapments or crosslinkers side reactions. For R values below peak modulus, there will be a significant number of dangling, or pendant, chains that are not elastically effective since only one end is attached to the network. At extremely low *R* values, extraction studies show that significant portions of the precursor networks strands are never incorporated into the network. For *R* values higher than peak, we expect strand end-capping, or crosslinker that only has one reacted junction functionality. The peak values of *R* are 1.27 for M_n=15200, 1.48 for M_n=22300, and 1.60 for M_n=41200, indicating a monotonic increase of R with strand molecular weight. Previous work using Monte Carlo simulations suggests that, for a

system of 50 repeat units (approximately 3700 molecular weight), kinetic and topological constraints give a maximum number of effectively elastic networks strands at an *R* value of 1.2.[22, 23] This formulation does not take into account effects of polydispersity or of potential crosslinker side reactions.

Several papers have shown that, even at low temperatures, up to 10% of silane crosslinker functionality is consumed in side reactions.[1, 26] Patel, et al., also observed similar trends for *R* values for minimum equilibrium swelling.[20] Using strand precursor molecular weights of M_n=2500 to M_n=58000, they found peak *R* values were between 1.44 and 2.05 with no trend between strand molecular weight and optimal *R*. Other work with PDMS and PDES (polydiethylsiloxane) shows similar values for *R*.[8, 25] These higher *R* values and data lacking a trend with molecular weight lead to the conclusion that considerable vinyl endgroup defects may be present in those networks. Additionally, this is supported in Patel's work by preliminary titration data showing higher vinyl functionality than 2 per network strand. Our values fall between other experimental and simulation work, indicating that our networks have relatively few defects but do have some measurable quantity of crosslinker-crosslinker side reaction occurring.

Since we also prepare networks in diluted conditions where polymer volume fraction is as low as 0.5, it was necessary to determine whether *R* would change under these conditions as compared to those in the melt. Figure 2.4B shows a plot of melt-prepared networks and two diluted preparation systems; there is not a significant shift in maximum *R*. Due to changes in kinetic entrapment effects and fewer entanglements at lower polymer volume fractions, we expected *R* to decrease slightly under diluted preparation conditions. Surprisingly, there is not an appropriate a priori theory available to determine this type of parameter. As such, all networks of a specific molecular weight are prepared at the same value of *R*.

In figure 2.2, oscillatory frequency sweeps over four orders of magnitude are performed

for networks polymerized at optimum *R* value and a lower *R* value (< 1). The network crosslinked at optimum *R* (model network) shows a plateau modulus for *G'* across the full frequency range. Conversely, the network formed with a dearth of crosslinker, or imperfect network, shows a monotonic increase in elastic modulus with increasing frequency. This behavior indicates that additional elastic modes of response are elicited in higher frequency regimes. Since these networks have been fully extracted, the non-homogeneous frequency response must be due to pendant, or dangling chains in the network that are not permanently elastically effective.
It is interesting to note that, although the example of an imperfect network in the figure 2.2 has a storage modulus nearly an order of magnitude smaller than the model network, viscous moduli are nearly equivalent. This indicates that the relative level of imperfections (as suggested by *G'* / *G''*) in the model network is signficantly less than that for networks cured at sub-optimal *R* values.

2.3.4. Curing moduli and scaling behavior for networks with initial diluent

When using an initial diluent during cure, we expect the network modulus to decrease due to decreased numbers of entanglements. As dilution increases, fewer chains are present within the radius of gyration of a single chain. Since, as was discussed earlier in this chapter, the entanglement molecular weight of PDMS is relatively low (near 10,000 g/mol), all three precursor molecular weights that we use should exhibit some increase in modulus when polymerized in the melt as compared to what is expected for purely chemical crosslinks. As percent dilution during cure is increased, the likelihood of entanglement decreases, and scaling behavior should alter analogously. If we examine equation 2.1 and eqution 2.3, we can see that, by replacing ϕ with ϕ_0 in equations 1 and 2, the behavior of a single precursor molecular weight will scale as :

$$Gb^3 \cong (b/a)^2 \phi_0^1 \tag{2.4}$$

for non-entangled systems and

$$Gb^3 \cong (b/a)^2 \phi_0^{7/3} \tag{2.5}$$

for networks dominated by entanglements in theta solvent conditions. Figure 2.3B shows experimental behavior of networks prepared with three different molecular weights from 0% to 50% dilution. Using a least squares regression, the power law exponents are:

$$G' \propto \phi_0^{1.96} \text{ for Mn = 15200 g/mol} \tag{2.6a}$$

$$G' \propto \phi_0^{2.21} \text{ for Mn = 22300 g/mol} \tag{2.6b}$$

$$G' \propto \phi_0^{2.34} \text{ for Mn = 41200 g/mol} \tag{2.6c}$$

These results confirm the notion that, at the molecular weights we use, entanglements are the dominant junction points in the network; all scaling behaviors are much closer to the 7/3 exponent for entangled networks than the linear exponent established for permanently crosslinked systems.

However, the results for the lowest molecular weight, M_n=15200 g/mol, are somewhat different than is expected from theory[17] where entanglements should still be a relatively minor contribution at the lowest molecular weight we examine. Our results are partially corroborated by experiments performed by Sivisailam and Cohen,[3] however; 9900 MW precursors show a scaling exponent of 1.52. This indicates that entanglements or chain entrapments (such as are present in looped systems) occur even at relatively low molecular weights. Using simple radius of gyration arguments, this explanation does not seem unlikely; at the entanglement molecular weight of 10000 g/mol, there are approximately 4 chains present in the volume subsumed by a single chain.

When the precursor molecular weight is increased to 41200 g/mol, we obtain a scaling exponent of 2.34. This value is very close to the theoretical expectations of 2.33 for highly entangled networks. Since the precursor molecular weight is only four times the entanglement molecular weight, it is somewhat unexpected to find such concurrence between experiment and theory. If higher precursor molecular weights were also examined, it would be interesting to note if experimental results would plateau at the theoretical exponent for this power law scaling behavior.

Cured networks are then extracted by the procedures indicated in the experimental methods sections. When extracted, network modulus increases significantly compared to diluted systems because of network collapse. The theoretical increase can be obtained using Eq (3). Qualitatively, a quick comparison of figure 2.3A and figure 2.3B shows an increase in modulus for extracted networks. To determine scaling behavior for these extracted networks, equation 2.1 and equation 2.3 can be used where we let ϕ=0. This results in:

$$Gb^3 \cong (b/a)^2 \phi_0^{2/3} \tag{2.7}$$

for non-entangled systems and

$$Gb^3 \cong (b/a)^2 \phi_0^2 \tag{2.8}$$

for entangled systems. Figure 2.3A shows the experimental scaling behavior for the three precursor molecular weight systems. The experimental power law exponents are:

$$G' \propto \phi_0^{1.33} \text{ for Mn = 15200 g/mol} \tag{2.9a}$$

$$G' \propto \phi_0^{1.44} \text{ for Mn = 22300 g/mol} \tag{2.9b}$$

$$G' \propto \phi_0^{1.87} \text{ for Mn = 41200 g/mol.} \tag{2.9c}$$

For the network formed from the lowest molecular weight precursor, we again see behavior that is intermediate between fully entangled and non-entangled regimes. For higher molecular weight precursors, behavior approaches theoretical values for power law exponents as is expected from results on diluted systems.

2.3.5. Comparison of ideal network behavior with synthesized model networks

Ideal network behavior, as indicated in the introduction, will show that the number of crosslinks per unit volume is directly proportional to the modulus of the network. We find significant departure from ideal behavior for our networks. Figure 2.5 shows three precursor molecular weight systems where modulus is plotted against precursor molecular weight at four different values of ϕ_0. The horizontal line at 2.1×10^5 Pa is the plateau modulus for high molecular weight uncrosslinked PDMS.[4] This equates to an entanglement molecular weight of approximately 12000 g/mol using affine junction theory and compares well with previous entanglement molecular weight determinations. The lower line in the plot shows affine crosslinking behavior which follows the simple equation:

$$G = \nu RT \tag{2.10}$$

where G is the shear modulus, ν is the number of moles of elastic chains per unit volume, T is absolute temperature, and R is the gas constant. Interestingly, networks polymerized in the melt have a modulus that is higher than expected if only entanglements are providing network structure. For high dilution ratios during cure, we are also able to access shear moduli that are below what is expected from affine modulus predictions. There are several potential mechanisms that may place the modulus in this regime: pendant chains, loops, and large-scale heterogeneities that lead to non-affine swelling and deformation. Patel, et al., have shown that for significant numbers of pendant chains, the shear modulus does not exhibit a plateau modulus in the

frequency region that we examine.[20] For short chain PDMS (<5000 MW) simulations have shown that the number of loops formed during highly diluted cure is < 10%.[22, 29] Also, large scale heterogeneities are known to exist in cured PDMS networks.[7, 30-32] These network heterogeneities have two potential means of formation: kinetically controlled crosslinking and very high functionality crosslinker. Since a silane-silane crosslinker side reaction has been shown to occur at less than 10 percent for reaction temperatures of 35 °C,[26] little high functionality crosslinker will be present in this system. Regardless, even if high functionality junctions were formed, previous results have shown little total modulus change regardless of crosslinker functionality.[33-35] Thus, the potential combination of more loops forming and increased kinetically produced heterogeneities at dilute conditions seems to be a reasonable explanation of the low shear modulus.

2.4. Conclusions

We have synthesized model PDMS networks using well-defined and low PDI precursors. These networks are shown to have little soluble weight fraction after cure and few pendant chains are present; rheology data indicates that most chains are elastically effective. The ratio of crosslinker to midblock endgroup functionality was optimized for each molecular weight system, was shown to be greater than a stoichiometric ratio, and exhibited an increase based on increasing precursor molecular weight. These effects can be explained with small amounts of silane-silane crosslinking reactions and kinetic chain entrapment during cure. Networks polymerized in a theta solvent were shown to follow theoeretical scaling predictions for modulus and preparation polymer volume fraction. This behavior shows that melt polymerization incorporate significant numbers of entrapped entanglements. Overall, the careful control of network modulus and extent of entanglements allows us to lay the foundation for examination of other properties, such as

equilibrium swelling and interaction parameters, modulus of intercalated model network systems with photopolymerized materials, and reaction kinetics with necessary accuracy to glean important experimental results.

2.5. Tables

Table 2.1. Molecular weight and polydispersity of linear vinyl endcapped PDMS.

α–ω vinyl precursor	M_n (NMR)	M_n(g/mol) GPC-MALS)	PDI[a] (GPC-MALS)
PDMS-A	16300	15200	1.11
PDMS-B	24900	23200	1.18
PDMS-C	N/A	41200	1.24

[a]PDI = Poldispersity Index (M_w/M_n)

Table 2.2. Network properties including modulus and soluble network fraction for networks prepared at multiple precursor concentrations

Sample #	$M_{precursor}$	ϕ_0	$10^2\ \omega_{sol}$	E'_{cured} (10^5Pa)
M84-15	15200	1	0.375	8.23
M69-15	15200	0.85	0.436	5.97
M52-15	15200	0.7	0.512	4.20
M33-15	15200	0.5	1.023	2.09
M77-22	22300	1	0.644	7.58
M64-22	22300	0.85	0.736	5.58
M47-22	22300	0.7	0.363	3.41
M29-22	22300	0.5	0.944	1.73

2.6. Figures

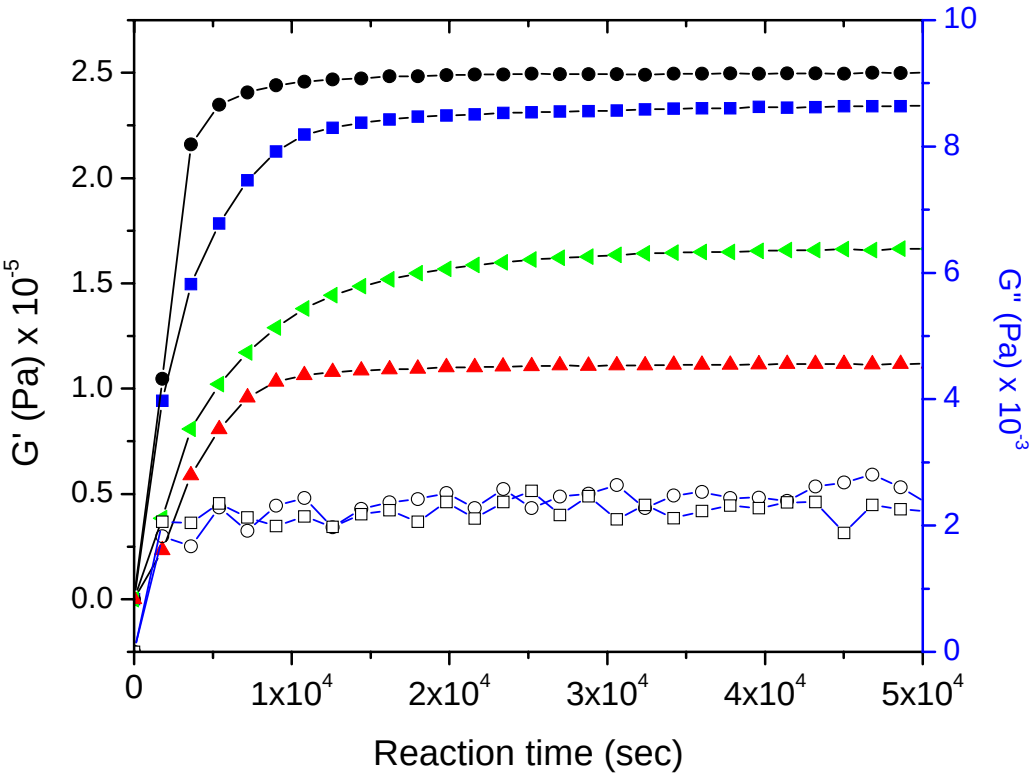

Figure 2.1 Progressive modulus increase with cure time at 35°C for several precursor molecular weights and ϕ_0 (initial polymer concentration). In all systems, G' and G" reach asymptotic values within 10 hours. Filled points are G', unfilled points are G". ● is 15200 g/mol, ■ is 22300 g/mol, ◀ is 22300 g/mol with ϕ_0=0.5, and ▲ is 41200 g/mol.

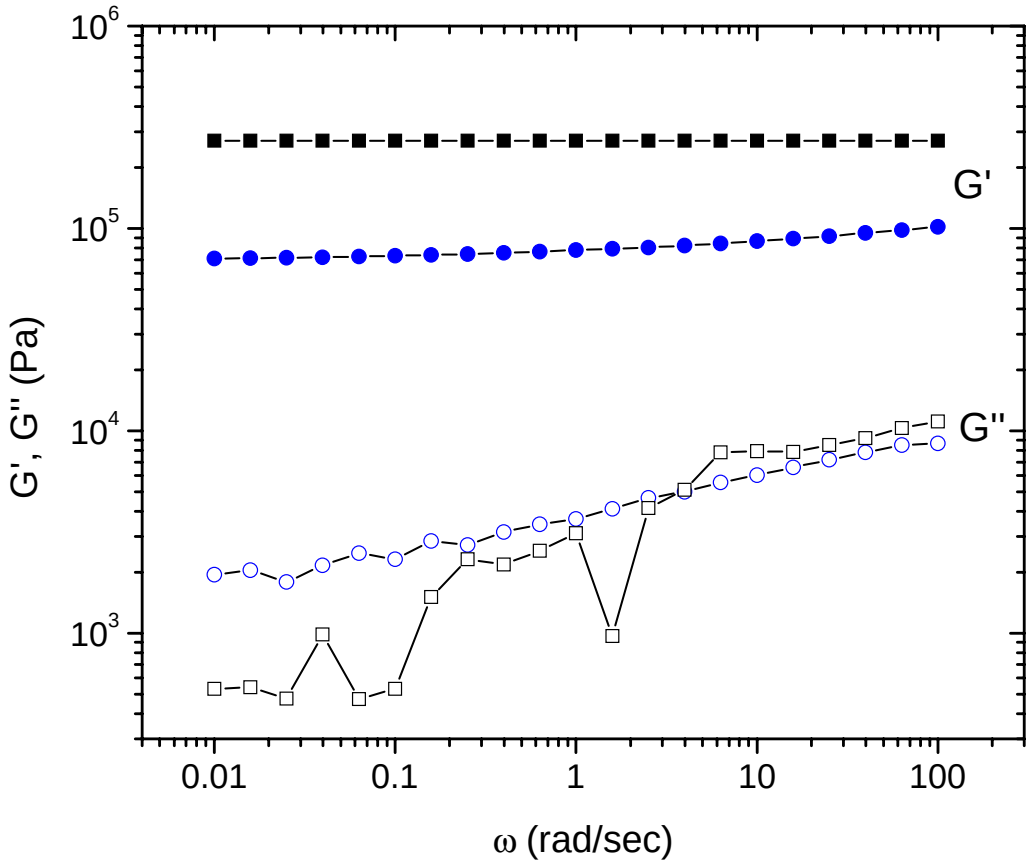

Figure 2.2 G' and G" for model and imperfect networks. Note the plateau modulus extends four decades in frequency for the model network (15200 g/mol, R = R_{opt}), whereas the imperfect network (15200 g/mol, R < R_{opt}) shows a monotonic increase in G' with frequency. ■ and □ are G' and G", respectively, for a model network, ● and ○ are G' and G", respectively, for an imperfect network.

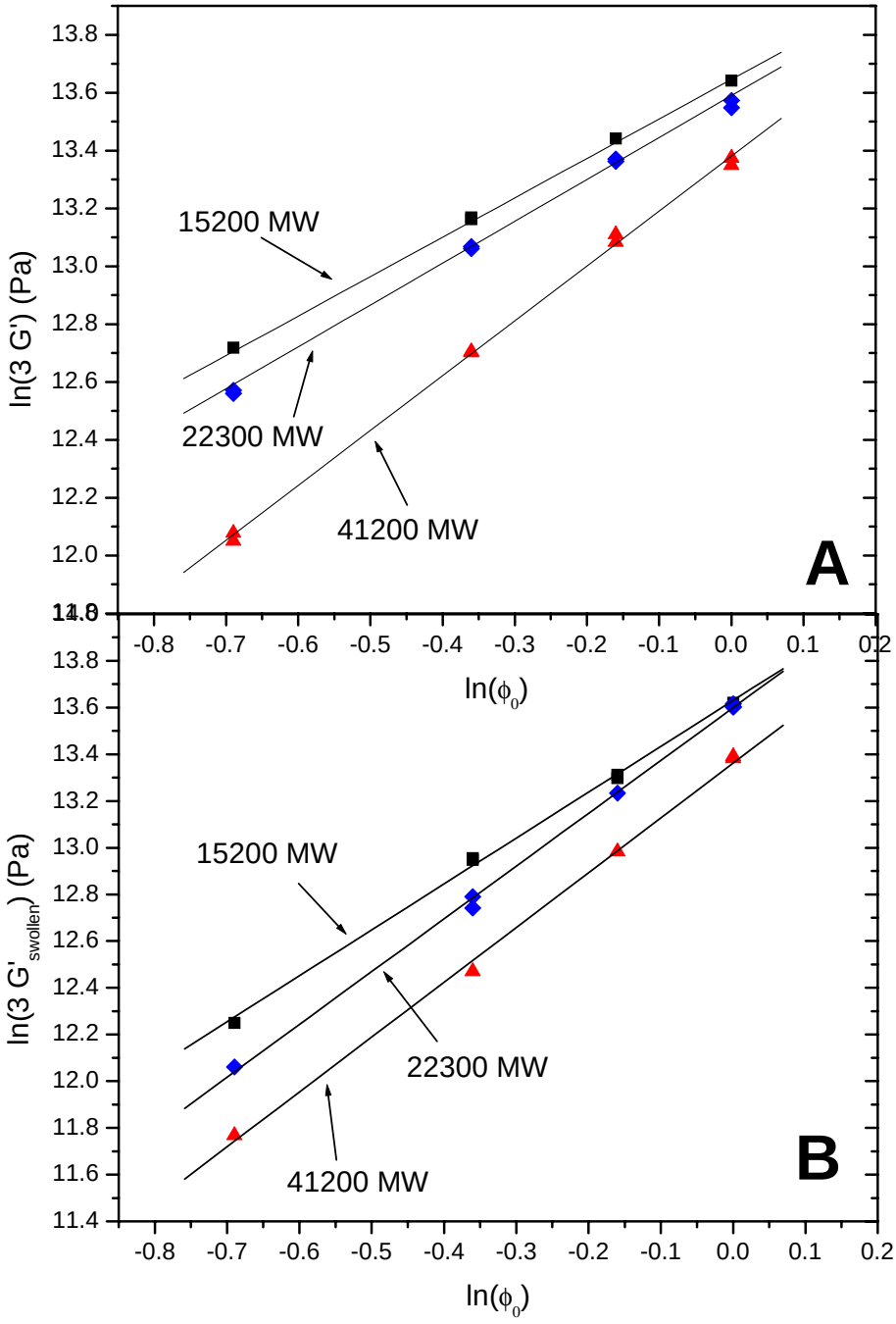

Figure 2.3 Plot A shows scaling behavior for three different molecular weight precursors for networks cured and measured after diluent was extracted. Plot B shows the same networks before extraction. *G'* is shear modulus and ϕ_0 is polymer volume fraction at preparation.

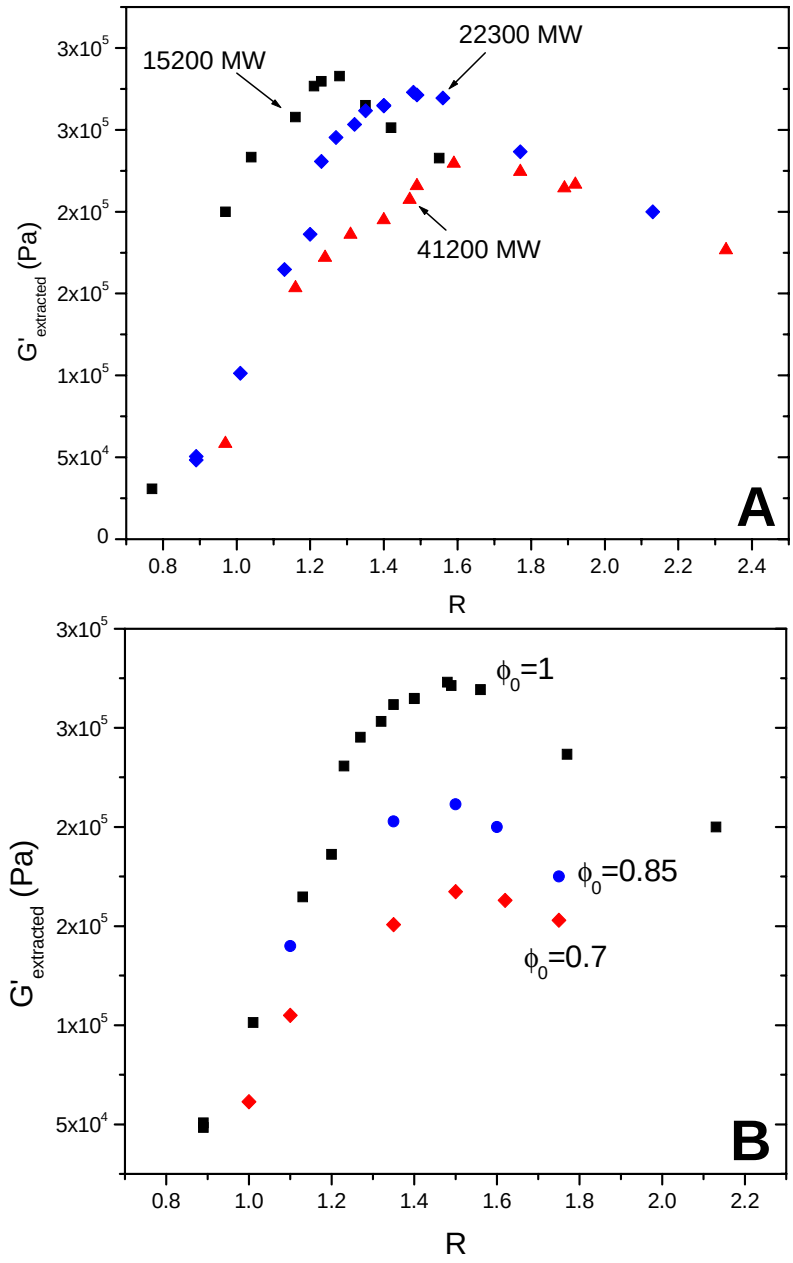

Figure 2.4 Plot A shows modulus reaches a peak at different ratios of silane to vinyl groups, *R*, for different network precursor molecular weights. Plot B shows how extracted modulus changes with initial diluent present at cure for 22300 MW precursors.

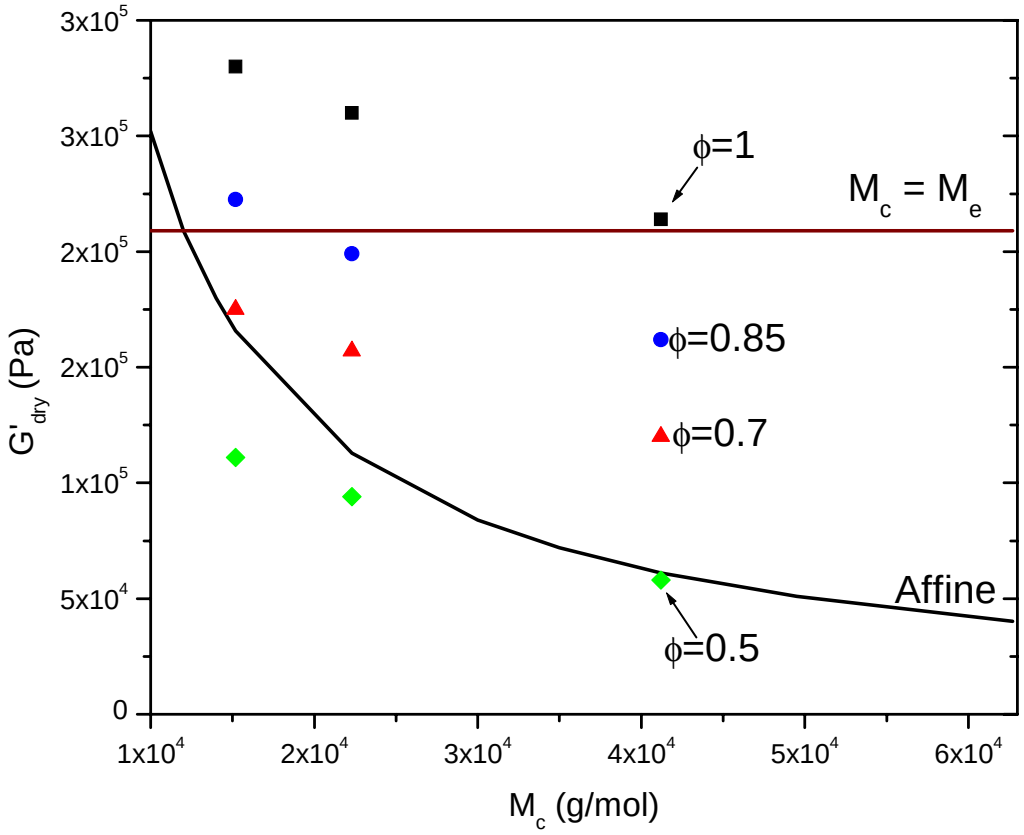

Figure 2.5 Shear modulus of extracted networks is plotted against network strand molecular weight (M_n = 15200, 22300, 41200). Each strand molecular weight is polymerized at four polymer volume concentrations (1, 0.85, 0.7, and 0.5). As the polymer volume concentration decreases, the dry modulus also decreases due to fewer entanglements. The horizontal line is the modulus expected if all strands were of the entanglement molecular weight. The line labeled "Affine" is the theoretical modulus expected for affine ideal networks with no entanglements. For each network precursor molecular weight, modulus regimes above the entanglement molecular weight and below the affine modulus predictions are reached.

2.7. References

1. Gottlieb, M., C. W. Macosko, G. S. Benjamin, K. O. Meyers, and E. W. Merrill, Equilibrium Modulus of Model Poly(Dimethylsiloxane) Networks. *Macromolecules,* 1981. **14**(4): p. 1039-1046.

2. Rennar, N. and W. Oppermann, Swelling Behavior and Mechanical-Properties of Endlinked Poly(Dimethylsiloxane) Networks and Randomly Cross-Linked Polyisoprene Networks. *Colloid and Polymer Science,* 1992. **270**(6): p. 527-536.

3. Sivisailam, K., Scaling Behavior: Effect of Precursor concentration and precursor molecular weight on the modulus and swelling of polymeric networks. *Journal of Rheology,* 2000. **44**(4): p. 897-915.

4. Valles, E. M. and C. W. Macosko, Properties of Networks Formed by End Linking of Poly(Dimethylsiloxane). *Macromolecules,* 1979. **12**(4): p. 673-679.

5. Erman, B. and I. Bahar, Effects of Chain Structure and Network Constitution on Segmental Orientation in Deformed Amorphous Networks. *Macromolecules,* 1988. **21**(2): p. 452-457.

6. Mark, J. E., Model Elastomeric Networks. *Rubber Chemistry and Technology,* 1981. **54**(4): p. 809-819.

7. Soni, V. K. and R. S. Stein, Light-Scattering-Studies of Poly(Dimethylsiloxane) Solutions and Swollen Networks. *Macromolecules,* 1990. **23**(25): p. 5257-5265.

8. Urayama, K., T. Kawamura, and S. Kohjiya, Elastic modulus and equilibrium swelling of networks crosslinked by end-linking oligodimethylsiloxane at solution state. *Journal of Chemical Physics,* 1996. **105**(11): p. 4833-4840.

9. Urayama, K. and S. Kohjiya, Crossover of the concentration dependence of swelling and elastic properties for polysiloxane networks crosslinked in solution. *Journal of Chemical Physics,* 1996. **104**(9): p. 3352-3359.

10. Valles, E. M. and C. W. Macosko, Structure and Viscosity of Poly(Dimethylsiloxanes) with Random Branches. *Macromolecules,* 1979. **12**(3): p. 521-526.

11. Ferry, J. D., *Viscoelastic Properties of Polymers, 3rd ed.* 1980. New York: John Wiley & Sons, Inc.

12. Orrah, D. J., J. A. Semlyen, and S. B. Rossmurphy, Studies of Cyclic and Linear Poly(Dimethylsiloxanes) .27. Bulk Viscosities above the Critical Molar Mass for Entanglement. *Polymer,* 1988. **29**(8): p. 1452-1454.

13. de Gennes, P. G., *Scaling Concepts in Polymer Physics*. 1979. Ithaca: Cornell University Press.

14. Candau, S., A. Peters, and J. Herz, Experimental-Evidence for Trapped Chain Entanglements - Their Influence on Macroscopic Behavior of Networks. *Polymer,* 1981. **22**(11): p. 1504-1510.

15. Zrinyi, M. and F. Horkay, On the Elastic-Modulus of Swollen Gels. *Polymer,* 1987. **28**(7): p. 1139-1143.

16. Bastide, J. and L. Leibler, Large-Scale Heterogeneities in Randomly Cross-Linked Networks. *Macromolecules,* 1988. **21**(8): p. 2647-2649.

17. Panyukov, S. V., Scaling Theory of High Elasticity. *Soviet Physics: JETP,* 1990. **71**(2): p. 372-379.

18. Obukhov, S. P., Network Modulus and Superelasticity. *Macromolecules,* 1994. **27**: p. 3191-3198.

19. Colby, R. H. and M. Rubinstein, *Polymer Physics*. 2003. New York: Oxford University Press, Inc.

20. Patel, S. K., S. Malone, C. Cohen, J. R. Gillmor, and R. H. Colby, Elastic-Modulus and Equilibrium Swelling of Poly(Dimethylsiloxane) Networks. *Macromolecules,* 1992. **25**(20): p. 5241-5251.

21. Patel, S. K., Dynamic Light Scattering from Swollen Poly(dimethylsiloxane) Networks. *Macromolecules,* 1992. **25**: p. 5252-5258.

22. Gilra, N., A Monte Carlo study of the structural properties of end-linked polymer networks. *Journal of Chemical Physics,* 2000. **112**(15): p. 6910-6916.

23. Gilra, N., A. Panagiotopoulos, and C. Cohen, Monte Carlo simulations of free chains in end-linked polymer networks. *Journal of Chemical Physics,* 2001. **115**(2): p. 1100-1104.

24. Braun, J. L., J. E. Mark, and B. E. Eichinger, Formation of poly(dimethylsiloxane) gels. *Macromolecules,* 2002. **35**(13): p. 5273-5282.

25. Hedden, R. C., H. Saxena, and C. Cohen, Mechanical properties and swelling behavior of end-linked poly(diethylsiloxane) networks. *Macromolecules,* 2000. **33**(23): p. 8676-8684.

26. Macosko, C. W. and J. C. Saam, The Hydrosilylation Cure of Polyisobutene. *Polymer Bulletin,* 1987. **18**(5): p. 463-471.

27. Venkataraman, S. K., L. Coyne, F. Chambon, M. Gottlieb, and H. H. Winter,

Critical Extent of Reaction of a Polydimethylsiloxane Polymer Network. *Polymer,* 1989. **30**(12): p. 2222-2226.

28. Macosko, C. W. and D. R. Miller, New Derivation of Average Molecular-Weights of Nonlinear Polymers. *Macromolecules,* 1976. **9**(2): p. 199-206.
29. Gilra, N., A. Panagiotopoulos, and C. Cohen, Monte Carlo simulations of polymer network deformation. *Macromolecules,* 2001. **34**(17): p. 6090-6096.
30. Horkay, F., A. M. Hecht, M. Zrinyi, and E. Geissler, Effect of cross-links on the structure of polymer gels. *Polymer Gels and Networks,* 1996. **4**(5-6): p. 451-465.
31. Geissler, E., A. M. Hecht, and F. Horkay, Structure of polymer solutions and gels containing fillers. *Macromolecular Symposia,* 2001. **171**: p. 171-180.
32. Geissler, E., F. Horkay, and A. M. Hecht, Structure and Thermodynamics of Flexible Polymer Gels. *Journal of Chemical Physics,* 1994. **100**(11): p. 8418-8424.
33. Mark, J. E. and M. A. Llorente, Model Networks of End-Linked Polydimethylsiloxane Chains .5. Dependence of the Elastomeric Properties on the Functionality of the Network Junctions. *Journal of the American Chemical Society,* 1980. **102**(2): p. 632-636.
34. Llorente, M. A. and J. E. Mark, Model Networks of End-Linked Poly(Dimethylsiloxane) Chains .8. Networks Having Cross-Links of Very High Functionality. *Macromolecules,* 1980. **13**(3): p. 681-685.
35. Tang, M. Y., L. Garrido, and J. E. Mark, The Effect of Crosslink Functionality on the Elastomeric Properties of Bimodal Networks. *Polymer Communications,*

1984. **25**(11): p. 347-350.

Chapter III: Characterization of PDMS Gels with Photopolymerized Short-chain PDMS Analogues

3.1. Introduction

Polydimethylsiloxane (PDMS) has been studied extensively as a model system for homogeneous and interpenetrating networks. By adding a second component to a well characterized material, it is possible to change optical, mechanical, and other properties of a network. We are particularly interested in examining the change in mechanical properties and underlying structure during photopolymerization of macromers in different model networks.

Interpenetrating networks (IPNs) are prepared by either sequential and simultaneous synthesis. Sequential synthesis is performed by curing a host network (A), dissolving a second network precursor (B), and then polymerizing the second network. Simultaneous materials are formed by mixing and then simultaneously curing two different polymer precursors (A and B) that have independent cross-linking chemistries. These two methods of IPN synthesis create very different materials in terms of mechanical properties and phase separation behavior. Assuming network precursors are initially miscible, phase separation in both sequential and simultaneous IPNs begins only once the reaction progresses. Four distinct stages have been observed during

formation of microscale morphologies in simultaneous IPNs.[1-3] At short times, monomer and polymer (part B) remain miscible with monomor and polymer (part A); the material remains optically transparent. As time progresses, the system becomes cloudy as part B polymer begins to phase separate. This phase separation may begin with nucleation of droplets or with the onset of spinodal decomposition (SD). The third step is grain coarsening; spinodal decomposition continues until interconnected cylinders of part B are present in the sample. The final step is due to gellation of the sample. Heterogeneities become locked in as diffusion is minimized. Depending on the relative rates of reaction and diffusion, these four phases may become blurred. If part A and part B polymer phase separate before network gellation, phase domains will be relatively large. The subsequent gellation effectively locks these inhomogeneities in place. If, however, network gellation occurs before phase separation, network crosslinks will limit localized swelling and phase separation. For sequential IPNs, part A polymer network is always present so phase separation will be limited to small size scales by part A crosslinks.[1] The induced phase separation during cure of sequential IPNs will lead to changes in the mechanical properties of the networks. Several theories have been proposed to examine the increased mechanical properties of dispersed and bicontinuous IPNs.[4-6]

IPNs can phase separate into two classes of morphologies. First, one phase can be non-continuous and completely dispersed inside of a continuous phase. The dispersed phase can attain different geometries depending on the thermodynamics of phase separation. The most common dispersed geometries are spherical and cylindrical domains. Spherical domains, or nodules, are created when phase separation is due to nucleation. Cylindrical domains are exhibited when a system spinodally decomposes. The second phase class is bicontinuous networks. Here, the two phases exhibit no chemical crosslinks, but are completely percolated within a single network. Small scale structure of bicontinuous phases may also share significant morphological

characteristics with dispersed systems. For example, spinodal decomposition to thermodynamic equilibrium often leads to a continuous cylindrical dispersed phase.

Multiple groups have analyzed size scales and structure of interpenetrating networks. In sequential polyisobutene-poly(methylmethacrylate) (PMMA) systems, tapping mode atomic force microscopy (AFM) shows a size scale of 50nm nodules with no distinct morphology in a bicontinuous network.[7] Sequential polydimethylsiloxane (PDMS) polystyrene (PS) IPNs have been shown with SEM to have approximately 1μm size scale; connectivity of PS morphology is dependent on weight percent.[8] PDMS-PMMA sequential IPNs show a trend in increased domain size with decreased reaction rate of the second cured network, that of PMMA.[9, 10] Using a UV initiated polymerization of PMMA with high absorbency, domain sizes were imaged throughout the depth of a sample using fluorescent confocal imaging techniques. Images at the sample surface show smaller domains than those receiving less light; minimum domain sizes appear to be on the order of microns. It is interesting to note that, in deep sections and slower cure rates, domain geometry progresses towards a interconnected spherical to cylindrical structure expected from spinodal decomposition.

If the phase separated domains have different material properties, the IPN will have a significantly different network modulus than either of the individual materials. Several theories been proposed for dispersed[4, 11-13] and continuous[5, 6] IPNs. Although considerable literature has been published on polymer reinforcement by fillers[14-17] and sequential IPNs[18, 19], the mechanism of reinforcement is still not well understood. In particular, we are not aware of any studies using curing photoreactive macromers into an elastomer networks to form a sequential IPN.

Static light scattering provides an effective method for analyzing both structure and size scales of density (or refractive index) fluctuations on the order of tens of nanometers to microns. Based on results from previous work in PDMS, this range seems eminently feasible to examine.

Since chemically crosslinked polymer, and in particular, PDMS, networks are known to have large scale heterogeneities,[20-25] it would also be interesting to correlate IPN structure size with host network heterogeneity size. These large scale heterogeneities, measured to be on the size scale of 10 nm to slightly less than 1 μm with light, X-ray, and neutron scattering, are significantly larger than the expected blob size of 1 to 2 nm that is found either in the melt or in crosslinked networks. These spatial density fluctuations are caused by inhomogeneous reactions that get locked into the network as the polymer gels; there is a direct relationship between this size scale and the modulus and equilibrium swelling properties of the network. For networks with a lower elastic modulus, heterogeneities occur on a larger size scale.

Scattering behavior can be analyzed with several methods depending on the expected structure and distribution of the scatterers. For randomly distributed spherical scatterers with sharp density delineation, Debye and Bueche proposed a simplification of Porod's Law such that:[26, 27]

$$I(q) \cong \frac{8\pi K a_c^{\,3} \left\langle \eta^2 \right\rangle}{\left(1 + q^2 a_c^{\,2}\right)^2} \tag{3.1}$$

where I is the scattering intensity at reduced scattering angle q; $K = 4\pi^2 n^2/\lambda_0^{\,4}$ where λ_0 is the wavelength of incident radiation in a vacuum and n is the refractive index of the medium; a_c is the correlation length for scattering particles; $<\eta^2>$ is the mean squared refractive index fluctuation in the medium; and $q = (4\pi/\lambda)\sin(\theta/2)$ where λ is the wavelength of incident light in the medium and θ is the angle between incident and scattered rays as measured in the medium. This formulation will be appropriate for phase separated regions with distinct boundaries, such as might be expected for equilibrated spinodal decomposition in IPNs. If we do not have sharp

boundaries between dispersed spherical particles (such as in swollen polymers in a dilute solution), the Ornstein-Zernicke function for scattering may be applied.[21, 28]

$$I(q) \cong \left(\frac{2}{\pi}\right)^{1/2} \frac{a_c{}^3 \langle \eta \rangle^2}{1 + q^2 a_c{}^2} \tag{3.2}$$

Both of these equations apply only as limited behavior as q becomes large. As such, it would be interesting to use a generalized analysis method to examine other size scales. Glatter uses a generalized form of Porod's Law, which gives the distance probability function for particles and provides a technique to smooth, desmear, and Fourier transform scattering data to obtain a size scale for scatterers.[29, 30] This technique may be applied throughout the q range, allowing us to use non-terminal high q scattering data.

In this chapter, we use model PDMS networks as discussed in Chapter II, swell them with photopolymerizable endcapped PDMS macromer, and photocure the macromer. We then examine the extent of modulus change with cure for a homologous molecular weight series of macromers and for different network structures. Turbidity and static light scattering are used to elucidate the size scale of phase separation and to potentially determine the thermodynamic decomposition of an initially miscible network-macromer blend.

3.2. Experimental Section

3.2.1. Synthesis of photopolymerizable macromer

Macromer is synthesized using a one pot acid catalyzed ring opening polymerization (figure 3.1). Octamethylcyclotetrasiloxane (D_4) and 1,3-bis(3-methacryloxypropyl) tetramethyldisiloxane (MPS), and phenylmethylcyclotrisiloxane (D_3^{Ph}) from Gelest Chemicals

and trifluoromethanesulfonic acid (triflic acid) from Sigma-Aldrich were used as received. D_4 and MPS were mixed under argon for 1 hour before addition of triflic acid. The reaction was allowed to continue for 24 hours and was quenched using a saturated sodium bicarbonate solution. Solvent was evaporated under vacuum and the reaction product was filtered to 0.2 μm. Macromer was further purified under 200 mtorr vacuum at 70 °C for 72 hours to remove short chain and cyclic impurities. The D_4 to MPS ratio was altered to obtain product molecular weights from M_n=500 to M_n=5000 g/mol.

Macromers with a combination of phenylmethylsiloxane and dimethylsiloxane backbone units were also synthesized. The synthesis procedure remains identical to macromer with pure methylsiloxane backbone; the appropriate fraction of D_3^{Ph} is substituted for D_4 as a reactant to obtain desired phenyl substitution.

3.2.2. Characterization of macromer synthesis product

Synthesis product is characterized using ^{1}H NMR, GPC, and refractive index measurements. ^{1}H NMR spectra were used to obtain the number average molecular weight, M_n, from the ratio of diene hydrogens in the bismethacrylate endcaps to methyl hydrogens from the backbone pendant groups. Phenyl incorporation into the macromer synthesis product was determined by evaluating rations between diene endcap hydrogens, methyl backbone hydrogens, and phenyl backbone hydrogens. Although a previous study found relatively poor incorporation of phenyl from cyclic PMPS for slightly different reaction conditions,[31] we find that over 95% of total phenyl content is presented in the final synthesized and purified product.

Gel permeation chromatography/light scattering (GPC-LS) was used to determine absolute macromer molecular weights. A Wyatt Dawn EOS 18 angle system was used for light scattering measurements where toluene was used for a solvent. Refractive indices of the

macromer and network precursors are measured with an Abbe refractometer at a wavelength of 590nm and 25 °C.

3.2.3. Preparation of photopolymerizable macromer doped network

Model PDMS networks are synthesized per the procedure in Chapter II. Multiple molecular weight precursors are used (15200, 22300, 41200). Precursor α–ω vinyl chains are catalytically crosslinked at 35 °C with tetrakis(dimethylsiloxy)silane at the ratio of crosslinker silane functionality to vinyl endgroup functionality, *R*, that was shown to give the highest modulus. The catalyst used was cis-dichlorobis(diethylsulfide)platinum(II). Networks were also prepared in the diluted state at polymer precursor volume fraction, ϕ_0, from 0 to 0.5 in a short chain linear PDMS theta solvent. Prepared networks were fully extracted to obtain dry networks and modulus was measured with a Rheometrics Scientific RSA III at 1% strain (linear viscoelastic regime) and 1 Hz in oscillatory tension mode.

Macromer as synthesized in section 3.2.1 was mixed with 2,2-dimethoxy-1,2,-diphenylethan-1-one (DMPO), a radical photonitiator with a strong absorbance band in the UV spectrum. The weight ratio of DMPO / macromer is held fixed at 2%. Fully cured, dry networks are swollen with macromer and minimally exposed to radiation sources.

Dry networks readily sorbed 10-30% by total weight of macromer and DMPO at 35 °C when placed on a single surface of a 1 mm thick slab. After short times (<48 hours), no macromer is visible on the surface of the gel for all network matrices and all macromer molecular weights. Samples are allowed to equilibrate for 7 days before being used for further experiments. Sample dimensions are measured before and after swelling to ensure that the sol is evenly

distributed throughout the sample on a macroscopic basis.

3.2.4. Photopolymerization of macromer swollen in PDMS matrix

Macromer swollen in model networks is photocured using irradiation dosage at 365 nm. A 500W Oriel Hg-Xe arc lamp is used as the collimated emission source. An interference filter with maximum transmittance at 365 ± 0.5 nm and 5 nm HWHM is used to select the 365nm emission line. Samples 1mm thick x 8mm diameter are placed on a quartz disc and loaded into a quartz windowed chamber. The chamber is purged with argon for 15 minutes before irradiation to minimize oxygen inhibition during reaction cure. Samples are irradiated for 40 minutes at 4 mW/cm^2 intensity to ensure complete macromer conversion. Irradiation intensity is measured before and after polymerization with a calibrated photodiode.

Complementary polymerization experiments were performed on macromer-swollen PDMS melts. Three different molecular weight (approximately 1, 50, and 500 kg/mol) melts are mixed with 10-30% macromer. For melts of 1 and 50 kg/mol, mixing could be accomplished with mechanical stirring. Macromer was incorporated into the 500 kg/mol melt by iterative “kneading” followed by time for diffusion. This mixed sol is then placed in a 1mm thick x 8mm diameter aluminum mold with quartz windows on both sides of the sample. Macromer-melt samples are polymerized within the mold in the same sample irradiation setup as macromer doped networks. The quartz-windowed cell allows us to perform both light scattering and turbidity measurements on polymerizing samples *in situ*.

3.2.5. Experimental methods to determine extent of cure

Since we were interested in fully cured macromer for the measurements in this chapter, it was necessary to determine the extent of cure. Two *ex situ* methods were used: IR spectroscopy

and extractable weight fraction. A significant acrylate vinyl stretching band is present at 1639 cm^{-1}. Spectra were measured before and after cure. Complete absence of the absorption peak was used as one criterion for complete cure.

To determine extractable weight fraction, polymerized samples were placed in 50x excess of toluene for 48 hours; three fresh cycles of toluene were used during this time period. Toluene was removed by cosolvent extraction with methanol; samples were successively placed in increasing methanol:toluene rations of 50:50, 75:25, and 1:0. After toluene extraction, samples were dried under vacuum for 24 hours and weighed.

3.2.6. Rheological measurements

Ex situ rheological measurements were performed on a Rheometric Scientific RSA III in a simple tension geometry under oscillatory mode. Samples were approximately 1 cm x 3 cm x 1 mm in size. Young's modulus was measured at 25 °C. Since relatively small strains (< 1%) were used for reporting modulus values, changes in cross-sectional area were neglected. Strain and frequency sweeps were run on each sample. Strain sweeps were performed from 0.01-4% to determine the linear viscoelastic regime. For all samples used, 1% strain rate was within this regime. Frequency sweeps were run from 0.01-100 Hz. In all cases, samples exhibit a nearly flat (< 1% deviation) plateau modulus across this frequency domain. In this chapter, data reported as G' (shear modulus) has been converted from Young's modulus data using the relationship $E=3G$, which is appropriate for these networks (Poisson ratio of 1/2).

3.2.7. Turbidity measurements

Turbidity measurements, both during and after cure, give an indication as to the extent of heterogeneities both inherent to network crosslinking and those that develop from macromer

photopolymerization. A 15mW 500:1 vertically polarized HeNe laser with 1mm beam waist is aimed perpendicular to the face of a sample as shown in figure 3.2. A calibrated 5 mm diameter photodiode detector was placed at a distance of 250 mm from the sample. Turbidity was measured in situ during cure for samples with macromer content from 10 to 30%, macromer length from 500 to 5000 g/mol, phenyl content of 0 and 5%, and network Young's modulus from 340kPa to 840kPa.

3.2.8. Static light scattering

Angular distribution of scattered light was measured for cured and uncured samples between an angular scattering vector, q, of 2.8×10^{-2} to 5×10^{-5} nm^{-1} using two methods. Large size scales (80nm-20 μm) are examined using a modification of the turbidity apparatus (figure 3.2). A 15 mW vertically polarized HeNe laser is directed through a 1 mm thick sample. A translucent viewing screen is placed behind the sample, and a CCD camera is used to image the viewing screen. The camera, a Photometrics Sensys 400 series, has extremely low dark current, negligible pixel bleed, and 16 bit linear well depth. For 30 second dark exposures, azimuthal integration of the radial region we examine reveals a net zero average intensity for each q. Measurements taken at multiple points on a single sample show similar scattering patterns. This indicates that the large size of the sampling beam provides an effective ensemble average of scattering particles and that the sample is macroscopically homogeneous.

Preliminary static light scattering measurements have also been performed on a slightly smaller size scale; a Wyatt Dawn EOS multi-angle light scattering (MALS) apparatus was used to measure angular intensity from 11 different detectors at angles of 32 to 117 degrees. Corresponding q vectors are 8×10^{-3} to 2.5×10^{-2} nm^{-1}, where $q=(4\pi n/\lambda)\sin(\theta/2)$, θ is the scattering angle, λ is the wavelength of incident light, and n is the refractive index of the medium. The

scattering light source is a 30 mW gallium arsenide laser emitting at 690 nm. Samples were swollen in 0.02 μm filtered toluene and scattering measurements were performed in scintillation vials. Because of heterogeneities in the vials, scattering measurements were taken 6 times from each sample with small angular sample rotations between acquisition. Measurements were then averaged to obtain a final result.

3.3. Results and Discussion

3.3.1. Physical property characterization of macromers

The six macromers used in this study (table 3.1) span a decade in molar mass at fixed composition (dimethylsiloxane) and up to 10% methyl substituents replaced by phenyl at a fixed macromer length (1000 g/mol only). The refractive index measured at 25 °C (n^{25}) of all macromers is greater than that of PDMS. For pure dimethylsiloxane macromers, this increase is due to the higher refractive index of methacrylate endgroups. Incorporation of phenyl groups further increases n^{25}.[31] Based on the catalytic ring opening polymerization used for macromer synthesis, we expect a Gaussian distribution of molecular weights. After purification, GPC-LS analysis shows that polydispersity (PDI) values range from 1.42 for 1000 g/mol methacrylate endcapped PDMS to 1.65 for 5000 g/mol materials. For radii of gyration (R_g) less than 5nm, we expect isotropic scattering for a wavelength of 591nm. Because 500 g/mol and 1000 g/mol macromers in toluene have Rg less than 10 nm, it is important to corroborate these molecular weight values via another method. ^{1}H NMR measurements are used in both this capacity and to determine the amount of phenyl incorporation into random polymethyl phenylsiloxane (PMPS) backboned macromer. Molecular weights measured both by GPC-LS and NMR are similar; this indicates that light scattering should be an appropriate method for determination of PDI.

3.3.2. Extent of cure for photopolymerized macromer

After forming model networks and synthesizing methacrylate endcapped macromer, we dope the network with a small (10%-30% wt/wt) amount of macromer. The system is allowed to equilibrate and is then irradiated with UV light to photopolymerize the macromer. Prior to polymerization, macromer exhibits a strong absorbance peak at 1639 cm^{-1}. After polymerization, no peak is present. However, more quantitative measurements for both partial and complete photopolymerization are performed by measuring mass of extractables as discussed in the experimental section. For all macromers, the weight percent of extractables is less than 2%. Although most reaction byproducts have been removed during the purification process, it is likely that some cyclics or non-functionalized siloxanes remain in the final macromer product. However, this relatively small amount of non-reacting material does not significantly change any results.

3.3.3. Modulus changes interpenetrating photopolymerized networks

As we noted, no macromer was extractable after this polymerization; however, it was uncertain as to whether this was due to a percolated macromer network or to non-interconnected nodules of cured macromer that were intercalated with host network. If the host network plays a significant role in preventing macromer network dissolution, then photopolymerization of macromer diluted in a host melt should elucidate whether macromer forms a percolated network or isolated nodules. Macromer, at 30% by weight, was mixed with three different viscosities of pure PDMS fluid: 50 cS, 50,000 cS, and a high molecular weight melt with G' G'' crossover at approximately 20 kPa. The low viscosity fluid is significantly below the entanglement molecular weight of PDMS whereas the other two samples are well entangled melts. For all three melts,

extraction of the melt from the photopolymerized macromer leaves a percolated gel. As in photopolymerized macromer doped host networks, less than 2% of the macromer is extracted. Thus, photopolymerized macromer in a host network forms a bicontinuous network. Although a continuous macromer network forms when photopolymerized, its structure could range from nodules with minimal interconnection or a highly connected homogeneous network. We therefore measure the modulus of a 50 cS melt with 30% 1000 g/mol photocured macromer; the modulus is approximately 1 kPa. If all the macromer were elastically effective, the estimated modulus is approximately 1 Mpa based on:

$$G = \nu RT \tag{3.3}$$

where G is the shear modulus, ν is the number of moles of elastic chains per unit volume, T is absolute temperature, and R is the gas constant. The factor of 1000 difference between $G'_{observed}$ and that expected for 100% elastically effective chains suggests that small polymerized macromer nodules form that are only minimally connected.

Since photocured macromer forms a gel even at 10% loading, if it is bicontinuous with a host network we expect to see an enhancement of elastic modulus. First, we are interested in elucidating the effect of the host PDMS network on the final modulus of the bicontinuous materials. The initial network modulus of the dry matrix, E'_{dry}, is dictated by the molecular weight of network precursors, M_h, and polymer volume fraction at preparation, ϕ_0. When the dry matrix is swollen with unreacted macromer modulus decreases. After the macromer is polymerized, the modulus increases to a value that exceeds E'_{dry}. In figure 3.3, a normalized modulus of photocured materials is plotted against weight percent macromer for different precursor networks. The normalized modulus is the modulus of photopolymerized material divided by the modulus of an unswollen model host, or dry, network. For all values of M_h, networks prepared with ϕ_0 of 1, 0.85, 0.7, and 0.5 were swollen with 1000 g/mol macromer and photopolymerized. All three plots show

that preparation dilution of the host network does not change the effective modulus increase of intercalated networks; data from each value of ϕ_0 are overlapping. Since modulus increase is independent of ϕ_0 we collapse these values for each M_h and plot normalized modulus against weight percent of macromer. Figure 3.4 shows that data from all three M_h values used overlaps. This combination of data overlap from different M_h and ϕ_0 values indicates that, similar to swelling behavior as will be seen in Chapter 4, the effects of entanglements and chemical crosslinks are equivalent.

Macromer molecular weight, M_d, also had a significant effect on the extent of network stiffening. Figure 3.5 shows normalized modulus plotted against macromer loading for four different values of M_d. For M_d = 500 g/mol, at 10% macromer loading the photopolymerized systems have a modulus increase of 1.15; at 30% loading, the modulus increase is approximately 2.2. For 5000 g/mol macromer, modulus increase at 30% loading was only a factor of 1.3. Intermediate molecular weights show intermediate absolute change in modulus. For all M_d, not only is there a monotonic increase in modulus change with percent macromer doping, but the slope of normalized modulus against weight percent macromer also increases. This increasing slope can be explained by the increasing density of macromers in the polymerizing system. A simple calculation using monomer size estimates for pure PDMS shows an overlap concentration of approximately 3%.[32, 33] At 10% macromer loading, we are then merely 3x the overlap concentration; during photopolymerization, the number of polymer chains within the pervaded volume of a single chain is relatively small. Since the macromers are end-capped at both sides of the molecule and have relatively flexible siloxane midblocks, they have the potential to form small intramolecular loops; ring strain in siloxane cyclics is relatively insignificant after 5 monomer repeat units. Assuming all methacrylate endgroups have identical reactivity and the reaction is diffusion limited, the chances of forming an intramolecular loop vs. an intermolecular

association is purely related to diffusivities. For intramolecular loops, Kuhn monomer diffusion is the limiting rate; for intermolecular associations, the limiting rate depends on solution concentration. For high concentrations (such as in the melt), Kuhn monomer diffusion is the limiting step for intermolecular reactions. For lower concentrations, such as we see at 10% macromer loading, macromer center of mass diffusion will be the rate limiting step. Making the simple assumption that macromer is a linear PDMS chain and does not contain methacrylate endgroups, we expect approximately 3 Kuhn monomers;[33] this indicates that, for Rouse-like diffusion, intramolecular reactions should occur at least three times higher than intermolecular reactions in non-concentrated systems. As the solution becomes more and more dilute, intramolecular loops are more likely; conversely, as the system becomes more concentrated, intermolecular reactions become more likely. In the limit of the melt, intra- and inter-molecular reactions will have a similar probability. Thus, as we increase macromer concentration, we should see relatively more intermolecular reactions and an increasing change in modulus with weight percent photopolymerized macromer.

Comparison of experimental data to two theories for modulus of interpenetrating networks also promote this interpretation of concentration dependence. The two theories that we will consider interpret interpenetrating networks either as a disperse phase or as bicontinuous networks. If we consider spherical particles randomly distributed throughout a disperse phase, one can obtain:[4]

$$E = E_1\left[\frac{\phi_1}{15(1-\sigma_1)} + \frac{\phi_2 E_2}{(7-5\sigma_1)E_1 + (8-10\sigma_1)E_2}\right] \tag{3.4}$$

where E, E_1, and E_2 are the modulus of the interpenetrated network, host phase, and dispersed phase; ϕ_1 and ϕ_2 are the volume fraction of host and dispersed phases; and σ_1 is Poisson's ratio for

the host phase. If the dispersed phase has a considerably higher modulus than the host phase, this equations simplifies to:

$$E = E_1\left[1+\frac{15(1-\sigma_1)\phi_2}{2(4-5\sigma_1)\phi_1}\right] \tag{3.5}$$

Figure 3.6A shows a comparison of the simplified version of the dispersed phase equation for 500 g/mol macromer in the complete array of model networks. Although modulus was not measured for pure photopolymerized macromer, polymerized 500 g/mol material forms an extremely brittle polymer. Thus, qualitatively, we suggest that cured macromer may have a high enough modulus for the assumption to be appropriate. Looking at data for low macromer weight percent, we see that this theory overpredicts modulus increase, although not significantly. This would indicate that the assumption of extremely high photopolymerized macromer modulus is not completely appropriate. However, the trend for theory matches well for low macromer weight percent and indicates that we very possibly have a macromer dispersed phase in this region. As we increase macromer weight percent to 30%, experimental data begins to significantly deviate from theory. There are two possibilities for this deviation: the networks are becoming bicontinuous as opposed to one phase dispersed in another; or the intermolecular macromer polymerization is becoming more prevalent as discussed previously. If intermolecular reactions increase, fewer loops and more elastically effective chains and network junctions are created. This increase in elastically effective chains will then increase material modulus.

If the IPNs are bicontinuous, increased modulus should be explained by theory for bicontinuous networks as proposed by Davies.[5, 6]

$$E^{1/5} = \phi_1 E_1^{1/5} + \phi_2 E_2^{1/5} \tag{3.6}$$

The basic premise for this expression is that the interpenetrated network is a composite of two

materials with moduli of $E + \Delta E$ and $E - \Delta E$. Figure 3.6B shows a comparison of this expression for bicontinuous networks compared with the same experimental data presented in figure 3.6A. Interestingly, due to the construction of the expression in Equation 3.6, the change in modulus is highly dependent on the host network modulus. Theoretical predictions for four different host moduli are also plotted in this figure. It is immediately obvious that experimental data do not exhibit a trend in modulus change that is in any way dependent on host modulus. Also, experimental results for high macromer weight percents are equally as underpredicted for bicontinuous network theory as they were for dispersed network theory. This leads us to the conclusion that intramolecular associations dominate in macromer photopolymerization at low concentration and intermolecular associations become more prominent for higher concentration systems. Although these plots only show behavior for 500 g/mol macromer molecular weight, other molecular weights show similar trends as compared to theory. However, for larger macromer molecular weights, the simplified version of disperse IPN theory greatly overpredicts modulus changes. This overprediction occurs because higher molecular weight photopolymerized macromer has a lower modulus than for short chain materials. However, equation 3.5 assumes that the disperse phase is infinitely stiff.

As will be discussed later in this chapter, some amount of microphase separation occurs during the photopolymerization of macromer doped networks. Although different macromer molecular weights have different interaction parameters with pure PDMS networks (due to the relative effect of endgroup vs. midblock length), they also change other parameters important to modulus determination such as midblock length. Adding phenyl content to the macromer allows us to retain similar midblock length while significantly changing thermodynamic interaction parameters. As is discussed in Chapter IV, PMPS macromer containing either 5% or 10% phenyl is significantly less miscible in pure PDMS than the PDMS macromer analogue. If different

amounts of phase separation occur for PMPS and PDMS macromer (i.e., PMPS remains in a disperse phase at the same concentration where PDMS is in a bicontinuous phase), we would expect different mechanical properties on cure. When systems containing from 10% to 30% PMPS macromer (10%-25% for PMPS macromer containing 10% phenyl due to miscibility concerns) are cured, modulus does not change as compared to using PDMS macromers. This indicates that microstructure is similar even for macromer phases with significantly different chemical properties.

3.3.4. Turbidity measurements

When polymerizing macromer doped networks, many systems exhibit significant decreases in optical clarity. The obvious reason for systems becoming translucent is microphase separation of macromer from the host network during photopolymerization. Since the two phases have different refractive indices, we see significant scattering. We measure turbidity to help elucidate the structure changes during photopolymerization. It is important to note that, in many regards, turbidity only provides qualitative information; no information is garnered regarding size scales of scatterers. Table 2 provides selected *ex situ* turbidity data; for reference, the last data point is for host networks that do not contain photopolymerized macromer. Looking at networks swollen in 10% to 30% 1000 g/mol macromer and then cured, we see that turbidity increases with increasing weight percent. For phase separated systems, the number of scatterers will increase with increasing macromer content. We also see that, for 1000 g/mol macromer at 0 and 5 weight percent phenyl, that turbidity increases radically with phenyl content. Since scattering intensity is proportional to the square of the refractive index difference between scattering centers and surrounding medium and Δn of PMPS macromer and pure PDMS is greater than Δn of PDMS macromer and pure PDMS, we expect increased turbidity.

If microstructure were consistent regardless of molecular weight, we would expect turbidity to increase with increasing refractive index by the same argument as that given for scattering in PMPS macromer. Although we see this trend from M_d = 5000 g/mol to M_d = 1000 g/mol, turbidity decreases between M_d = 1000 g/mol to M_d = 500 g/mol. This indicates that there is another process that is important in determining microscale phase separation. In sequential IPNs for both spinodal decomposition and nucleated growth, the relative rate of reaction kinetics to diffusion is important to determine the final material topology. As will be seen in Chapter 5 (diffusion) and Chapter 6 (reaction kinetics), there are significant differences in these values for differing macromer molecular weight.

Qualitative visual measurements of backscattering (relative opaqueness) also indicate that turbidity does not tell a complete story for length scale of microphase separation. Turbidity is equivalent when a specific macromer molecular weight is polymerized in different host network moduli. However, visual inspection shows that increased back-scattering occurs for lower modulus networks. Since the host and macromer refractive indices are the same for this series of experiments, extent of density fluctuations should play a minimal role in this increased scattering. As host network crosslink density decreases, larger microphase separated domains will form and increase backscattering.

3.3.5. Static light scattering measurements

Static light scattering is used to help provide insight into the structure and length scale of microphase separated interpenetrating networks. Using two different light scattering setups, we are able to probe length scales from 20 μm down to 40 nm. Figure 3.7 shows a log-linear plot of arbitrary scattering intensity against q^{-1} for an unswollen model network and a network swollen, but not cured with, 30% 1000 g/mol macromer. For the q values examined, there is a monotonic

decrease in scattering intensity in both systems; minimal deviations are seen between data sets. This concurrence of data, along with high sample transparency, also indicates that there is no decomposition into phase separated systems before macromer photopolymerization. For spinodal decomposition, a scattering maximum will occur at some non-zero *q* value.[34] Figure 3.8 compares the scattering intensities of a host network swollen but uncured with 30% macromer against the same system after photopolymerization. Although there is a systematic increase in scattering intensity at all scattering angles, an intensity maximum is not seen throughout the *q* range examined. Looking at the propagation of phase separation in IPNs, we expect nucleated growth to initially occur followed by spinodal decomposition. The PDMS networks that we use are relatively tightly crosslinked; this combined with relatively slow macromer diffusivity and the capability to quickly form gelled systems indicates that it is very unlikely that a true equilibrium spinodal decomposition will occur. Contrarily, nucleated growth and SD will occur to some degree, but initial heterogeneities in phase separation will be locked in with macromer gellation.

In figure 3.9, we plot high *q* scattering data for a model network swollen in macromer using the Ornstein-Zernicke formulation. The non-linear data indicates that, down to 100 nm size scales, we do not see a single size scale for network heterogeneities. Additional data obtained using a Wyatt Dawn EOS allows us to examine size scales down to 40 nm; no linear behavior is seen even at these values of *q*. Soni and Stein used static light scattering measurements to determine the size of large-scale heterogeneities as compared to network equilibrium swelling values in toluene.[20] They found an effect that was moderately invariant of *Q* (total mass of toluene and polymer at equilibrium swelling divided by polymer mass); oddly, results show increasing heterogeneity size scales with decreasing equilibrium swelling. Correlation lengths for $Q = 6.2$ are around 320 nm, whereas for $Q = 3$ and $Q = 2$, they are 364 nm and 380 nm. Since we examine materials that have *Q* values in toluene from 6.2 to 3.5, we would expect to see

scattering data in the linear regime for our range of q values. More recent work with neutron scattering indicates that these heterogeneities may be on a much smaller size scale.[24, 25] Using Q values between 22 and 3.1 in toluene, correlation lengths were shown to be between 175 nm and 6.4 nm with decreasing length scales for decreasing equilibrium swelling. In particular, the correlation length at $Q = 7.7$ is only 21.8 nm. This data suggests that light scattering may not be an effective method for probing network heterogeneities and explains why a linear scattering regime was not observed when our data was plotted in the Ornstein-Zernicke formulation. Data for swollen networks was also plotted using the Debye-Bueche formulation for completeness; again, no linear regime was seen.

If there are distinct boundaries between phase separated regions of polymerized macromer and host network, we would expect high q behavior plotted with the Debye-Bueche formulation to be linear. Figure 3.9 shows $I^{-1/2}$ plotted against q^2 for a high modulus macromer; surprisingly, we do not see linear behavior even at 100 nm size scales. Extended scattering data (data not shown) increases this range down to 40 nm. In light of the relatively large (μm) size scale of dispersed phase in other PDMS IPNs,[7-10] this result is rather surprising. If the phases showed gradient boundaries, a plot of I^{-1} against q^2 should be linear (Ornstein-Zernicke). However, q independent behavior was also seen in this case. Since only high q data are used for analysis with the Debye-Bueche equation this technique can potentially miss larger size scale inhomogeneities. We therefore use a combination smoothing and Fourier transform approach pioneered by Glatter.[29, 30] No distinct size scale appropriately fit scattering data for polymerized IPNs. These combined scattering data suggest the following explanation for microscale phase separation. Initially, the sol macromer phase is quite miscible in the host network. As the macromer begins to photopolymerize, nucleated phase growth begins. However, due to network constraints and fast gelling of the cured macromer (because of two reactive endgroups), the

system is never allowed to thermodynamically equilibrate. This leads to very small (nm scale) and polydisperse inclusions or nodules of interconnected polymerized macromer within a host network. Similar non-linear results are found for all network moduli, indicating that complete spinodal decomposition is not present for any of our systems due to either network constraints or photopolymerization kinetics.

Although we are unable to establish specific size scales with light scattering data, there are some qualitative trends that are interesting to examine. Figure 3.11 shows a plot of scattering intensity against q for different percent cure in photopolymerized IPNs. Cure was determined by stopping the reaction and extracting the soluble fraction of non-polymerized macromer. At 0% cure, we see that there is minimal scattering; as percent cure increases, so does absolute scattering for all scattering vectors. Even at high percent conversion, we still see significant increases in scattering intensity. This suggests that significant amounts of monomer are still free to diffuse through the system to alter phase separated nodules even at high levels of methacrylate conversion. This trend can be attributed to large amount of intramolecular chemical crosslinks as discussed earlier. Figure 3.11 shows scattering intensity plotted against scattering vector for IPNs with different weight percent of macromer. Similar to results obtained from turbidity measurements, we see a monotonic increase in scattering intensity for all q values with increasing percent cured macromer.

3.4. Conclusions

We have formed interpenetrating networks (IPNs) from well-defined constituents and measured mechanical properties and microphase structure of the materials. Increase in modulus for IPNs as compared to a pure host network were relatively small and were independent of network structure. However, theories for the modulus of bicontinuous and dispersed phases

consistently underpredicted modulus increases for high weight percent of macromer. We also found that mechanical properties were independent of photopolymerization conditions; increased photoinitiator content and irradiation intensity did not alter the material modulus. There are two future lines of work, both with *in situ* rheological measurements, that could provide additional insight into the dynamics of phase separation. Measuring the modulus of macromer swollen networks during photopolymerization in tensile geometry would offer insight into how phase separated structures builds up with conversion. Also, *in situ* modulus measurements during polymerization for macromer-swollen melts would provide information on macromer interconnectivity and gelation.

Contrary to previous work with PDMS IPNs, we did not find μm size scale heterogeneities in our systems with light scattering measurements. This has two potential causes: relatively high miscibility for our PDMS analogue macromers in a PDMS host network; or slow diffusion rates and fast gellation of relatively large macromer molecules with reactive groups on either end of the molecule. However, we do see trends that indicate greater scattering for higher macromer content, larger domain sizing for less highly crosslinked networks, and increased scattering with the extent of photopolymerized conversion of macromer in a host network. Additional work with transmission electron microscopy (TEM) and neutron or x-ray scattering would be extraordinarily beneficial to help elucidate the exact nature of the nanometer scale phase separated inclusions in these IPNs.

3.5. Tables

Table 3.1. Molecular weights, polydispersity, and refractive indices of methacrylate endcapped macromer

Nominal MW	M_n (NMR)	M_n(g/mol) (GPC-MALS)	PDI[a] (GPC-MALS)	n^{25}	% phenyl[b]
500	520	480	1.44	1.438	0
1000	1010	990	1.42	1.423	0
1000	1020	N/A	N/A	1.440	4.8
1000	1000	N/A	N/A	1.454	9.7
3000	2920	2940	1.53	1.410	0
5000	4890	4880	1.65	1.407	0

[a]PDI = Poldispersity Index (Mw/Mn)
[b]percent of backbone sidegroups that contain phenyl instead of methyl moiety

Table 3.2. Selected turbidity measurements for different macromer molecular weights, phenyl content, and doped macromer content

$M_{macromer}$	wt % macromer	% phenyl	% transmittance
500	30	0	70
1000	10	0	65
1000	20	0	45
1000	30	0	4
1000	10	5	< 1
1000	20	5	< 1
1000	30	5	< 1
3000	30	0	60
5000	30	0	85
N/A	0	0	90

3.6. Figures

Synthesis of Silicone Macromers

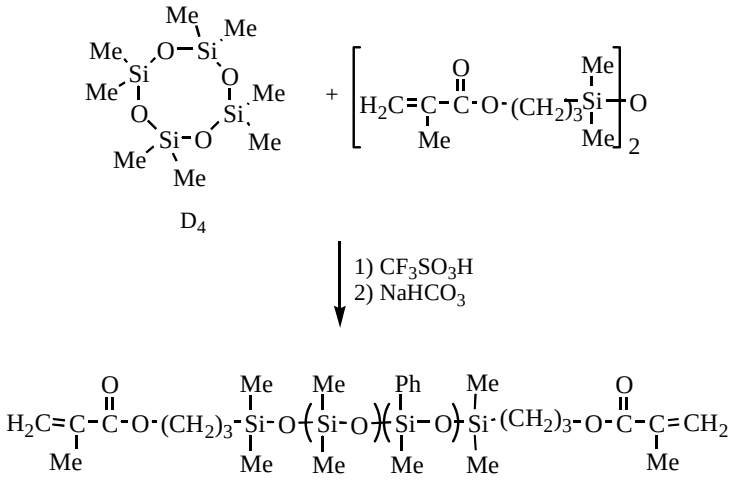

Figure 3.1. Standard reaction scheme to produce controlled molecular weight silicone macromers.

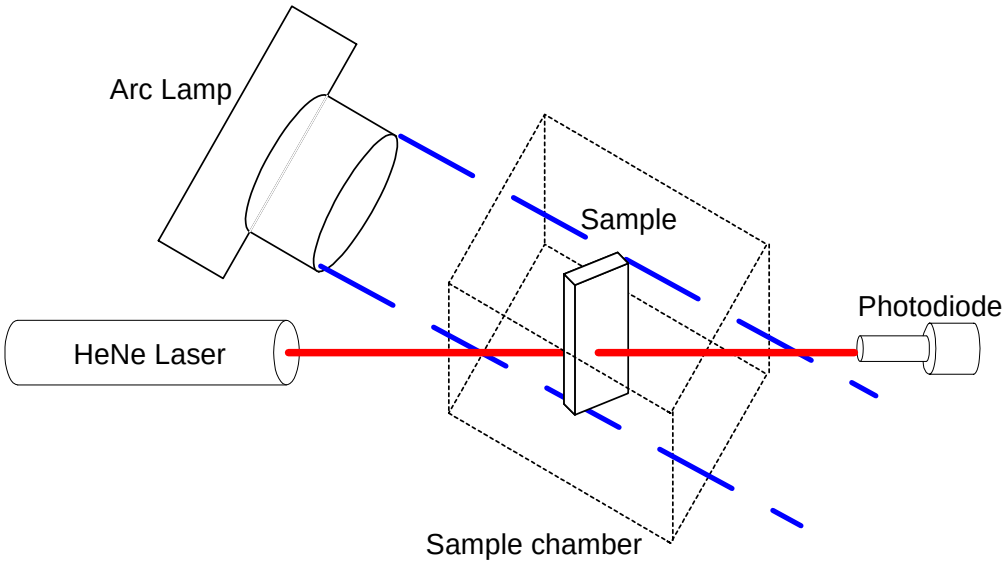

Figure 3.2. Experimental apparatus for polymerization and turbidity measurement. The quartz sample holder is not pictured. The chamber surrounding the samples is purged with argon and the Hg-Xe arc lamp is equipped with a 365 nm interference filter. Irradiation is normal to the large face of the sample. A similar setup (replacing the photodiode with an imaging screen and low-dark current CCD camera) is used to measure 2-d static light scattering patterns.

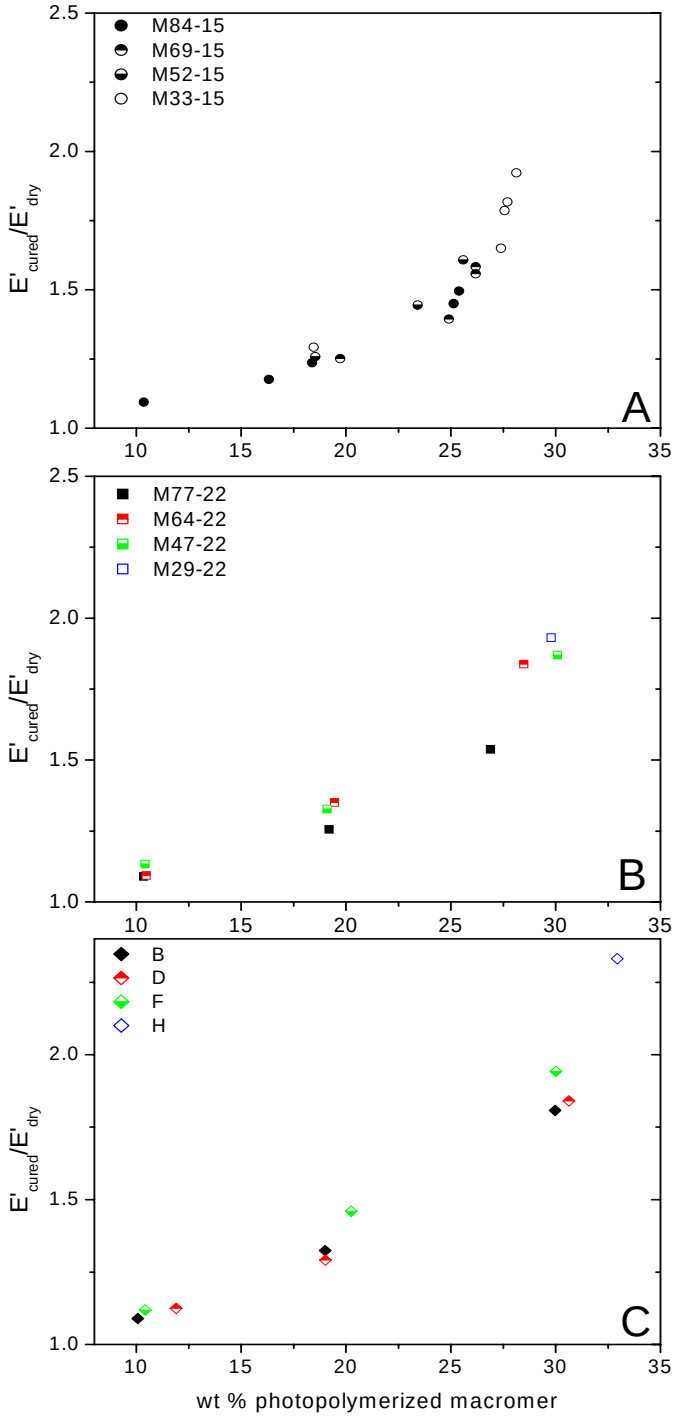

Figure 3.3. Fractional change in modulus on photopolymerization of swollen sol gel systems plotted against weight percent sol. 1000 g/mol macromer is swollen in model networks with different precursor molecular weight and ϕ_0, or polymer volume fraction at preparation.

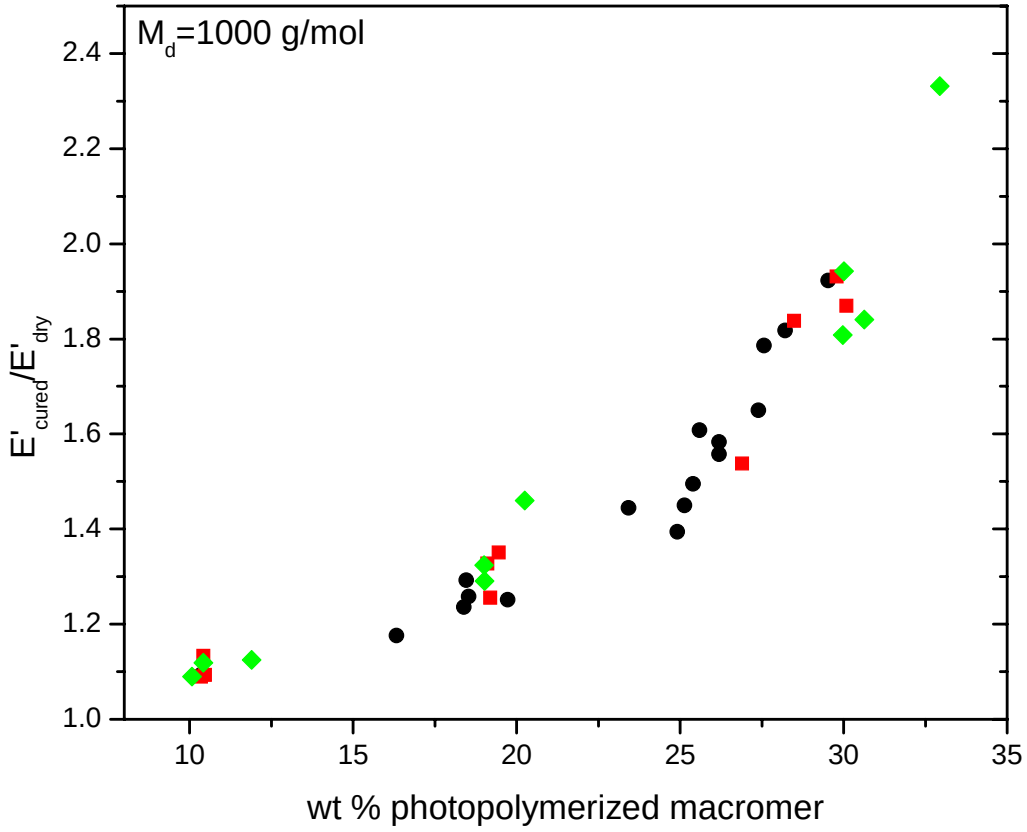

Figure 3.4. Fractional change in modulus after photopolymerization of swollen networks plotted against weight percent cured macromer. 1000 g/mol macromer is swollen in model networks with precursor molecular weight of ● 15200 g/mol, ■ 22300 g/mol, and ◆ 41200 g/mol.

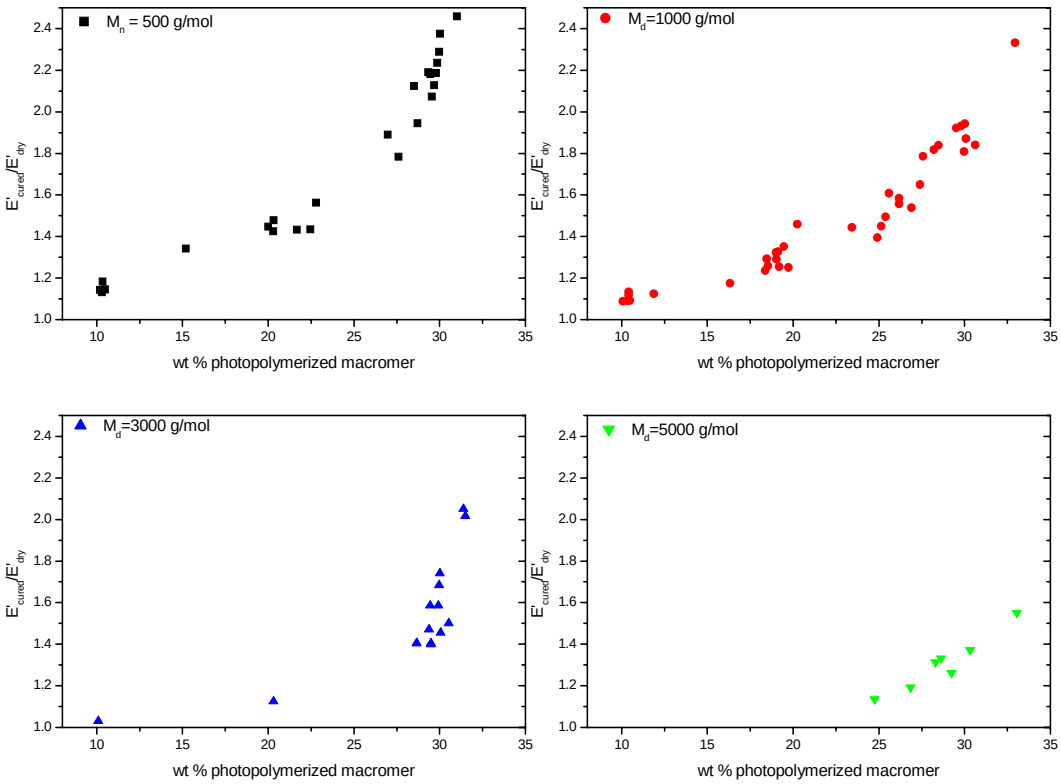

Figure 3.5. Fractional change in modulus on photopolymerization of swollen sol gel systems plotted against weight percent sol. 500 g/mol, 1000 g/mol, 3000 g/mol, and 5000 g/mol macromers are swollen and cured in different model networks.

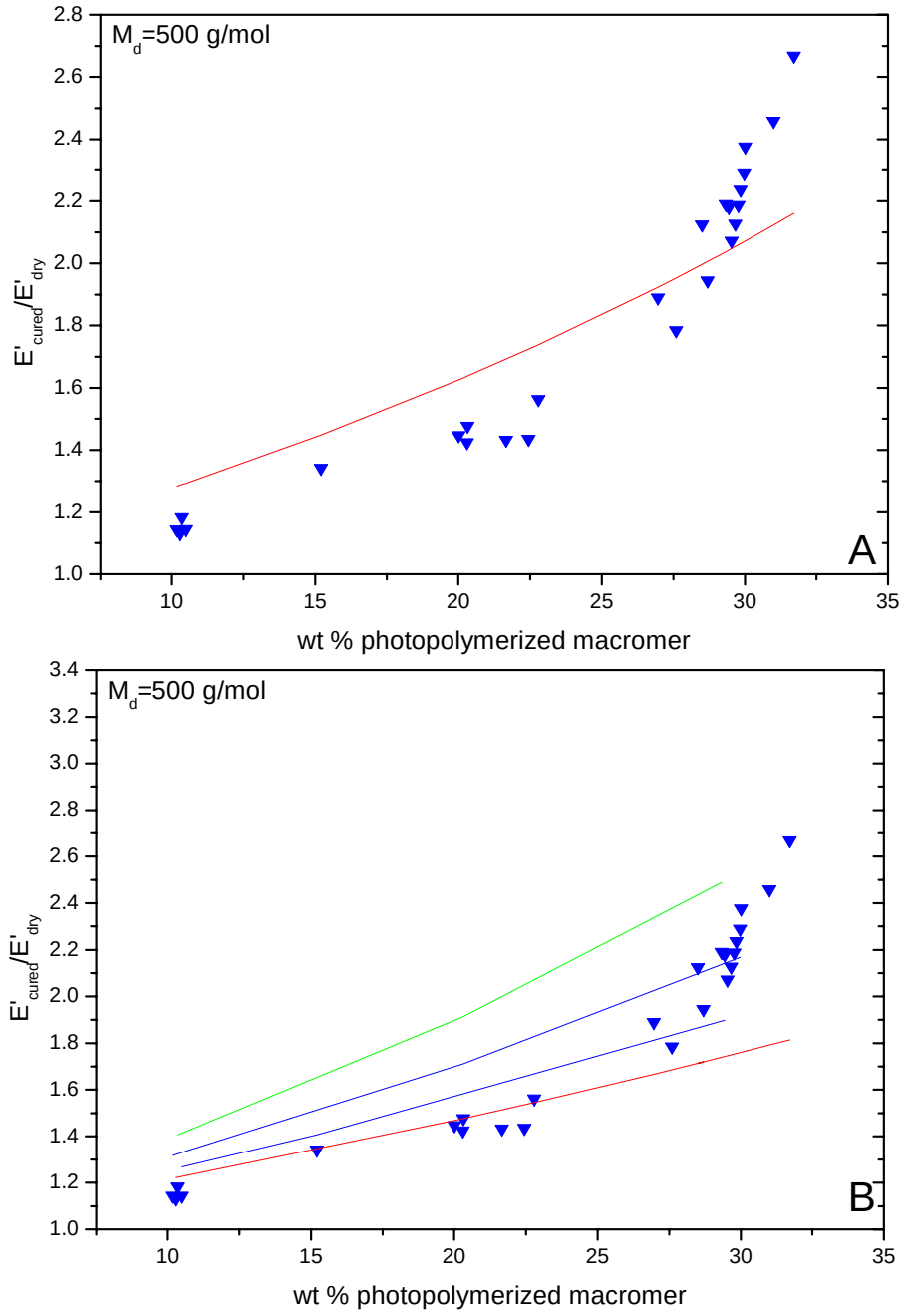

Figure 3.6. Fractional change in modulus on photopolymerization of swollen sol gel systems plotted against weight percent sol for 500 g/mol. The experimental data (▼) is the same as is presented in Figure 5. The line in plot A is a simplified version of the Kerner equation. The lines in Plot B are for the Davies equation. Each line indicates a different E'_{dry}. The lines, from top down, are for a modulus of E'=334 kPa, E'=490 kPa, E'=668 kPa, and E'=840 kPa.

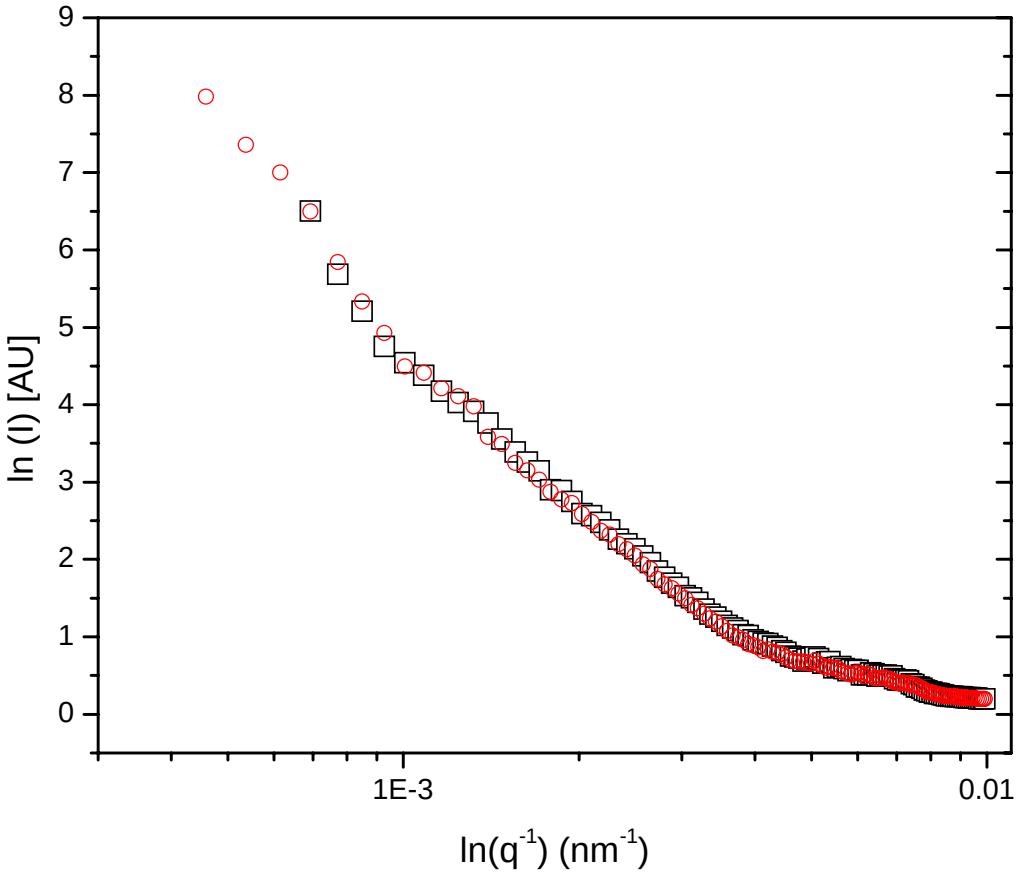

Figure 3.7. Intensity plotted against the inverse scattering vector for unswollen and swollen model networks. The data sets parallel each other throughout the scattering range we use. □ is for 17200 g/mol precursor network prepared at ϕ_0=0, ○ is for the same model network swollen with 30% by weight 1000 g/mol methacrylate endcapped macromer.

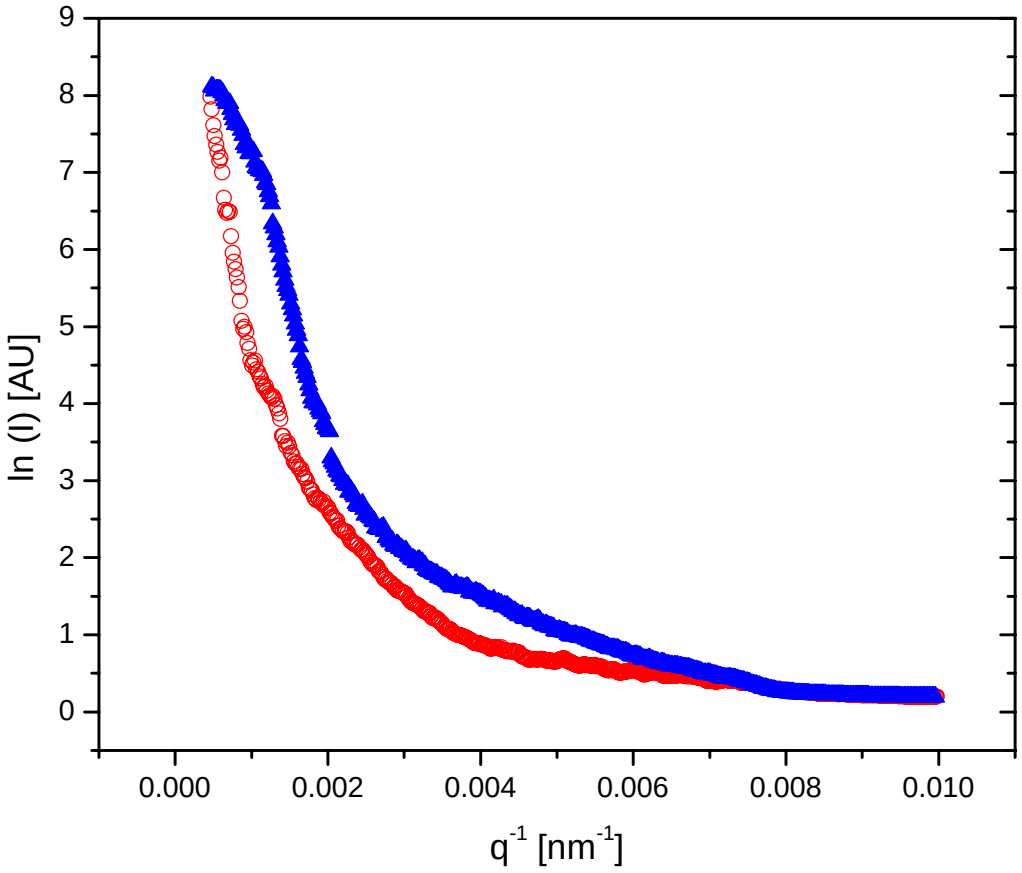

Figure 3.8. Intensity plotted against the inverse scattering vector for swollen model networks in the photopolymerized and non-photopolymerized states. ○ is for 17200 g/mol precursor network prepared at ϕ_0=0 and swollen with 30% by weight 1000 g/mol methacrylate endcapped macromer, ▲ is for the same system that has been fully photopolymerized.

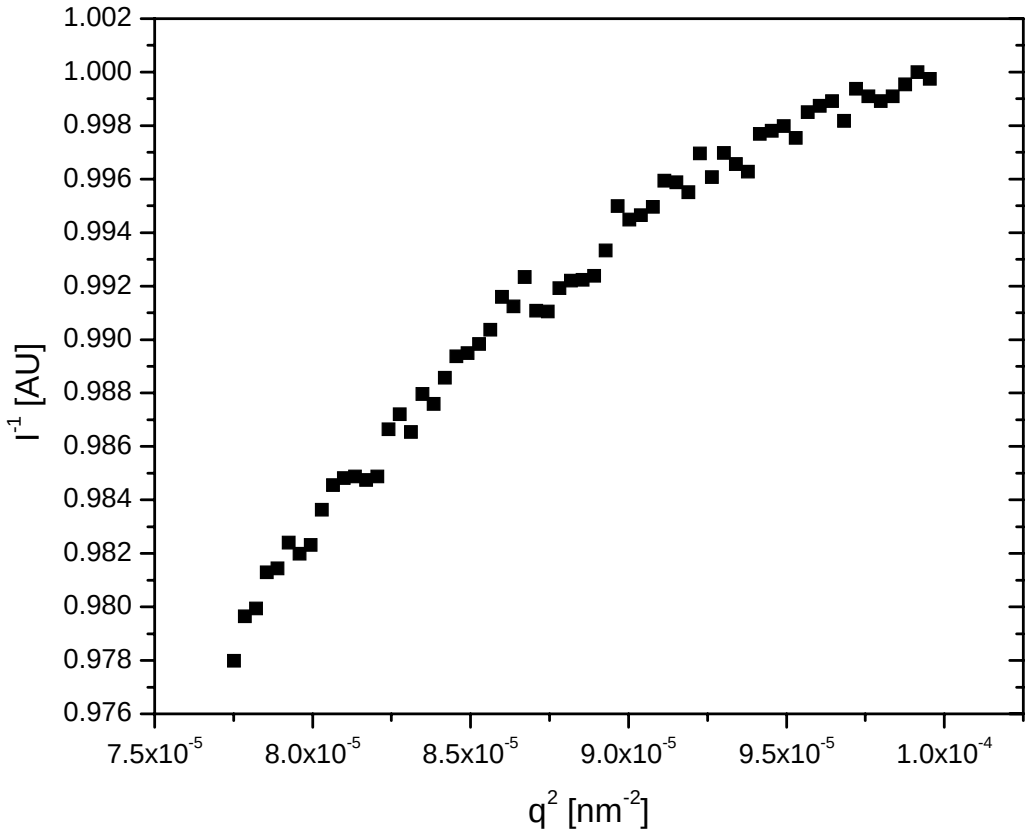

Figure 3.9. Ornstein-Zernicke plot of high q for a model network with modulus of *E'*=840 kPa that is swollen with 30% 1000 g/mol photpolymerized methacrylate endcapped PDMS macromer.

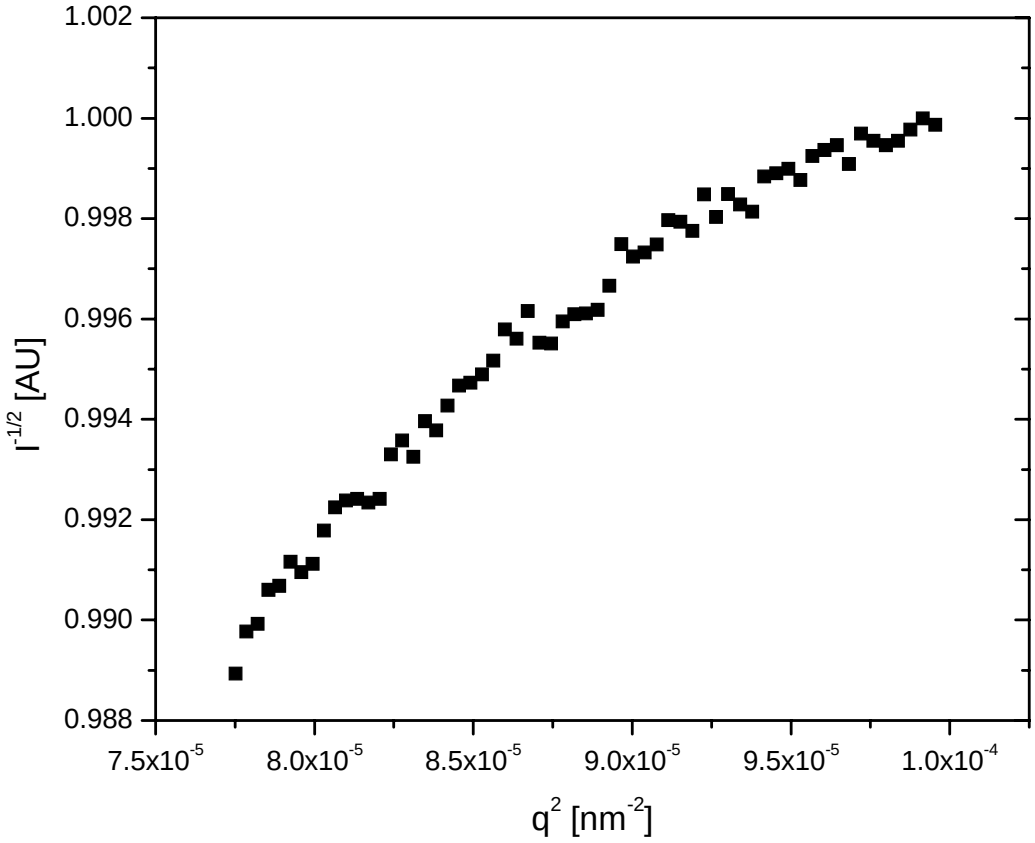

Figure 3.10. Debye-Bueche plot of high q for a model network with modulus of *E'*=840 kPa that is swollen and cured with 30% 1000 g/mol photpolymerized methacrylate endcapped PDMS macromer.

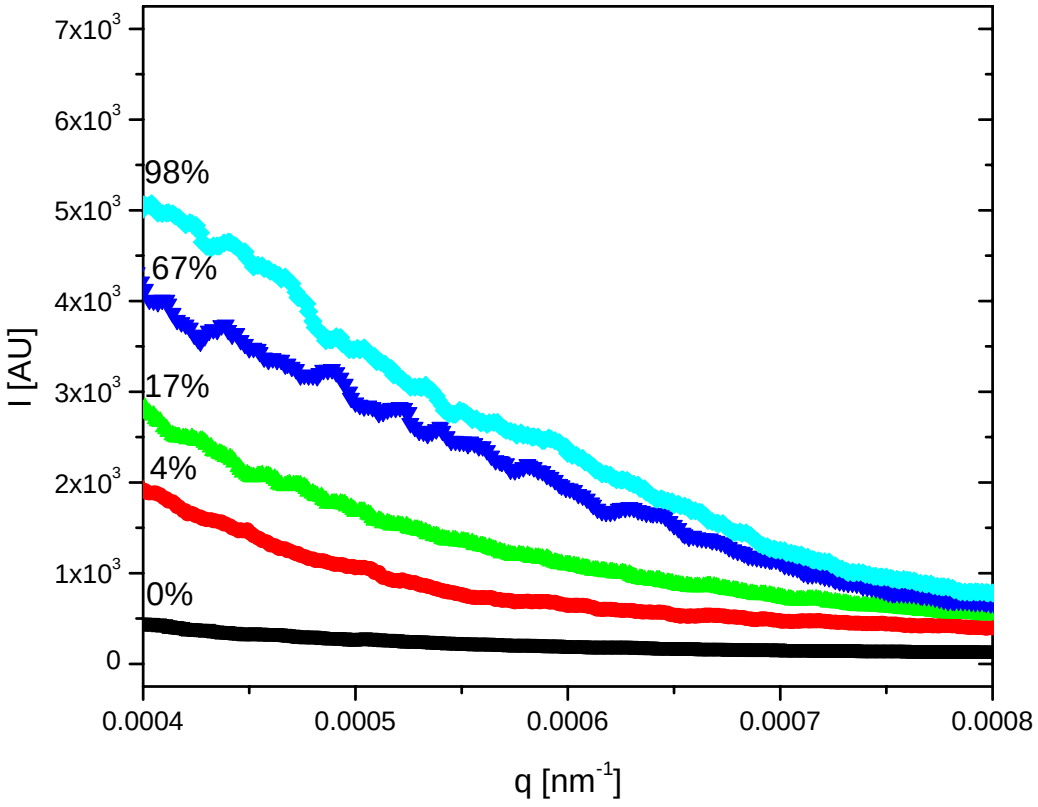

Figure 3.11. Scattering intensity plotted against scattering vector for different levels of cured macromer swollen in a model network. Extent of cure was determined by extracting unpolymerized macromer. 1000 g/mol macromer swollen to 30% by weight in a *E'*=840kPa was used for the experiments in this plot.

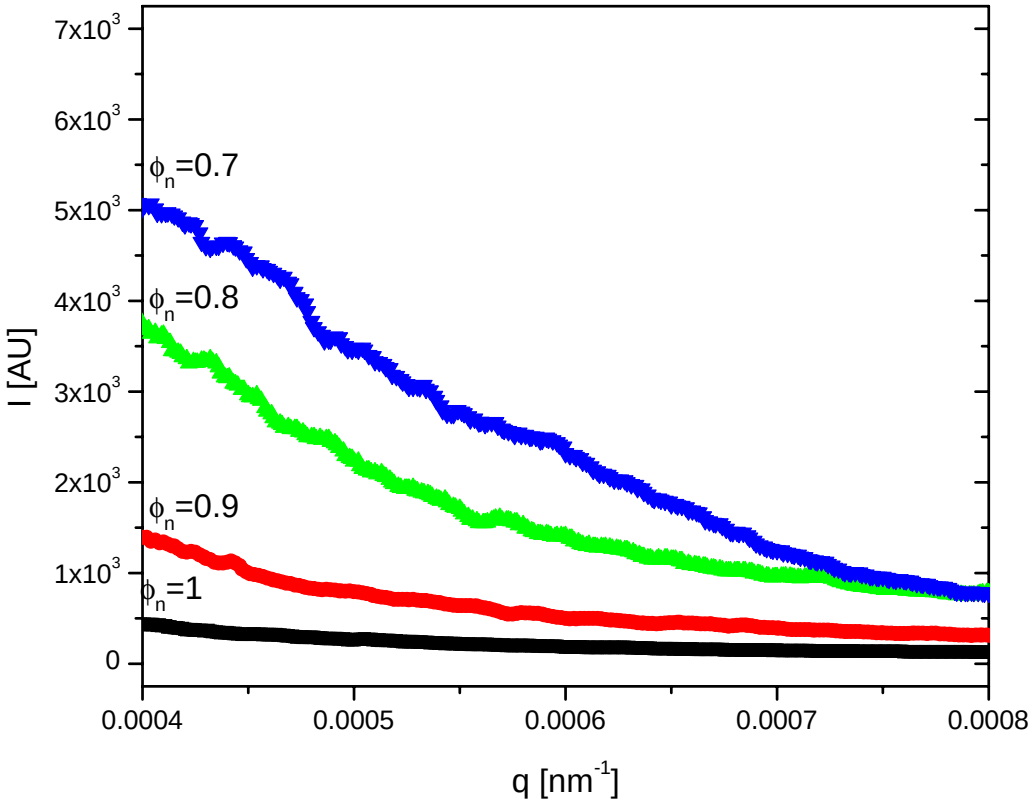

Figure 3.12. Scattering intensity plotted against scattering vector for different weight percent cured macromer swollen in a model network. 1000 g/mol macromer swollen to 10%, 20%, and 30% by total weight in a E'=840kPa network was used for the experiments in this plot. ϕ_n is polymer weight fraction.

3.7. References

1. Klempner, D., L. H. Sperling, and L. A. Utracki, eds. *Interpenetrating Polymer Networks*. Advances in Chemistry Series. Vol. 239. 1994. American Chemical Society: Washington, D.C.
2. Sperling, L. H., C. S. Heck, and J. H. An, Ternary Phase-Diagrams for Interpenetrating Polymer Networks Determined During Polymerization of Monomer-Ii. *ACS Symposium Series,* 1989. **395**: p. 230-244.
3. Lipatov, Y. S., O. P. Grigoryeva, G. P. Kovernik, V. V. Shilov, and L. M. Sergeyeva, Kinetics and Peculiarities of Phase-Separation in the Formation of Semi-Interpenetrating Polymer Networks. *Makromolekulare Chemie-Macromolecular Chemistry and Physics,* 1985. **186**(7): p. 1401-1409.
4. Kerner, E. H., The Elastic and Thermo-Elastic Properties of Composite Media. *Proceedings of the Physical Society of London Section B,* 1956. **69**(8): p. 808-813.
5. Davies, W. E. A., Theory of Elastic Composite Materials. *Journal of Physics D-Applied Physics,* 1971. **4**(9): p. 1325.
6. Davies, W. E. A., Elastic Constants of a 2-Phase Composite Material. *Journal of Physics D-Applied Physics,* 1971. **4**(8): p. 1176.
7. Vancaeyzeele, C., O. Fichet, S. Boileau, and D. Teyssie, Polyisobutene-poly(methylmethacrylate) interpenetrating polymer networks: synthesis and characterization. *Polymer,* 2005. **46**(18): p. 6888-6896.
8. Dong, J., Z. L. Liu, N. F. Han, Q. Wang, and Y. R. Xia, Preparation, morphology, and mechanical properties of elastomers based on alpha,omega-dihydroxy-polydimethylsiloxane/polystyrene blends. *Journal of Applied Polymer Science,* 2004. **92**(6): p. 3542-3548.

9. Turner, J. S. and Y. L. Cheng, Preparation of PDMS-PMAA interpenetrating polymer network membranes using the monomer immersion method. *Macromolecules,* 2000. **33**(10): p. 3714-3718.

10. Turner, J. S. and Y. L. Cheng, Morphology of PDMS-PMAA IPN membranes. *Macromolecules,* 2003. **36**(6): p. 1962-1966.

11. Halpin, J. C., Stiffness and Expansion Estimates for Oriented Short Fiber Composites. *Journal of Composite Materials,* 1969. **3**: p. 732.

12. Nielsen, L. E., Generalized Equation for Elastic Moduli of Composite Materials. *Journal of Applied Physics*, 1970. **41**(11): p. 4626.

13. Lewis, T. B. and L. E. Nielsen, Dynamic Mechanical Properties of Particulate-Filled Composites. *Journal of Applied Polymer Science,* 1970. **14**(6): p. 1449.

14. Shim, S. E. and A. I. Isayev, Rheology and structure of precipitated silica and poly(dimethyl siloxane) system. *Rheologica Acta*, 2004. **43**(2): p. 127-136.

15. Burnside, S. D. and E. P. Giannelis, Nanostructure and properties of polysiloxane-layered silicate nanocomposites. *Journal of Polymer Science Part B-Polymer Physics,* 2000. **38**(12): p. 1595-1604.

16. Osman, M. A., A. Atallah, G. Kahr, and U. W. Suter, Reinforcement of poly(dimethylsiloxane) networks by montmorillonite platelets. *Journal of Applied Polymer Science,* 2002. **83**(10): p. 2175-2183.

17. Takeuchi, H., Reinforcement of Poly(dimethylsiloxane) Elastomers by Chain-End Anchoring to Clay Particles. *Macromolecules,* 1999. **32**: p. 6792-6799.

18. Mark, J. E., C. Y. Jiang, and M. Y. Tang, Simultaneous Curing and Filling of Elastomers. *Macromolecules,* 1984. **17**(12): p. 2613-2616.

19. Gent, A. N., Experimental Study of Molecular Entanglement in Polymer Networks.

Journal of Polymer Science: Part B: Polymer Physics, 1994. **32**: p. 271-279.

20. Soni, V. K. and R. S. Stein, Light-Scattering-Studies of Poly(Dimethylsiloxane) Solutions and Swollen Networks. *Macromolecules,* 1990. **23**(25): p. 5257-5265.
21. Mallam, S., A. M. Hecht, E. Geissler, and P. Pruvost, Structure of Swollen Poly(Dimethyl Siloxane Gels. *Journal of Chemical Physics,* 1989. **91**(10): p. 6447-6454.
22. Mallam, S., F. Horkay, A. M. Hecht, A. R. Rennie, and E. Geissler, Microscopic and Macroscopic Thermodynamic Observations in Swollen Poly(Dimethylsiloxane) Networks. *Macromolecules,* 1991. **24**(2): p. 543-548.
23. Urayama, K., T. Kawamura, Y. Hirata, and S. Kohjiya, SAXS study on poly(dimethylsiloxane) networks with controlled distributions of chain lengths between crosslinks. *Polymer,* 1998. **39**(16): p. 3827-3833.
24. Falcao, A. N., J. S. Pedersen, and K. Mortensen, Structure of Randomly Cross-Linked Poly(Dimethylsiloxane) Networks Produced by Electron-Irradiation. *Macromolecules,* 1993. **26**(20): p. 5350-5364.
25. Falcao, A. N., J. S. Pedersen, K. Mortensen, and F. Boue, Polydimethylsiloxane networks at equilibrium swelling: Extracted and nonextracted networks. *Macromolecules,* 1996. **29**(3): p. 809-818.
26. Debye, P., H. R. Anderson, and H. Brumberger, Scattering by an Inhomogeneous Solid .2. The Correlation Function and Its Application. *Journal of Applied Physics,* 1957. **28**(6): p. 679-683.
27. Debye, P. and A. M. Bueche, Scattering by an Inhomogeneous Solid. *Journal of Applied Physics,* 1949. **20**(6): p. 518-525.
28. Higgins, J. S. and H. C. Benoit, *Polymers and Neutron Scattering*. 1994. Oxford: Clarendon Press.

29. Glatter, O., New Method for Evaluation of Small-Angle Scattering Data. *Journal of Applied Crystallography,* 1977. **10**(OCT1): p. 415-421.

30. Glatter, O., Interpretation of Real-Space Information from Small-Angle Scattering Experiments. *Journal of Applied Crystallography,* 1979. **12**(APR): p. 166-175.

31. Yang, M. H., H. T. Lin, and C. C. Lin, Synthesis and characterization of phenyl modified PDMS/PHMS copolymers. *Journal of the Chinese Chemical Society,* 2003. **50**(1): p. 51-57.

32. Brandrup, J. and E. H. Immergut, eds. *Polymer Handbook, 3rd ed.* 1989. John Wiley and Sons: New York.

33. Colby, R. H. and M. Rubinstein, *Polymer Physics*. 2003. New York: Oxford University Press, Inc.

34. Sperling, L. H., The current status of interpenetrating polymer networks. *Polymers for Advanced Technologies,* 1996. **7**: p. 197-208.

Chapter IV: Thermodynamics of Swelling Behavior for Short-chain PDMS Analogues in Model Crosslinked PDMS Networks

4.1. Introduction

Model elastomer networks have long been studied to elucidate theoretical predictions for rubber elasticity. Swelling behavior of these networks, and particularly equilibrium swelling behavior, is a powerful method to determine network crosslink densities and network strand molecular weights. In the process of synthesizing photopolymerizable sol gel systems, we have run into several issues that previous work in network behavior has not addressed. Although significant work is available on network swelling in good solvents[1-5] and theta solvents[6-11], little work has been performed for poorer solvent qualitites.[12] In addition, we use multiple molecular weights of sol to swell networks, each of which will have different entropic and enthalpic effects on the extent of swelling. We also prepare sols that have identical molecular weight but are of different solvent quality.

There are two methods, both resting on the same theoretical cornerstone, that we will use to examine this thermodynamic behavior. Initially, we will use scaling arguments originating

from the concept that swelling equilibrium can be discussed in terms of free energy equivalencies: an osmotic pressure portion of free energy swells the network and an elastic portion of the free energy restricts swelling.[13] Prior work has established an effective method to determine scaling with affine deformation on swelling.[14, 15] We can write an equation for the free energy due to osmotic pressure of the material using de Gennes blob sizes which store *kT* of osmotic energy.[16]

$$F_{os} \propto kT\left(\frac{b}{\xi}\right)^3 \propto \phi^3 \tag{4.1}$$

Here, *k* is Boltzmann's constant, *T* is absolute temperature, *b* is the Kuhn length and ξ is blob size ($\xi = b\phi^{-3/4}$). It is important to note that we perform this derivation only under the auspices of theta solvent conditions; good solvents elicit significantly different scaling behavior. To determine the elastic effects of free energy, we can use an analogue of Hooke's law for the free energy of elasticity.[14]

$$F_{el} \propto kTb^3\nu\left(\frac{\lambda R_0}{R}\right)^2 \tag{4.2}$$

In equation 4.2, ν is network strand number density, λ is a linear expansion factor, R_0 is the RMS end to end distance of a network strand in the initial prepared state, and *R* is the end to end distance of a chain with equivalent length in solution at a polymer fraction ϕ. ν is defined as

$$\nu \cong \phi b^{-3} N^{-1} \tag{4.3}$$

where *N* is the average degree of polymerization. Using semidilute solution theory for a theta solvent, we then determine the relative size for unattached network strands.[16]

$$\nu \propto \phi b^{-3} N^{-1} \tag{4.4}$$

To extend this derivation, we make an assumption of affine deformation. Affine behavior indicates fractal swelling behavior that has identical scaling properties throughout size scales. In particular, it says network junctions are dispersed isotropically throughout the network and, during swelling, the junctions move away from each other the same amount as we see macroscopically. An opposing view, the c* theorem, suggests that networks strands disinterpenetrate and junctions dissociate in a non-isotropic manner.[16] There is considerable amount of work involving neutron, X-ray, and visible light scattering that shows larger scale homogeneities in PDMS networks[17-22] and other gels[23-25]. In particular, the c* theory allows for greater equilibrium swelling than affine network theory. Since several groups have found moderately good scaling behavior agreement using the affine assumption with theta to good solvents and we use solvents with poor to theta quality, the affine assumption is used in this derivation. The coefficient of linear expansion for an affine system, λ, is given by Eq (5).

$$\lambda \propto \left(\frac{\phi}{\phi_0} \right)^{-1/3} \tag{4.5}$$

In this formulation, ϕ is polymer volume fraction and ϕ_0 is the polymer volume fraction at preparation.

By combining the previous equations and equating free energy terms, we obtain the following result.[26 13]

$$F_{el} \cong Gb^3 \cong \frac{kT}{N} \phi_0^{2/3} \phi^{1/3} \tag{4.6}$$

If we then minimize the total free energy (osmotic + elastic), we can determine scaling behavior

for equilibrium swelling. In particular, the swelling ratio Q is defined as the ratio of total volume in the swollen state divided by the total volume in the unswollen state, or the inverse of the polymer volume fraction in the swollen state.

$$Q \cong N^{3/8}\phi^{-1/4} \tag{4.7}$$

It is interesting to note that several other derivations present in literature obtain slightly different scaling results for good and theta solvent behavior.[13, 15, 16, 27]

Since this whole system is postulated on the free energy equivalency approach, we can then take the previous two equations (equationss 4.6 and 4.7) and combine them.

$$G_{swollen} \cong \frac{kt}{b^3}Q^{-3} \tag{4.8}$$

Thus, the swollen modulus scales with the swelling ratio to the exponent α, where α =-3. This prediction has been examined for several different polymer-solvent systems: polyvinylacetate in isopropyl alcohol where α=-3.04,[28] PDMS and short chain PDMS gives α=-2.93,[7] and polystyrene in cyclohexane α= 3.7.[29] This scaling result is independent of network precursor strand length and polymer volume fraction at network preparation. Thus, it is equally effective at predicting behavior for both predominantly chemically crosslinked and entanglement dominated networks.

However, in this chapter, we are particularly interested in the scaling behavior between dry network modulus and swelling behavior. Again combining equations 4.5 and equations 4.6, but this time setting ϕ=1, we obtain the following scaling behavior in regards to dry networks.

$$G_{\phi=1} \propto b^{-3}kTQ^{-8/3} \tag{4.9}$$

Although significant work has been performed to establish the validity of the good solvent

relationship between dry modulus and equilibrium swelling ratio, little work has been performed under theta conditions. Sivisailam and Cohen, using M_n = 3800 g/mol PDMS diffusants in several different network strand molecular weight systems, obtained a scaling exponent of -2.29.[7] Rennar and Opperman, in an earlier study, found that $G_{\phi=1} \cong Q^{-1.65}$ for similar, although more imperfect, networks.[30] It is interesting to note that both of these results suggest an intermediate behavior between theta and good solvent conditions. This may be explained if networks have high degrees of inhomogeneity.

Although equation 4.9, similar to equation 4.7, is ostensibly independent of network precursor strand molecular weight and polymer volume fraction at network formation, this assumption fails for values of ϕ_0 that approach 0 when precursor molecular weight is large enough ($\sim MW_{entanglement}$). Under these preparation conditions, networks strands will have few entanglements during the network formation process; after deswelling, network collapse is significant enough to create temporary crosslinks. However, the point at which this becomes important is around ϕ_0=0.1 in good solvent.[31] Thus, since in a theta solvent equilibrium swelling will be less than that in a good solvent, even lower ϕ_0 values would be required to invalidate this scaling relationship.

The free-energy equivalency approach to determine meaningful equilibrium swelling results can also be viewed through an approach pioneered by Flory.[13, 27, 32] For a tetrafunctional network with affine deformations, the result is:

$$\ln(1-\upsilon_2) + \upsilon_2 + \chi\upsilon_2 = \mathrm{v}_1 \nu \left[\frac{\upsilon_2}{2} - \upsilon_2^{1/3} \right] \tag{4.10}$$

where v_2 is polymer volume fraction, χ is the interaction parameter, v_1 is solvent molar volume, and ν is number density of precursor chains. Using the phantom network model (network

crosslinks are allowed to move non-affinely), the result is modified to

$$\ln(1-\upsilon_2)+\upsilon_2+\chi\upsilon_2=-\mathrm{v}_1\left(\nu-\mu\right)\upsilon_2^{1/3} \tag{4.11}$$

where υ is molar density of network junctions ($G_e^{phantom}=(\nu-\mu)RT$). Rearranging this equation and letting the density of the solvent and network be equivalent, we obtain:

$$Q^2\ln(1-Q^{-1})+Q+\chi+\frac{Ms}{Mc}\left(Q^{5/3}-\frac{2Q}{f}\right)=0 \tag{4.12}$$

where M_s is the molecular weight of the solvent, M_c is the molecular weight of network strands, and f is network junction functionality. In the case of network precursors that are below the entanglement molecular weight, $M_c=M_{precursor}$. However, if precursor molecular weight are long, $M_c=M_{entanglement}$.

In this chapter, we are particularly interested in examining the swelling parameters for a different molecular weights and compositions of bismethacrylate endcapped PDMS oligomers. Both model PDMS networks and networks intercalated with photopolymerized macromer are employed as the host for these measurements.

4.2. Experimental section

4.2.1. Preparation of swollen sol-gel systems

Ideal gel networks are synthesized per the procedure in Chapter II. Multiple molecular weight precursors are used (15200, 22300, 41200 g/mol) with 0%, 15%, 30%, and 50% dilution in a theta solvent during cure. Precursor α–ω vinyl chains are catalytically crosslinked at 35 °C with tetrakis(dimethylsiloxy)silane at an *R* value (ratio of crosslinker silane functionality to vinyl

endgroup functionality) that results in the highest modulus. The catalyst used was cis-dichlorobis(diethylsulfide)platinum(II). Prepared networks are then fully extracted and modulus is measured with a Rheometrics Scientific RSA III at 1% strain (linear viscoelastic regime) and 1 Hz in oscillatory tension mode.

Macromer as synthesized in Chapter III is mixed with 2,2-dimethoxy-1,2,-diphenylethan-1-one (DMPO), a radical photonitiator with a strong absorbance band in the UV spectrum. For fully cured systems, 2% wt/wt DMPO/macromer is fully dissolved in macromer with minimal exposure to UV radiation sources.

Dry networks are swollen with 10-30% by total weight macromer and DMPO at 35 °C. After short times (< 48 hours), no macromer is visible on the surface of the sol gel systems for all networks and all macromer molecular weights. Samples are allowed to equilibrate for 7 days before being used for further experiments. Macroscopic sample dimensions are measured at multiple points before and after swelling to ensure that the sol is evenly distributed throughout the sample.

4.2.2. Photopolymerization of macromer swollen model networks

Macromer swollen in model networks is cured using controlled exposure times and intensities at 365 nm. A 500W Oriel Hg-Xe arc lamp is used as the collimated emission source. A 5nm HWHM interference filter with maximum transmittence at 365 +-0.5 nm provides frequency filtering. Sol-gel samples are placed on a quartz disc and loaded into a quartz windowed chamber. The chamber is purged with argon for 15 minutes before irradiation to minimize oxygen inhibition during reaction cure. For complete polymerization, samples are irradiated for 40 minutes at 4 mW/cm^2 intensity. Complete polymerization is corroborated by experiments and results presented in Chapter III.

4.2.3. Swelling measurements and gravimetric analysis

Dry networks, both pure PDMS model networks and photopolymerized intercalated networks, are swollen to equilibrium with different molecular weights of acrylate endcapped macromer. Samples approximately 1 mm thick and 8 mm in diameter were immersed in different molecular weight and phenyl content macromer at 35 °C. Dimensional measurements are repeated after swelling to ensure macroscopic affine behavior. Weight measurements were taken at defined intervals until samples reached equilibrium (< 0.1% change in weight over a 24 hour period). To ensure no crosslinking or macromer reaction had taken place, selected samples were fully extracted in toluene and reweighed.

4.2.4. Rheological measurements on swollen and nonswollen gels

Ex situ rheological measurements were performed on a Rheometric Scientific RSA III in a simple tension geometry under oscillatory mode. Samples were approximately 1 cm x 3cm x 1 mm in size. Young's modulus was measured at 25 °C. Since relatively small strains (< 1%) were used for reporting modulus values, changes in cross-sectional area were neglected. Strain and frequency sweeps were run on each sample. Strain sweeps were performed from 0.01-4% to determine the linear viscoelastic regime. For all samples used, 1% strain rate was within this regime. Frequency sweeps were run from 0.01-100 hz. In all cases, samples exhibit a nearly flat (< 1% deviation) plateau modulus across this frequency domain.. In this chapter, data reported as G' (shear modulus) have been converted from Young's modulus data using the relationship $E=3G$. This relationship holds true for a poisson ratio of 1/2, which is exhibited for most elastomeric systems.

4.3. Results and discussion

4.3.1. Storage modulus dependence on degree of equilibrium swelling

Three different molecular weight series of precursor network chains are used to elucidate equilibrium swelling behavior for different macromer formulations. As discussed in the experimental section, each network precursor molecular weight was prepared at four different dilution ratios. Examining equation 4.8, it is readily apparent that scaling behavior between prepared network modulus and ultimate equilibrium swelling ratio should be independent of both the molecular weight of the network precursor chains and the polymer volume fraction at preparation. For four different molecular weights of endcapped macromer (M_n=500, 1000, 3000, 5000 g/mol) and two different phenyl contents (M_n=1000 g/mol, phenyl=5% and 10%), this behavior was seen. In particular, figure 4.1, using 1000 g/mol macromer as the network diluent, shows the near perfect swelling behavior overlap between different model networks. However, the scaling exponent of α=-3.01 is quite different than the theoretically predicted value of α=-8/3 for affine deformation in a theta solvent. This is expected due to the relatively large size of the methacrylate endcaps compared to the total molecular weight of the oligomer. As such, the macromer should have characteristics between a theta and poor solvent.

Having determined that network precursor molecular weights and preparation volume fractions may be neglected for scaling behavior between equilibrium swelling and modulus, we now examine the effect of macromer molecular weight on scaling relationships. Pure homologous series of PDMS oligomers are expected to swell a network to the same amount above some extent of polymerization threshold. It has been suggested that deviations in scaling behavior still occur due to entropic concerns for molecular weights at least up to 4000 g/mol.[7] Since we are using relatively short chain materials (< 5000 g/mol), we have some expectation that an entropic effect will be apparent in both scaling behavior and degree of equilibrium swelling. In this study we do

not use homologous PDMS series; a molecular weight of 256 g/mol for each macromer is dedicated to a photopolymerizable methacrylate endcap. Especially at low molecular weights, we might expect this endcap to sufficiently change solvent quality such that entropic effects may not be significant in comparison.

Examining swelling behavior for different molecular weight macromer, we find the following power laws:

$$G_{\phi=1} \cong Q^{-8.15} \text{ for 500 g/mol} \tag{4.13}$$

$$G_{\phi=1} \cong Q^{-3.01} \text{ for 1000 g/mol} \tag{4.14}$$

$$G_{\phi=1} \cong Q^{-2.97} \text{ for 3000 g/mol} \tag{4.15}$$

$$G_{\phi=1} \cong Q^{-2.91} \text{ for 5000 g/mol} \tag{4.16}$$

For 1000, 3000, and 5000 molecular weight macromer, we find scaling behavior that is moderately close to the expected power law of -8/3. The larger exponent found in experimental data can be directly attributed to the methacrylate endcaps. It is interesting to note the significant jump in scaling exponent between 1000 g/mol and 500 g/mol as compared to the rather minimal changes between other molecular weights. Overall, as the chains become longer and the methacrylate endgroup has less of an effect on the interaction parameter between network and diluent, the scaling law more closely approaches that expected of a theta solvent. If entropic effects due to short chains had greater effect than enthalpic considerations, we would expect the scaling exponent to be between theta and good solvent conditions. Even though scaling behavior exponents decrease monotonically with molecular weight, absolute values of equilibrium swelling do not, as can be seen in figure 4.2. The highest values of Q are exhibited for a

macromer molecular weight of 1000 g/mol. *Q* decreases respectively for 3000, 5000, and 500 g/mol in the network modulus region which we examine. This will be discussed in more depth in section 4.3.4.

Scaling behavior and extent of equilibrium swelling were also examined for several different phenyl contents in 1000 g/mol macromer. The power law exponent is:

$$G_{\phi=1} \cong Q^{-7.74} \text{ for 5\% phenyl} \tag{4.17}$$

$$G_{\phi=1} \cong Q^{-30.01} \text{ for 10\% phenyl} \tag{4.18}$$

Comparing these exponents to that of PDMS endcapped 1000 g/mol macromer, we see a significant change. This large negative value is indicative of significant deviation from theta and towards poor solvent behavior. Equilibrium swelling values also decrease monotonically with phenyl content. A more quantitative discussion follows in section 4.3.4.

4.3.2. Scaling behavior for partially swollen networks

Now that we have an array of model networks prepared and equilibrium swelling parameters have been determined, we would also like to examine how closely intermediate swelling relationships scale as compared to theory.[15, 16, 33] A more complete derivation for this analysis is provided in Chapter II and both parallels and extends similar scaling behavior presented earlier in this chapter.

$$Gb^3 \cong (b/a)^2 \phi_0^2 \phi^{1/3} \tag{4.19}$$

In this equation, *G* is the shear modulus, *a* and *b* are tube diameter and Kuhn length respectively, ϕ_0 is the preparation polymer volume fraction, and ϕ is the polymer volume fraction at the time of measurement. Although several papers have examined scaling behavior for equilibrium swelling

for hydrocarbon solvents[2, 3, 34] and linear PDMS[7, 8], little work has been done to analyze non-equilibrium, or intermediate, scaling behavior. Also, scaling behavior is analyzed using several new tools; we look at systems with different molecular weights and significantly different thermodynamic interaction parameters. In particular, it will be interesting to note whether the number of entanglements due to dilution on initial cure will change the scaling behavior for the modulus of a swollen material. Monte Carlo simulations for relatively short chains (< 50 repeat units) show that loop formation may be present at up to 10% for high initial levels of dilution.[35, 36] High levels of loop formation would lead to different scaling behavior for different ϕ_0.

For our samples, it seems that loop formation is not significant; slopes of different ϕ_0 in figure 4.4A all show similar power law behavior. Using network precursor molecular weights other than 15200, slopes remain constant regardless of ϕ_0. Replotting normalized modulus ($E'_{swollen}/E'_{extracted}$) values against ϕ, we can see in figure 4.4B that for all ϕ_0 values, the plots collapse onto a single power law exponent. Figure 4.4C shows a log-log plot of normalized modulus against polymer volume fraction for three different molecular weight precursors. The resultant power law behaviors are:

$$G \cong \phi^{0.53} \text{ for MW=15200} \tag{4.20}$$

$$G \cong \phi^{0.57} \text{ for MW=22300} \tag{4.21}$$

$$G \cong \phi^{0.64} \text{ for MW=41200} \tag{4.22}$$

Equation 19 suggests that the scaling exponent should be approximately 1/3 if we neglect the effect of ϕ_0 on G. Considering the poor concurrence of experimental data, this does not seem feasible. This reiterates the importance of entanglements when networks are polymerized in a concentrated regime.

4.3.3. Swelling behavior in photopolymerized macromer swollen networks

The systematic series of moduli for model networks was also swollen with 10% to 30% of macromer. These systems were then cured and reswollen with the same macromer variety (molecular weight, phenyl content). Overall values for absolute swelling parameters and scaling behavior may be examined fully in Table 1. For all photopolymerized macromer systems, the resulting scaling parameter α (where $G \cong Q^{\alpha}$) decreases. Also, the absolute value for Q decreases at equivalent modulus values. Figure 4.5 indicates the particular case of 30% cured 3000 g/mol macromer. For longer macromer chains, the siloxane backbone provides the dominant interaction between macromer and the network. As such, this triblock system will have a relatively low Flory interaction parameter when mixed with a pure PDMS network. After we have photopolymerized macromer in the network, we have added a significant number of methacrylate groups. Since the macromer used to reswell this photopolymerized system still has siloxanes as the main interacting group, we expect the interaction parameter to increase. Thus, the network shifts towards a poorer solvent quality for the macromer diluent.

This effect can be more thoroughly posited if, as we increase the photopolymerized macromer content, the Flory interaction parameter between the network and unpolymerized diluent macromer becomes increasingly positive. For 1000 g/mol macromer, 10%, 20%, and 30% macromer were polymerized in a model network and then reswollen. Figure 4.6 shows that we find the expected trend in scaling behavior; scaling exponents monotonically change from -3.01 for network with 0% cured macromer to -4.66 for networks with 30% cured macromer. Absolute equilibrium swelling values also decrease as cured macromer content increases. Similar trends for 500 g/mol macromer may also be identified using table 4.1. Although this behavior is expected for larger molecular weights, it is somewhat surprising to see in shorter macromer chains. For a molecular weight of 500 g/mol, fully half of the molecule by weight consists of non-siloxane

endgroups. It is not obvious that the interaction between macromer siloxane groups and network methacrylate groups will be more important than methacrylate-methacrylate interactions. Certainly, this seems to indicate that the macromer does not form microphase separated micelles where the methacrylate endgroups would be allowed to minimize contact area with network siloxanes. If this were the case, the shielding would allow for a both a larger scaling parameter and larger *Q*. However, this behavior does suggest that some type of heterogeneity may be polymerized into the network that alters the equilibrium swelling properties. For standard junction and network models for heterogeneity formation, this result is still counterindicated.

As with pure model networks swollen with phenyl containing macromer, we also want to look at equilibrium swelling for networks with photopolymerized macromer. For cured macromer containing both 5% and 10% phenyl content, equilibrium swelling and scaling behavior decrease as can be seen in figure 4.7. This movement away from theta solvent conditions to poorer solvent conditions can be explained using equivalent arguments as given for methacrylate endcapped PDMS macromer.

4.3.4. Change in interaction parameter based on molecular weight and phenyl containing analogues

In the previous section, we noted that, although scaling trends could be explained well without incorporating molecular weight knowledge, absolute swelling behavior could not. The absolute swelling trends for macromer molecular weight show that 1000 g/mol swells the most, followed by 3000, 5000, and 500 g/mol. Since we know M_n for each of these diluents, we can extract the entropic portion of the free energy contributing to swelling and purely retain molecular interactions by using an adapted Flory-Rehner equation. We then expect that the interaction parameter will decrease with increasing molecular weight and increase with higher

phenyl content. Figure 4.8 shows a comprehensive picture of the Flory interaction parameter for a wide array of molecular weights, phenyl content, and degree of equilibrium swelling. In particular, we see the two predicted trends: the interaction parameter decreases with increasing molecular weight, signifying a lesser effect of the methacrylate endgroups; and the interaction parameter increases significantly when phenyl groups are added. If a theta solvent were the diluent, we would not expect the interaction parameter to change with the degree of equilibrium swelling. However, there is an obvious concentration dependence; as a larger amount of macromer is present in the swollen system, χ decreases. This same behavior is seen in other poor solvent systems: in particular, both benzene and toluene as solvents in PDMS networks.[3] It is also important to establish whether absolute χ values are reasonable. Sivisailam et al. report a value of χ=0.09 for 3800 g/mol siloxane oligomer in a variety of PDMS networks.[7] For low Q (Q=1.63) and methacrylate end-capped 5000 g/mol macromer, we obtain χ=0.36. Considering the large methacrylate molecular weight contribution, this value seems reasonable.

In section 4.3.2., we found that when macromer was photopolymerized in a model network, trends in scaling behavior and absolute swelling indicate that successive equilibrium swelling leads to poorer solvent behavior. Figure 4.9 presents an array of interaction parameters for this type of network; in all cases, χ increases significantly (0.05 to 0.1) for intercalated networks. However, relative trends for molecular weight and phenyl content remain the same for model and intercalated networks. Note that all networks in figure 4.9 were swollen and polymerized with 30% macromer. To determine intermediate behavior between 0% and 30% intercalated network, similar swelling experiments were performed for 10% and 20% photopolymerized macromer. These results may be seen in figure 4.10; the monotonic increase in χ with intercalation is exactly what is expected based on the scaling behavior arguments and plots in section 4.3.2.

4.4. Conclusions

In this chapter, we have examined equilibrium and intermediate swelling behaviors for both model networks and model networks intercalated with photopolymerized macromer. The extent of equilibrium swelling is independent of both the network precursor molecular weight and, in the range we examine, the polymer volume fraction at preparation. Using four different molecular weights of methacrylate endcapped PDMS macromer, we show that as molecular weight increases, experimental scaling behavior approaches the theoretical value of $G \cong Q^{-8/3}$. However, absolute equilibrium swelling does not monotonically follow a molecular weight trend. Using a form of the Flory-Rehner equation, we show that this trend is created by the interplay in interaction parameter and entropic considerations due to macromer molecular weight. Intermediate swelling scaling behavior was also examined, and shown to coincide rather poorly with a priori expectations. This can be, however, be purely attributed to neglecting the effect of preparation polymer volume fraction on the elastic modulus.

Equilibrium swelling behavior was also examined for intercalated polymer networks. For all photopolymerized systems, the resulting swelling behavior indicated that macromer was now a poorer solvent than in model networks. Poor solvent behavior is indicated both through decreases in absolute swelling and power law exponents for modulus against equilibrium swelling ratio behavior. This trend followed for macromer with high phenyl content, also. This behavior is surprising, since the Flory interaction parameter is concentration dependent and decreases with decreasing polymer volume fraction. However, for intercalated networks, polymerized macromer increases the interaction parameter.

4.5. Tables

Table 4.1. Scaling parameter for model and interpenetrating networks.

Penetrant MW	% phenyl	% cured diffusant	α ($G \cong Q^{\alpha}$)
500	0	0	-8.15
500	0	10	-9.19
500	0	20	-9.76
500	0	30	-10.59
1000	0	0	-3.01
1000	0	10	-4.11
1000	0	20	-4.36
1000	0	30	-4.66
3000	0	0	-3.10
3000	0	30	-3.58
5000	0	0	-3.32
1000	5	0	-7.74
1000	5	30	-8.31
1000	10	0	-30.01
1000	10	20	-31.25

4.6. Figures

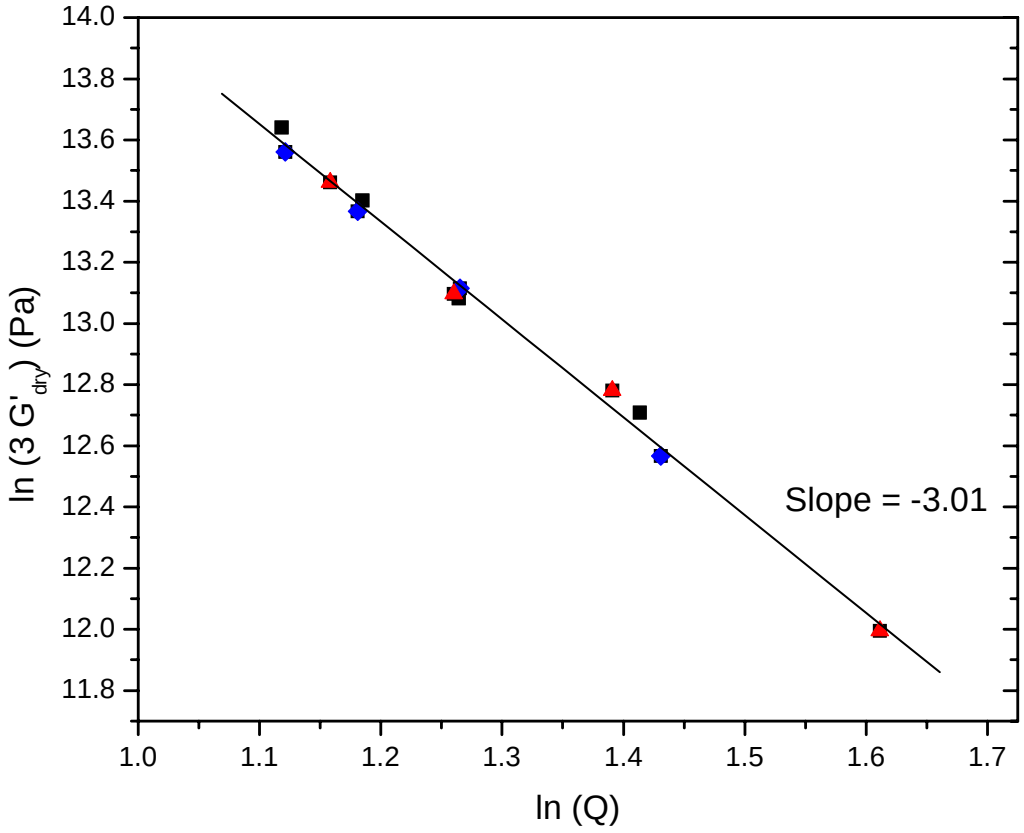

Figure 1 Log-log plot of Young's modulus for extracted samples against the equilibrium swelling parameter, Q. Three different matrix precursor molecular weights are swollen with 1000 g/mol bismethacrylate endcapped macromer. ■ is 15200 MW matrix precursor, ◆ is 22300 MW, and ▲ is 41200 MW. Each matrix precursor molecular weight series incorporates several different ϕ_0 values (0, 0.85, 0.7, 0.5). Values for all matrix molecular weights and ϕ_0s fall on a straight line with slope of -3.01.

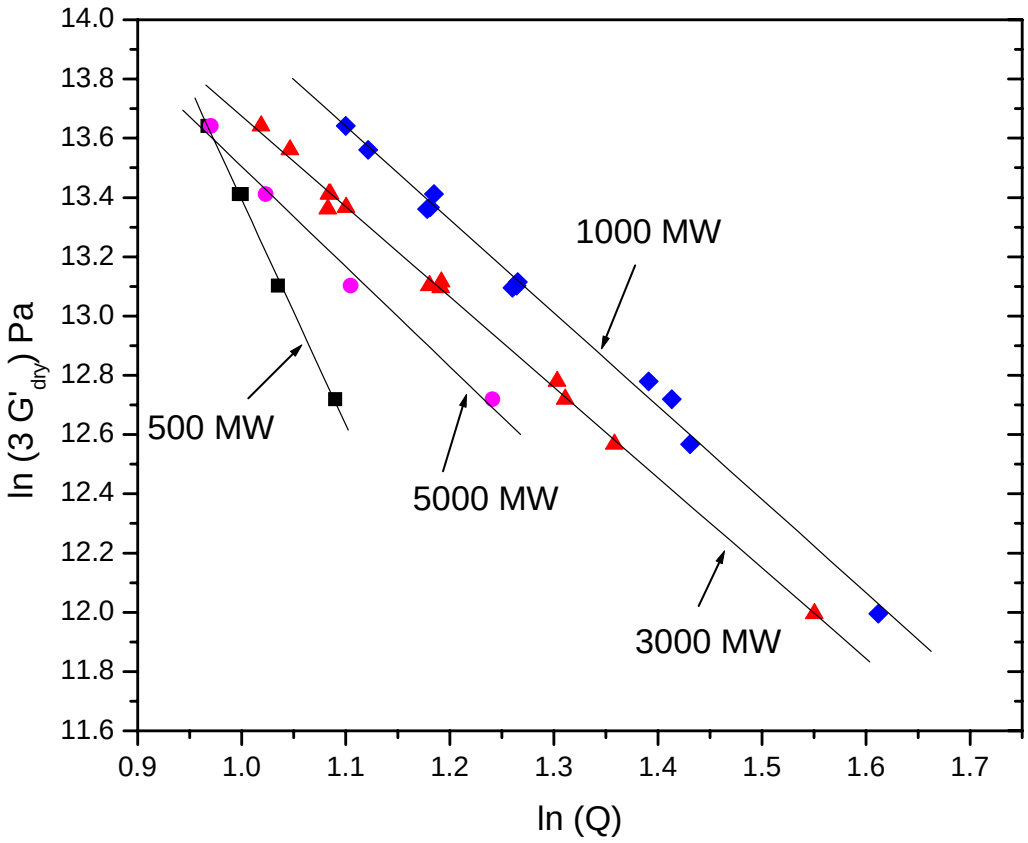

Figure 2 Log-log plot of Young's modulus for extracted samples against the equilibrium swelling parameter, Q. Model networks are swollen with different bismethacrylate endcapped macromer. ■ is 500 MW, ◆ is 1000 MW, ▲ is 3000 MW, and ▼ is 5000 MW. Lines are least squares linear regression and have slopes of -8.15 for 500 MW, -3.01 for 1000 MW, -2.97 for 3000 MW, and -2.91 for 5000 MW. It is interesting to note that, for a specific modulus, there is not a monotonic increase in Q with macromer molecular weight.

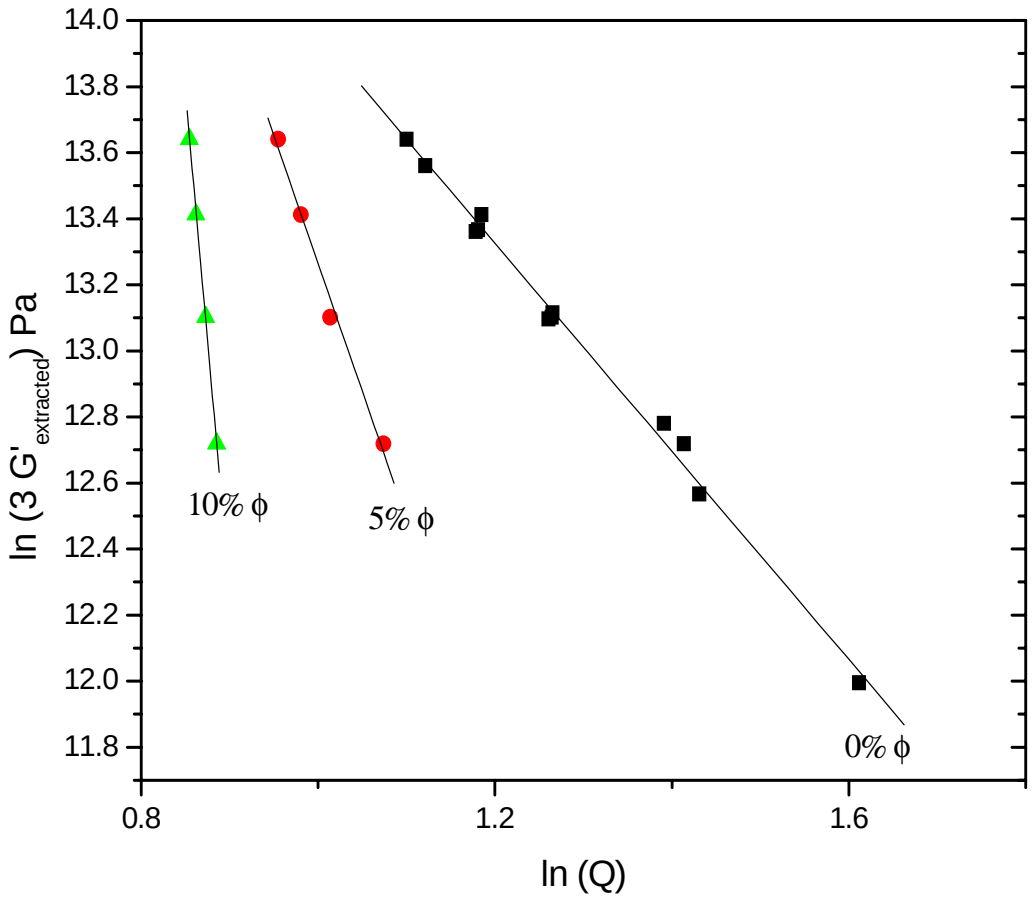

Figure 3 Log-log plot of Young's modulus for extracted samples against the equilibrium swelling parameter, Q. Model networks are swollen with 1000 molecular weight bismethacrylate endcapped macromer with different percents of phenyl (ϕ) incorporation. ■ is 0 % phenyl, ● is 5% phenyl , and ▲ is 10% phenyl. Lines are least squares linear regression and have slopes of -3.01 for 0% phenyl, -7.74 for 5% phenyl, and -30.01 for 10% phenyl.

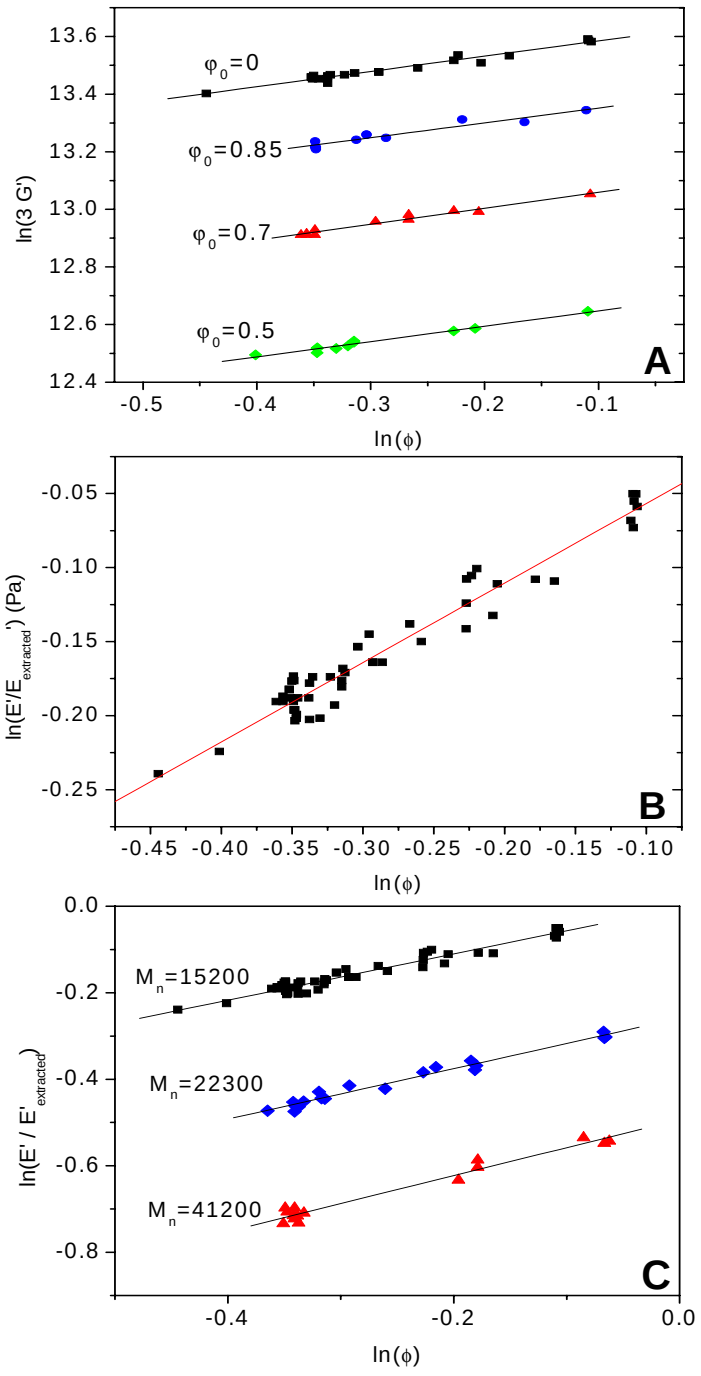

Figure 4 Part A shows a log-log plot of modulus vs. fill fraction for 15200 MW precursor systems at different initial diluent levels. Lines are least squares linear regression and have a slope of 0.53+-.004. Part B plots the same data with normalized elastic modulus. Note that all initial diluent levels collapse on top of each other. Part C compares the normalized moduli for three different precursor molecular weights. 22300 and 41200 MW have been shifted down by 0.2 and 0.4 to prevent data overlap. Lines are least squares linear regression and have slopes of 0.53 for MW=15200, 0.57 for MW=22300, and 0.64 for MW=41200.

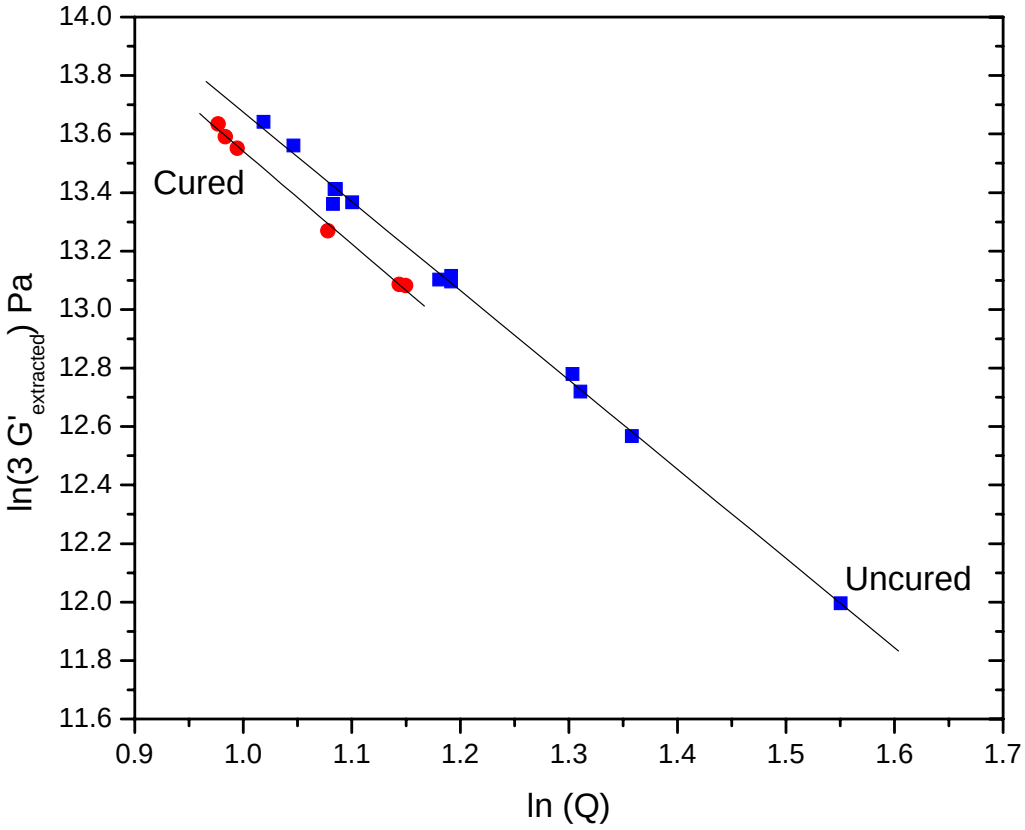

Figure 5 Log-log plot of Young's modulus for extracted samples against the equilibrium swelling parameter, Q. Model networks and networks cured with 30% 3000 g/mol macromer are swollen with 1000 molecular weight macromer. ■ is uncured model network and ● is results from the system with cured macromer. Lines are least squares linear regression and have slopes of -2.97 for the model system and -3.67 for system with 30% cured macromer.

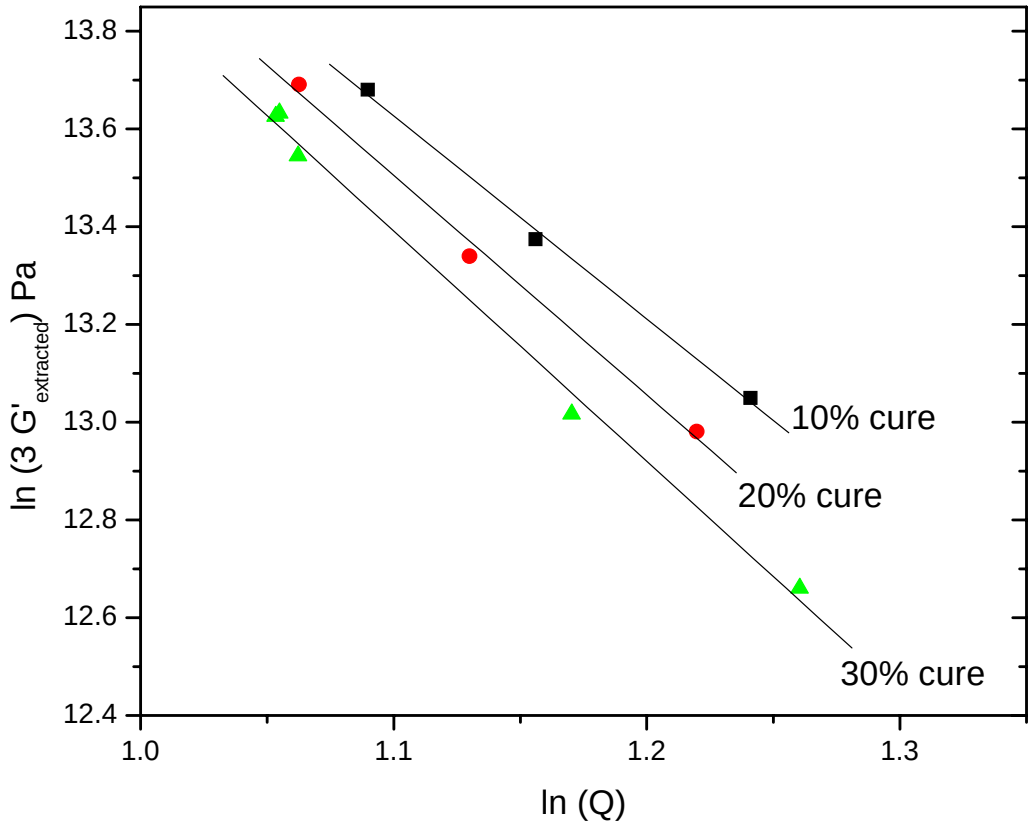

Figure 6 Log-log plot of Young's modulus for extracted samples against the equilibrium swelling parameter, Q. Model networks are swollen and cured with 10%, 20%, and 30% 1000 g/mol macromer. These samples are then reswollen to equilibrium with 1000 g/mol macromer. ■ is 10% cured macromer in model network, ● is 20% cured macromer in model network, and ▲ is 30% cured macromer in model network. Lines are least squares linear regression and have slopes of -4.11 for 10% cured macromer, -4.36 for 20% cured macromer, and -4.66 for 30% cured macromer.

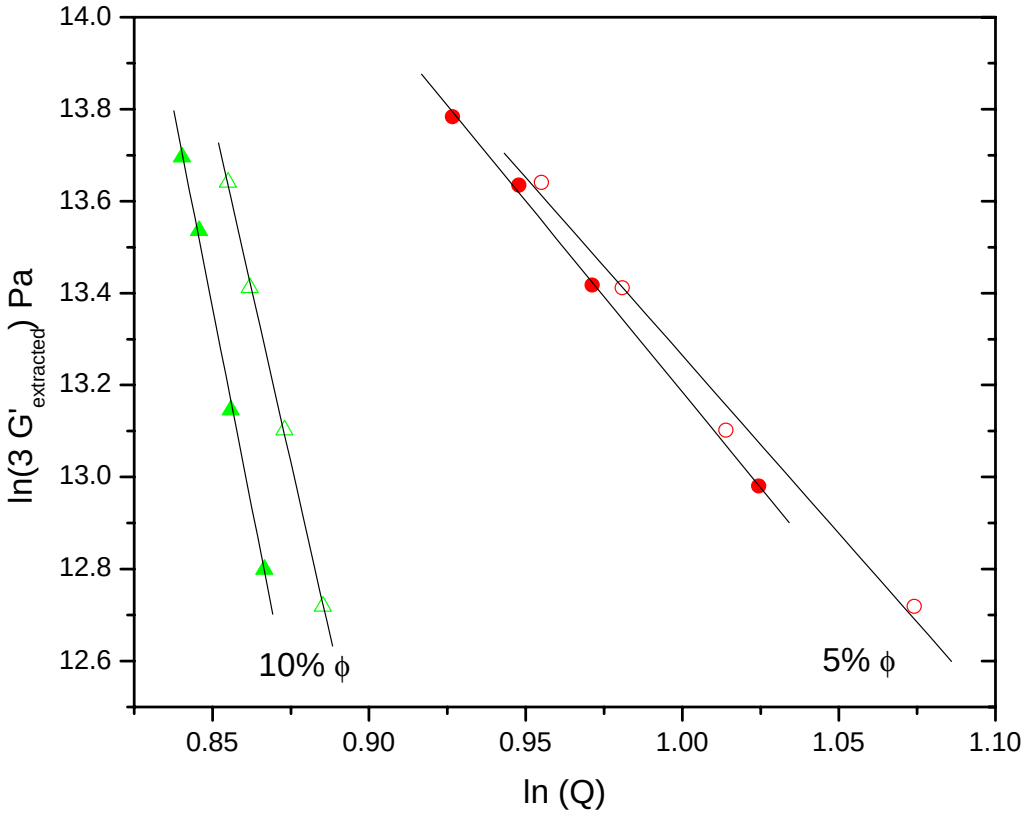

Figure 7 Log-log plot of Young's modulus for extracted samples against the equilibrium swelling parameter, Q. Model networks are swollen and cured with 30% macromer incorporating 5% phenyl or 20% macromer incorporating 10% phenyl. These samples are then reswollen to equilibrium with 1000 g/mol macromer with the same phenyl percent. ▲ is 1000 g/mol macromer with 10% phenyl and ● is 1000 g/mol macromer with 5% phenyl. Unfilled points refer to equilibrium swelling for model networks (no cured macromer). Lines are least squares linear regression and have slopes of -7.74 for the model system and 5% phenyl, -8.31 for the cured system with 5% phenyl, -30.01 for model system and 10% phenyl, and -31.246 for cured system with 10% phenyl.

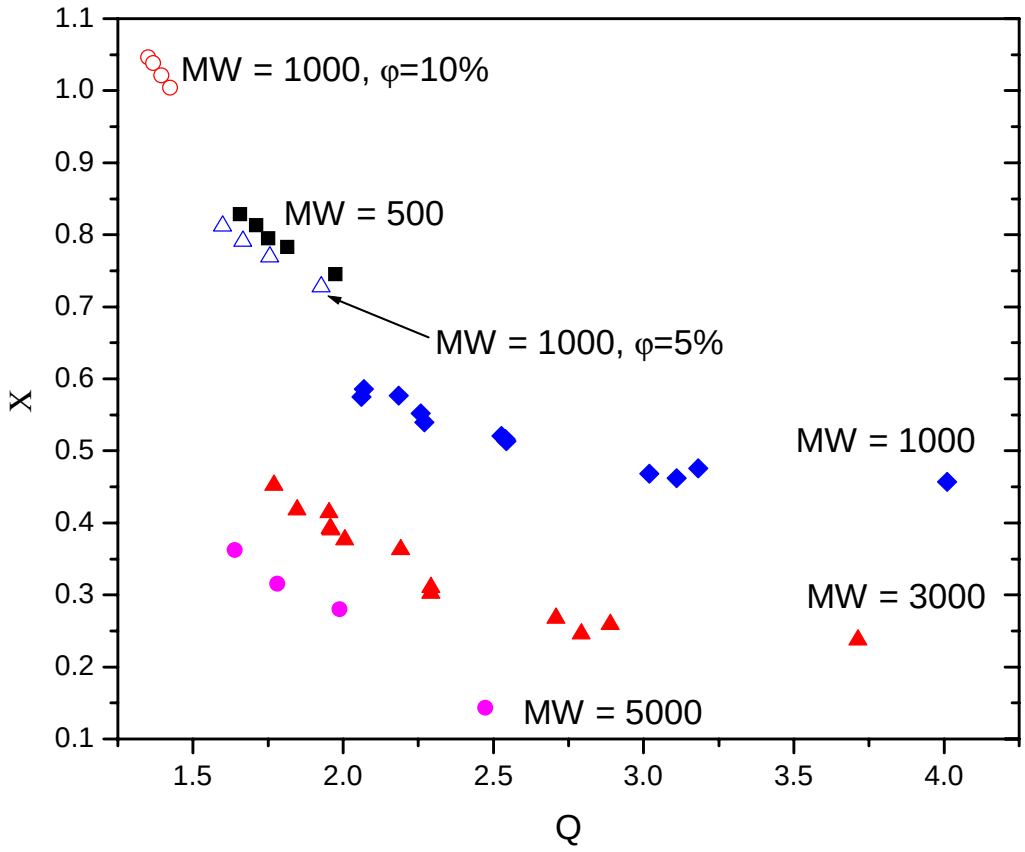

Figure 8 Plot of Flory interaction parameter for extracted samples against the equilibrium swelling parameter, Q. Model networks are swollen with different bismethacrylate endcapped macromer. ■ is 500 MW, ◆ is 1000 MW, ▲ is 3000 MW, and ● is 5000 MW. 1000 g/mol macromer with ○ 5% phenyl content and △ 10% phenyl content. There is a monotonic inverse relationship between the interaction parameter and molecular weight. Also, as we increase phenyl content, the interaction parameter increases.

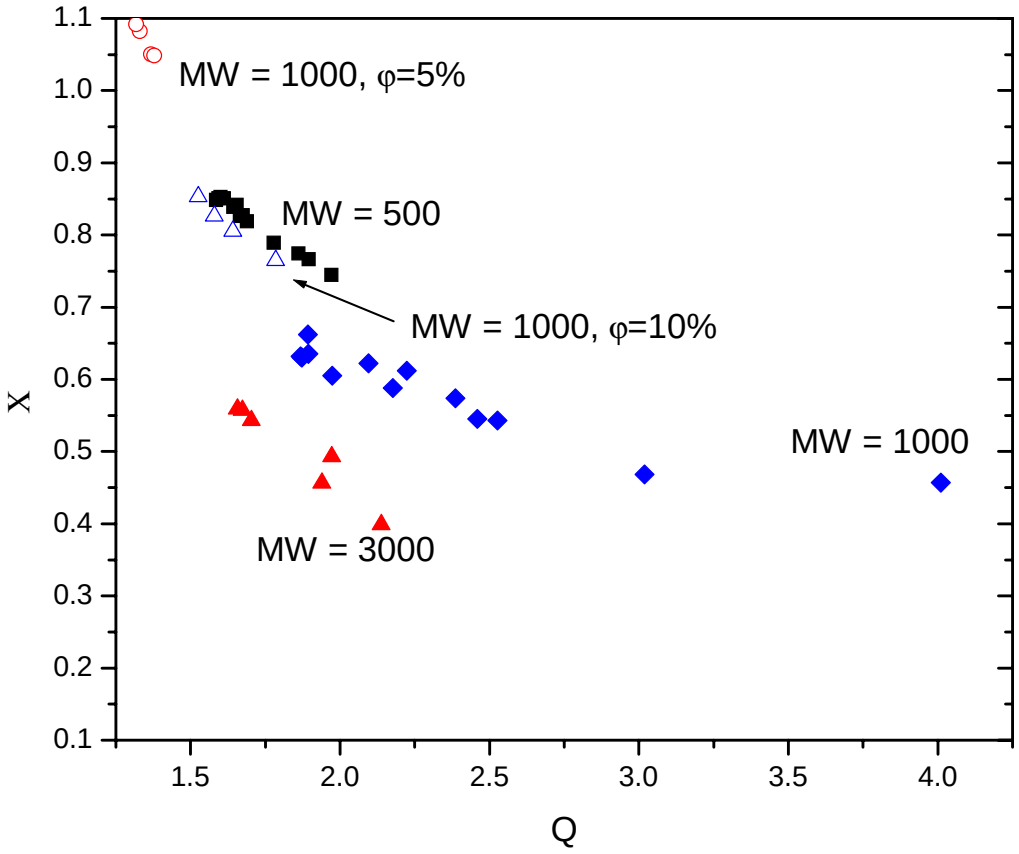

Figure 9 Plot of Flory interaction parameter for extracted samples that contain 30% photopolymerized macromer against the equilibrium swelling parameter, Q. Networks are then swollen with different bismethacrylate endcapped macromer. ■ is 500 MW, ◆ is 1000 MW, ▲ is 3000 MW, and ● is 5000 MW. 1000 g/mol macromer with ○ 5% phenyl content and △ 10% phenyl content. There is a monotonic inverse relationship between the interaction parameter and molecular weight. Also, as we increase phenyl content, the interaction parameter increases. Comparing this plot to Figure 8, we see that the addition of cured macromer to the model network increases the interaction parameter.

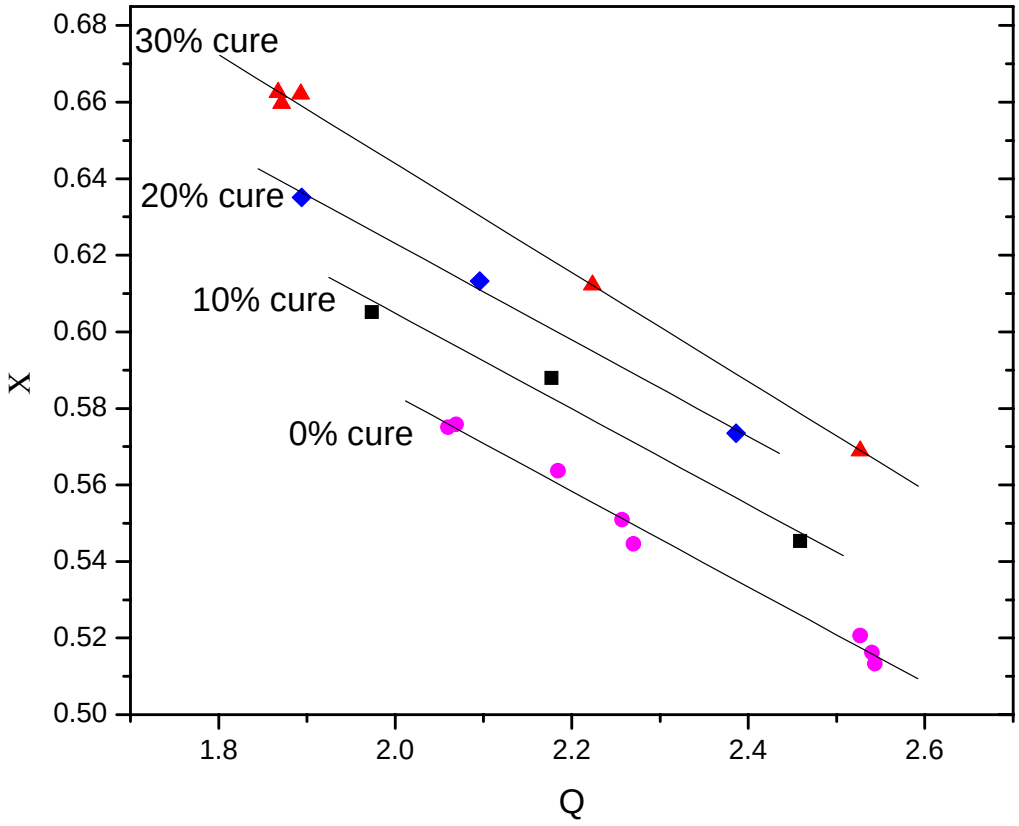

Figure 10 Plot of Flory interaction parameter for extracted samples that contain 0% to 30% photopolymerized macromer against the equilibrium swelling parameter, Q. Networks are swollen with 1000 g/mol bismethacrylate endcapped macromer to equilibrium. ● is 0% cured macromer, ■ is 10% cured macromer, ◆ is 20% cured macromer, and ▲ is 30% cured macromer. There is direct relationship between the interaction parameter and amount of cured macromer in the system.

4.5. References

1. Gottlieb, M., C. W. Macosko, G. S. Benjamin, K. O. Meyers, and E. W. Merrill, Equilibrium Modulus of Model Poly(Dimethylsiloxane) Networks. *Macromolecules,* 1981. **14**(4): p. 1039-1046.

2. Horkay, F., A. M. Hecht, and E. Geissler, Thermodynamic Interaction Parameters in Polymer Solutions and Gels. *Journal of Polymer Science Part B-Polymer Physics,* 1995. **33**(11): p. 1641-1646.

3. Patel, S. K., S. Malone, C. Cohen, J. R. Gillmor, and R. H. Colby, Elastic-Modulus and Equilibrium Swelling of Poly(Dimethylsiloxane) Networks. *Macromolecules,* 1992. **25**(20): p. 5241-5251.

4. Llorente, M. A. and J. E. Mark, Model Networks of End-Linked Poly(Dimethylsiloxane) Chains .8. Networks Having Cross-Links of Very High Functionality. *Macromolecules,* 1980. **13**(3): p. 681-685.

5. Braun, J. L., J. E. Mark, and B. E. Eichinger, Formation of poly(dimethylsiloxane) gels. *Macromolecules,* 2002. **35**(13): p. 5273-5282.

6. Garrido, L., Extraction and sorption studies using linear polymer chains and model networks. *Journal of Polymer Science: Polymer Physics Edition,* 1985. **23**: p. 1933-1940.

7. Sivisailam, K., Scaling Behavior: Effect of Precursor concentration and precursor molecular weight on the modulus and swelling of polymeric networks. *Journal of Rheology,* 2000. **44**(4): p. 897-915.

8. Gent, A. N., Diffusion and Equilibrium swelling of macromolecular networks by

their linear homologs. *Journal of Polymer Science : Polymer Physics Edition*, 1982. **20**: p. 2317-2327.

9. Gent, A. N., Diffusion of Linear Polyisoprene Molecules into Polyisoprene Networks. *Journal of Polymer Science: Part B: Polymer Physics*, 1989. **27**: p. 893-911.

10. Gent, A. N., Diffusion of Polymer Molecules into Polymer Networks: Effect of Stresses and Constraints. *Journal of Polymer Science: Part B: Polymer Physics*, 1991. **29**: p. 1313-1319.

11. Hedden, R. C., H. Saxena, and C. Cohen, Mechanical properties and swelling behavior of end-linked poly(diethylsiloxane) networks. *Macromolecules*, 2000. **33**(23): p. 8676-8684.

12. Clarson, S. J., An investigation of the properties of bimodal poly(dimethylsiloxane) elastomers upon swelling with a linear oligomeric phenylmethylsiloxane. *Polymer Communications*, 1986. **27**: p. 260-261.

13. Flory, P. J., Statistical Mechanics of Cross-linked polymer networks: II. Swelling. *Journal of Chemical Physics*, 1943. **11**(11): p. 521-526.

14. Panyukov, S. V., Scaling Theory of High Elasticity. *Soviet Physics: JETP*, 1990. **71**(2): p. 372-379.

15. Obukhov, S. P., Network Modulus and Superelasticity. *Macromolecules*, 1994. **27**: p. 3191-3198.

16. de Gennes, P. G., *Scaling Concepts in Polymer Physics*. 1979. Ithaca: Cornell University Press.

17. Soni, V. K. and R. S. Stein, Light-Scattering-Studies of Poly(Dimethylsiloxane) Solutions and Swollen Networks. *Macromolecules,* 1990. **23**(25): p. 5257-5265.

18. Mallam, S., F. Horkay, A. M. Hecht, A. R. Rennie, and E. Geissler, Microscopic and Macroscopic Thermodynamic Observations in Swollen Poly(Dimethylsiloxane) Networks. *Macromolecules,* 1991. **24**(2): p. 543-548.

19. Mallam, S., A. M. Hecht, E. Geissler, and P. Pruvost, Structure of Swollen Poly(Dimethyl Siloxane Gels. *Journal of Chemical Physics,* 1989. **91**(10): p. 6447-6454.

20. Falcao, A. N., J. S. Pedersen, and K. Mortensen, Structure of Randomly Cross-Linked Poly(Dimethylsiloxane) Networks Produced by Electron-Irradiation. *Macromolecules,* 1993. **26**(20): p. 5350-5364.

21. Falcao, A. N., J. S. Pedersen, K. Mortensen, and F. Boue, Polydimethylsiloxane networks at equilibrium swelling: Extracted and nonextracted networks. *Macromolecules,* 1996. **29**(3): p. 809-818.

22. Urayama, K., T. Kawamura, Y. Hirata, and S. Kohjiya, SAXS study on poly(dimethylsiloxane) networks with controlled distributions of chain lengths between crosslinks. *Polymer,* 1998. **39**(16): p. 3827-3833.

23. Kizilay, M. Y. and O. Okay, Effect of initial monomer concentration on spatial inhomogeneity in poly(acrylamide) gels. *Macromolecules,* 2003. **36**(18): p. 6856-6862.

24. Kizilay, M. Y. and O. Okay, Effect of swelling on spatial inhomogeneity in poly (acrylamide) gels formed at various monomer concentrations. *Polymer,* 2004.

45(8): p. 2567-2576.

25. Ozdogan, A. and O. Okay, Effect of spatial gel inhomogeneity on the elastic modulus of strong polyelectrolyte hydrogels. *Polymer Bulletin,* 2005. **54**(6): p. 435-442.

26. James, H. M. and E. Guth, Theory of the Increase in Rigidity of Rubber During Cure. *Journal of Chemical Physics,* 1947. **15**(9): p. 669-683.

27. Flory, P. J., *Principles of Polymer Chemistry*. 1953. Ithaca, N.Y.: Cornell University Press.

28. Zrinyi, M. and F. Horkay, On the Elastic-Modulus of Swollen Gels. *Polymer*, 1987. **28**(7): p. 1139-1143.

29. Richards, R. W. and N. S. Davidson, Scaling Analysis of Mechanical and Swelling Properties of Random Polystyrene Networks. *Macromolecules,* 1986. **19**(5): p. 1381-1389.

30. Rennar, N. and W. Oppermann, Swelling Behavior and Mechanical-Properties of Endlinked Poly(Dimethylsiloxane) Networks and Randomly Cross-Linked Polyisoprene Networks. *Colloid and Polymer Science,* 1992. **270**(6): p. 527-536.

31. Graessley, W. W., Polymer-Chain Dimensions and the Dependence of Viscoelastic Properties on Concentration, Molecular-Weight and Solvent Power. *Polymer,* 1980. **21**(3): p. 258-262.

32. Treloar, L. R. G., *The Physics of Rubber Elasticity, 3rd ed.* 1975. Oxford: Clarendon.

33. Colby, R. H. and M. Rubinstein, *Polymer Physics*. 2003. New York: Oxford

University Press, Inc.

34. Menge, H., S. Hotopf, S. Ponitzsch, S. Richter, K. F. Arndt, H. Schneider, and U. Heuert, Investigation on the swelling behaviour in poly(dimethylsiloxane) rubber networks using nmr and compression measurements. *Polymer,* 1999. **40**(19): p. 5303-5313.

35. Gilra, N., A Monte Carlo study of the structural properties of end-linked polymer networks. *Journal of Chemical Physics,* 2000. **112**(15): p. 6910-6916.

36. Gilra, N., A. Panagiotopoulos, and C. Cohen, Monte Carlo simulations of free chains in end-linked polymer networks. *Journal of Chemical Physics,* 2001. **115**(2): p. 1100-1104.

Chapter V: Diffusion Kinetics of Short-chain Macromers in Model Polymer Networks

5.1. Introduction

Effective application of time resolved spatially heterogeneous photopolymerization for sol gel systems necessitates the knowledge of sol diffusion rates. Although for spatially homogeneous polymerization system overall kinetics may be determined with knowledge only of reaction rates, heterogeneous polymerization allows non-polymerized free sol to re-equilibrate. Thus, there is competition between reaction kinetics and diffusion kinetics. In systems such as intraocular lenses or Bragg-type diffraction gratings, this interaction is extraordinarily important when determining optical characteristics, both in regards to refractive index and shape.

Several techniques, such as gravimetric swelling and extraction,[1-8] pulsed field gradient nuclear magnetic resonance (PFG-NMR),[9-13] forced Rayleigh scattering,[14-22] and forward recoil spectrometry (FRES)[23] have been used to examine diffusion theory in polymer melts and networks. Center of mass diffusion in polymer networks can be described in terms of diffusant molecular weight, M_d:

$$D \cong M_d^{-\alpha} \tag{5.1}$$

In this equation, D is the diffusivity coefficient and α is a variable scaling coefficients. For M_d values much less than the entanglement molecular weight, M_e, Rouse-like diffusion should occur where $\alpha = 1$. As M_d increases in size and approaches M_e, transverse chain movement is impeded by a "tube" of surrounding network chains, resulting in what de Gennes calls reptation.[24-26] For reptation, Rouse-like diffusion occurs for a series of Kuhn-length blobs along the tube, resulting in a scaling exponent of $\alpha = 2$. Neither of these basic relationships examine whether the molecular weight between crosslinks (M_c) in a network is important in diffusion rates. To our knowledge, there are no *a priori* models that predict how network crosslink densities will affect diffusivity.

Diffusive behavior of both entangled and non-entangled diffusants in networks has been extensively studied. Self-diffusivity, or diffusion rate of a penetrant in a network of the same molecular weight, has been reported to scale with $\alpha = 1.5$ to 2.0 in PDMS.[5, 26, 27] Sorption kinetics were used to determine diffusion rates and diffusants had a polydispersity index (PDI) of approximately 2. For lower PDI diffusants (PDI < 1.2), a scaling exponent of $\alpha = -2$ was found for M_d = 4200 g/mol to M_d = 12000 g/mol with PFG-NMR.[9] It is interesting to note that this $\alpha = 2$ behavior continues until $M_d < 1/2\ M_e$. This suggests that reptation may be occurring to some extent even for diffusants significantly below the entanglement molecular weight. However, Cosgrove, et al., report a scaling exponent of $\alpha = -1$ for systems where $M_d < 5M_e$.[7, 12] These experiments were performed using PFG-NMR at PDI < 1.3. Considering the different results for α obtained with similar materials and methodologies, it is difficult to determine from literature what diffusant molecular weights lead to Rouse-like and reptative diffusion.

Although scaling theory does not predict an effect of M_c on diffusivity, experiments have shown that network crosslink density does play an important role. Using mass uptake measurements, polyisoprene diffusants both above and below M_e with PDI < 1.08 showed

behavior of $D \cong M_c^{-0.2}$.[1] In PDMS, our analysis of reported data shows scaling behavior for M_c of α = -0.16 to -0.37 using sorption experiments.[5, 27] PFG-NMR measurements show a random mixture of positive and negative α values between -0.4 and 0.3 for different PDMS diffusant molecular weights.[9] For all of these literature values for α, M_c is precursor molecular weight, not effective molecular weight between junctions. Depending on initial reaction conditions, trapped entanglements or elastically ineffective chains may alter network modulus; the molecular weight between junctions has the potential to be significantly different than the precursor materials. Since prior work used networks prepared in the melt, it is likely that trapped entanglements will be important and molecular weight between crosslinks will be overpredicted. Well characterized model networks are therefore necessary for appropriate determination of scaling behavior between D and M_c.

Because there is a lack of consensus in literature for the effects of penetrant molecular weight and molecular weight between network junctions, we examine diffusion behavior particular to our system. Four penetrant molecular weights are swollen into a series of networks with different moduli, and diffusion rates are calculated from the time it takes to reach equilibrium values. Diffusion rates into interpenetrating networks (IPNs) are also examined to see if microstructure changes diffusion rates. Effects of diffusant polydispersity are also examined . For all systems, the relationship between diffusivity, molecular weight, and network properties is determined.

5.2. Experimental section

5.2.1. Preparation of swollen sol-gel systems

Ideal gel networks are synthesized per the procedure in chapter II. Multiple molecular

weight precursors are used (15200, 22300, 41200 g/mol) with 0%, 15%, 30%, and 50% dilution in a theta solvent during cure. Precursor α–ω vinyl chains are catalytically crosslinked at 35 °C with tetrakis(dimethylsiloxy)silane at an *R* value (ratio of crosslinker silane functionality to vinyl endgroup functionality) that results in the highest modulus. The catalyst used was cis-dichlorobis(diethylsulfide)platinum(II). Prepared networks are then fully extracted and modulus is measured with a Rheometrics Scientific RSA III at 1% strain (linear viscoelastic regime) and 1 Hz in oscillatory tension mode.

Macromer as synthesized in chapter III is mixed with 2,2-dimethoxy-1,2,-diphenylethan-1-one (DMPO), a radical photoinitiator with a strong absorbance band in the UV spectrum. For fully cured systems, 2% w/w DMPO / macromer is fully dissolved in macromer with minimal exposure to UV radiation sources.

Dry networks are swollen with 10-30% by total weight macromer and DMPO at 35 °C. After short times (< 48 hours), no macromer is visible on the surface of the sol gel systems for all networks and all macromer molecular weights. Samples are allowed to equilibrate for 7 days before being used for further experiments. Macroscopic sample dimensions are measured before and after swelling to ensure that the sol is evenly distributed throughout the sample.

5.2.2. Photopolymerization of macromer swollen model networks

Macromer swollen in model networks is cured using controlled exposure times and intensities at an irradiation wavelength of 365 nm. A 500W Oriel Hg-Xe arc lamp is used as the emission source. A 5 nm HWHM interference filter with maximum transmittance at 365 +-0.5 nm provides frequency filtering. Sol-gel samples are placed on a quartz disc and loaded into a quartz windowed chamber. The chamber is purged with argon for 15 minutes before irradiation to minimize oxygen inhibition during reaction cure. For complete polymerization, samples are

irradiated for 40 minutes at 4 mW/cm^2 intensity. Complete polymerization is corroborated by experiments and results presented in chapter III.

5.2.3. Diffusion measurements using gravimetric analysis

Dry networks, both pure PDMS model networks and photopolymerized intercalated networks, were swollen to equilibrium with different molecular weights of acrylate endcapped macromer. Samples approximately 1 mm thick and 8 mm in diameter were immersed in different molecular weight and phenyl content macromer at 35 °C. Dimensional measurements were repeated after swelling to ensure macroscopic affine behavior. Weight measurements were taken at defined intervals until samples reached equilibrium (< 0.1% change in weight over a 24 hour period). To ensure no crosslinking or macromer reaction had taken place, selected samples were fully extracted in toluene and reweighed.

To analyze the effect of selective adsorption, or molecular weight sieving behavior, bidisperse solutions of two different molecular weight macromers were allowed to diffuse into a network. Weights measurements were taken in the same manner as for single component diffusion experiments.

5.2.4. Rheological measurements of cured and uncured sol-gel systems

Ex situ rheological measurements were performed on a Rheometric Scientific RSA III in a simple tension geometry under oscillatory mode. Samples were approximately 1 cm x 3cm x 1mm in size. Young's modulus was measured at 25 °C. Since relatively small strains (< 1%) were used for reporting modulus values, changes in cross-sectional area were neglected. Strain and frequency sweeps were run on each sample. Strain sweeps were performed from 0.01 - 4% to determine the linear viscoelastic regime. For all samples used, 1% strain rate was within this

regime. Frequency sweeps were run from 0.01-100 Hz. In all cases, samples exhibit a nearly flat (< 1% deviation) plateau modulus across this frequency domain. In this chapter, data reported as G' (shear modulus) has been converted from Young's modulus data using the relationship $E=3G$. This relationship holds true for a Poisson ratio of 1/2, which is exhibited for most elastomer systems.

5.3. Results and discussion

5.3.1 . Measurement of diffusion coefficient

Diffusion coefficient values are analyzed by comparing mass uptake experiments with a numerical solution of the Fickian diffusion equation. The Fickian diffusion equation is

$$\frac{\partial C}{\partial t} = -D(C)\frac{\partial^2 C}{\partial^2 x} \tag{5.2}$$

where C is concentration, t is time, D is the diffusivity coefficient, and x is a spatial parameter. This equation is then solved as a function of mass uptake.[28]

$$\frac{M_t}{M_\infty} = 1 - \frac{8}{\pi^2}\sum_{m=0}^{\infty}\frac{1}{(2m+1)^2}\exp\left[-\frac{D(2m+1)^2\pi^2 t}{l^2}\right] \tag{5.3}$$

In this equation, M_t is mass at time t, M_∞ is mass at equilibrium swelling, and l is the length scale over which diffusion occurs. From equation 5.2, the slope of l plotted against $t^{1/2}$ will be D. Since mass uptake experiments directly measure M_t/M_∞, it is more convenient to plot normalized mass uptake against $t^{1/2}$ to obtain D. In figure 5.1, the data thus plotted exhibit a linear behavior at short times; from the slope of the short time regime we obtain values for concentration independent

diffusivity. At longer times (where $M_t/M_\infty > 0.5$), there is significant negative deviation of experimental data from theoretical predictions. This can be partially attributed to an increase in the linear dimension, *l*, in which diffusion is occurring. If the penetrant molecules are required to diffuse over greater distances as M_t / M_∞ increases, apparent diffusivities will decrease. Molecular sieving of polydisperse samples would also contribute to negative deviation of diffusivity values. At short times, a disproportionate number of small molecules diffuse into the network and contribute to a relatively high diffusivity. As time progresses and longer chains diffuse into the network, apparent diffusivities decrease. The effect of polydisperse samples is discussed in further depth as we progress through this chapter. If diffusivity were treated as concentration dependent, experimental data would exhibit positive deviation from theory because of faster constraint release from the short diffusant molecules as compared to longer molecular weights between network crosslinks. Thus, even if diffusivity is concentration dependent, the effect is completely overcome by that of molecular sieving.

5.3.2. Changes in diffusivity with penetrant molecular weight and network modulus

Four molecular weights of diffusants (500, 1000, 3000, and 5000 g/mol) are swollen into model networks with different elastic moduli. Measured diffusion rates for this array of samples are graphed against the diffusant molecular weight in a log-log plot (figure 5.2); each data set is for a specific network modulus. For each network modulus, least squares linear regression fits of data give the following scaling behavior.

$$D \cong M_d^{-0.59} \text{ for } E' = 8.40 \text{ x } 10^5 \text{ Pa} \tag{5.4}$$

$$D \cong M_d^{-0.60} \text{ for } E' = 6.68 \text{ x } 10^5 \text{ Pa} \tag{5.5}$$

$$D \cong M_d^{-0.62} \text{ for } E' = 4.90 \text{ x } 10^5 \text{ Pa} \tag{5.6}$$

$$D \cong M_d^{-0.73} \text{ for } E' = 3.44 \text{ x } 10^5 \text{ Pa} \quad (5.7)$$

In these equations, E' is Young's modulus. Since we are swelling a network with diffusant where $M_d < M_e$, we expect that equation 5.1 for Rouse-like diffusion should apply ($\alpha = 1$). The lower values of α that we obtain may be explained by differential diffusion rates for different molecular weight species of a polydisperse penetrant. Due to our cationic chemistry for synthesizing methacrylate endcapped PDMS, we have a diffusant with Gaussian length distribution and polydispersity greater than 1.5. Although the diffusant is purified and polydispersity is reduced slightly below initial values, we do not perform further fractionation because of limited batch size and proportionally large mass requirements for experimental work. Since diffusion rates are calculated at $M_t/M_\infty < 0.5$ for mass uptake experiments and the lower molecular weight species of the polydisperse penetrant preferentially diffuse into the network at early times, $\alpha < 1$. Not only are our experimental values for α significantly lower than theory predicts, but we also observe that as network modulus increases, exponents show greater deviation from Rouse-like scaling behavior.

This network contribution to diffusion is examined by plotting penetrant diffusivity against calculated molecular weight between crosslinks, M_c, for four different molecular weights of penetrant (figure 5.3). Contrary to previous work where scaling relationships were determined using network precursor molecular weights, M_c is based on actual tensile modulus measurements and therefore incorporates effects of chemical junctions and entrapped entanglements. Assuming affine deformation and that all chains are elastically effective, the following expression can be derived:

$$E' = \frac{3\rho RT}{M_c} \quad (5.8)$$

For $D \cong M_c^{-\beta}$,

$$\beta = 0.66 \text{ for } M_d = 500 \text{ g/mol} \quad (5.9)$$

$$\beta = 0.68 \text{ for } M_d = 1000 \text{ g/mol} \quad (5.10)$$

$$\beta = 0.90 \text{ for } M_d = 3000 \text{ g/mol} \quad (5.11)$$

$$\beta = 1.01 \text{ for } M_d = 5000 \text{ g/mol} \quad (5.12)$$

Although crosslink density should have little effect on actual diffusion rates for Rouse-like diffusion, even at very low molecular weights we see diffusivity has a large dependence on M_c. As diffusant chains get longer, β increases to a value of 1.01. This increase can be attributed to increased polydispersity for higher diffusant molecular weights (table 3.1). It is interesting to compare the value of our scaling exponents with those calculated from other work and discussed in the introduction.[1, 5, 27] Even with significantly higher PDI diffusants, other reported scaling exponents are significantly lower that what we see. This is likely caused by prior use of network precursor molecular weight instead of measured crosslink density for determination of scaling behavior. Table 5.1 summarizes all diffusivity values based on diffusant molecular weight, network precursor strand length, and network modulus.

5.3.3. Effects of intercalated networks and phenyl sidegroup incorporation

Several model networks were also swollen with 1000 g/mol macromer with either 5 or 10% phenyl content. Because materials with phenyl content have different backbone chain lengths than pure PDMS endcapped macromer, there was a possibility that diffusion rates might be different. However, even though equilibrium swelling was considerably different (chapter IV), both absolute diffusivities and scaling behavior remained constant regardless of phenyl content.

Diffusion rates into photopolymerized intercalated systems were also measured for the

full spectrum of macromer molecular weights. Because of potential differences in network structure between initial model networks and IPNs formed by polymerizing macromer in model networks, it was deemed important to determine whether the sole network factor determining diffusion rates is modulus (and, therefore, effective molecular weight between network crosslinks). For all host networks and penetrant molecular weights, diffusivity was a function only of network modulus; network intercalation created through use of 10% to 30% polymerized macromer made no significant difference in either scaling behavior or absolute values of diffusivity.

5.3.4. Bimodal macromer molecular weight distributions

Although it seems apparent from single molecular weight diffusion studies that our scaling behavior is dominated by diffusant polydispersity and the asymmetric time analysis of mass uptake data, we have also performed mass uptake experiments with a bimodal molecular weight distribution of penetrant. Several host networks with varying crosslink density were swollen in a mixture of 500 or 1000 g/mol macromer and 3000 g/mol macromer. Figures 5.4A and 5.4B plot diffusivity against host network modulus; Figure 5.4A shows diffusion rates macromer 500 g/mol, 3000 g/mol, and a 50:50 wt/wt mixture of the two molecular weights. Diffusivities for all three systems are at their maximum at high network modulus and monotonically decrease with decrease network modulus. By visual inspection, one can see that at high network modulus, diffusivity of the bimodal penetrant has a value intermediate to 500 and 3000 g/mol but slightly closer to 3000 g/mol. This value is not equidistant because the equilibrium swelling value for 3000 g/mol is greater than that for 500 g/mol. Thus, because diffusivities are based on equilibrium swelling, there will be a systematic shift of bimodal penetrant diffusivity to lower values. As network modulus is decreased, bimodal penetrant

diffusivity approaches the diffusivity of 3000 g/mol macromer. If no molecular sieving is present, the diffusion rate of the bimodal system should have retained the same relative distance between 500 g/mol and 3000 g/mol regardless of network modulus. A similar trend regarding molecular sieving behavior is seen in Figure 5.4B, where a bimodal mixture of 1000 g/mol and 3000 g/mol macromer is used as penetrant and relative diffusivity decreases with decreasing network modulus. However, the systematic shift in diffusivities is positive rather than negative because 1000 g/mol macromer has greater equilibrium swelling than 3000 g/mol.

5.4. Conclusions

In this chapter, we have examined the diffusion rates of several different molecular weights of bismethacrylate endcapped PDMS macromer in model networks with different cross-link densities. Diffusivity values show dependence both on molecular weight of the penetrant species and the modulus of the host network. In particular, we find that the scaling exponent α for $D \cong M_d^{-\alpha}$ is significantly lower than expected for Rouse-like diffusion. α is also dependent on the host modulus; for higher network moduli, there is greater deviation from predicted behavior. We also find that β (for $D \cong M_c^{-\beta}$) increase for more polydisperse diffusants. Additional measurements of diffusivity were performed on macromer containing up to 10% phenyl content. Diffusivities and scaling trends did not change for these materials as compared to PDMS based penetrants. Diffusivity of a series of different molecular weight macromers was also measured in photopolymerized intercalated networks. As with adding phenyl content to macromer, we found that penetrant molecular weight and host network modulus are the only two important variables in diffusivities. Bimodal molecular weight distributions were similarly swollen in a series of different modulus host networks. Absolute diffusion rates show the detrimental effect of using penetrants with different equilibrium swelling ratios; diffusion rates show systematic deviation

from actual values when using a mass uptake analysis method. Trends in diffusion rates also corroborate the previous analysis that significant molecular sieving is present for our macromers when diffusing in tightly crosslinked networks.

Table 5.1. Summary of diffusivity in different model networks with several macromer molecular weights.

$M_{macromer}$	$M_{precursor}$	ϕ_0	E' (Pa)	D ($x10^{-12}$ m^2/s)	% phenyl
500	17200	0	840000	23.5	0
	17200	15	668000	16.9	0
	17200	15	668000	18.1	0
	17200	30	490000	15.6	0
	17200	50	334000	11.9	0
1000	17200	0	840000	12.8	0
	17200	15	668000	9.7	0
	17200	15	668000	9.8	0
	17200	30	490000	8.2	0
	17200	50	334000	5.5	0
	28000	0	775000	11.5	0
	28000	15	638000	10.0	0
	28000	30	496000	8.1	0
	28000	50	287000	5.9	0
	43000	0	635000	10.4	0
	43000	15	487000	9.0	0
	43000	30	355000	6.9	0
	43000	50	162000	4.1	0
3000	17200	0	840000	6.8	0
	17200	15	668000	5.6	0
	17200	15	668000	5.0	0
	17200	30	490000	4.2	0
	17200	50	334000	2.9	0
	28000	0	775000	6.7	0
	28000	15	638000	5.9	0
	28000	30	496000	4.2	0
	28000	50	287000	2.8	0
	43000	0	635000	5.7	0
	43000	15	487000	4.8	0
	43000	30	355000	3.4	0
	43000	50	162000	2.0	0
5000	17200	0	840000	5.8	0
	17200	15	668000	4.9	0
	17200	30	490000	4.0	0
	17200	50	334000	2.2	0
1000	17200	0	840000	14.0	5
	17200	15	668000	11.8	5
	17200	30	490000	9.7	5
	17200	50	334000	8.0	5
1000	17200	0	840000	18.8	10
	17200	15	668000	18.0	10
	17200	30	490000	15.9	10
	17200	50	334000	14.3	10

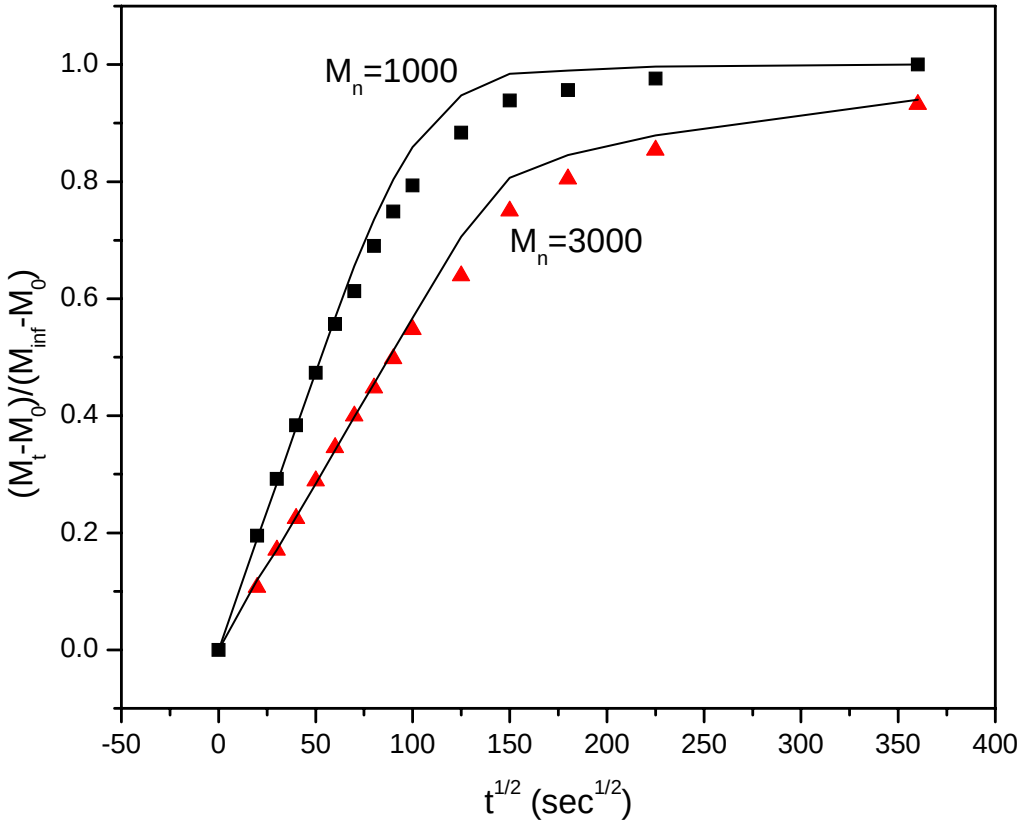

Figure 5.1. Sorption data plotted with normalized mass uptake against time. ■ is experimental data for 1000 g/mol macromer diffusing in a network with E'=840000, ▲ is 3000 g/mol macromer diffusing in the same network. Lines are data fits assuming Fickian diffusion. During data correspondence at early times, the slope of the line can be used to calculate the diffusion coefficient.

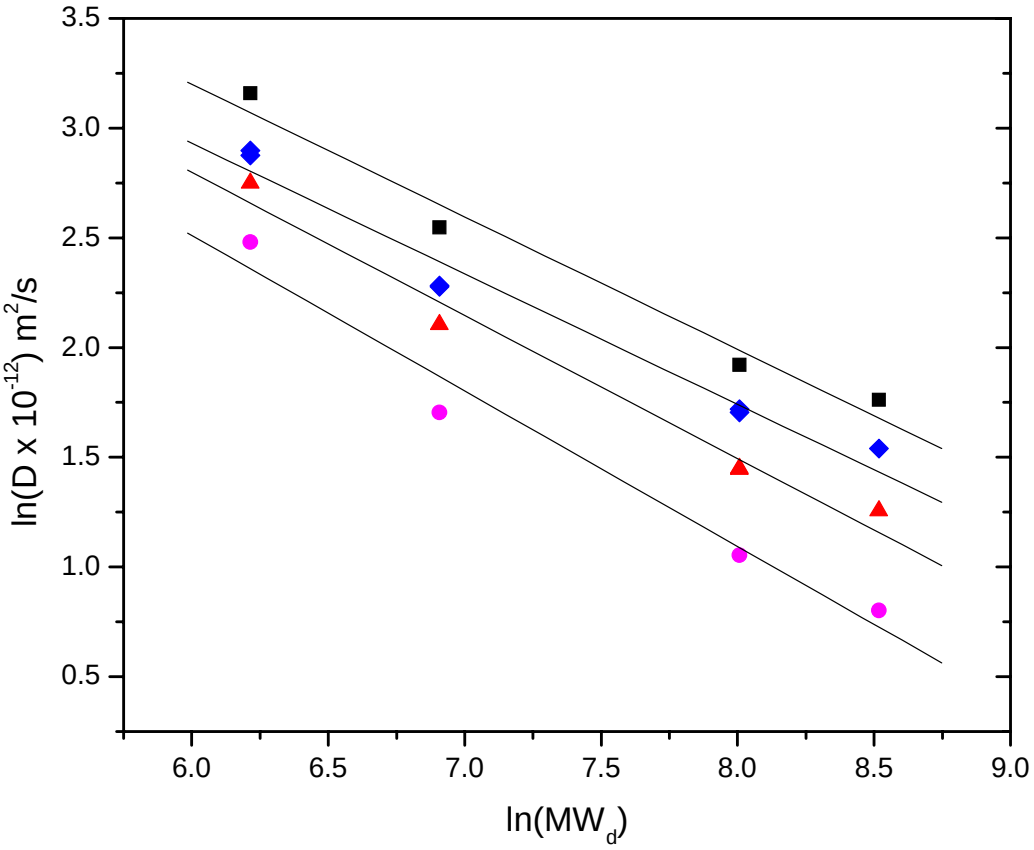

Figure 5.2. Log-log plot of macromer diffusivity against penetrant molecular weight. ■ is E'=8.40x10^5 Pa, ◆ is 6.68x10^5 Pa, ▲ is 4.90x10^5 Pa, and ● is 3.44x10^5 Pa. Lines are linear least squares regressions to the data. Line slopes are -0.59 for 8.40x10^5 Pa, -0.60 for 6.68x10^5 Pa, -0.62 for 4.90x10^5 Pa, and -0.73 for 3.44x10^5 Pa. Decreasing slopes with decreasing network modulus indicate that molecular sieving is less important for more loosely crosslinked networks.

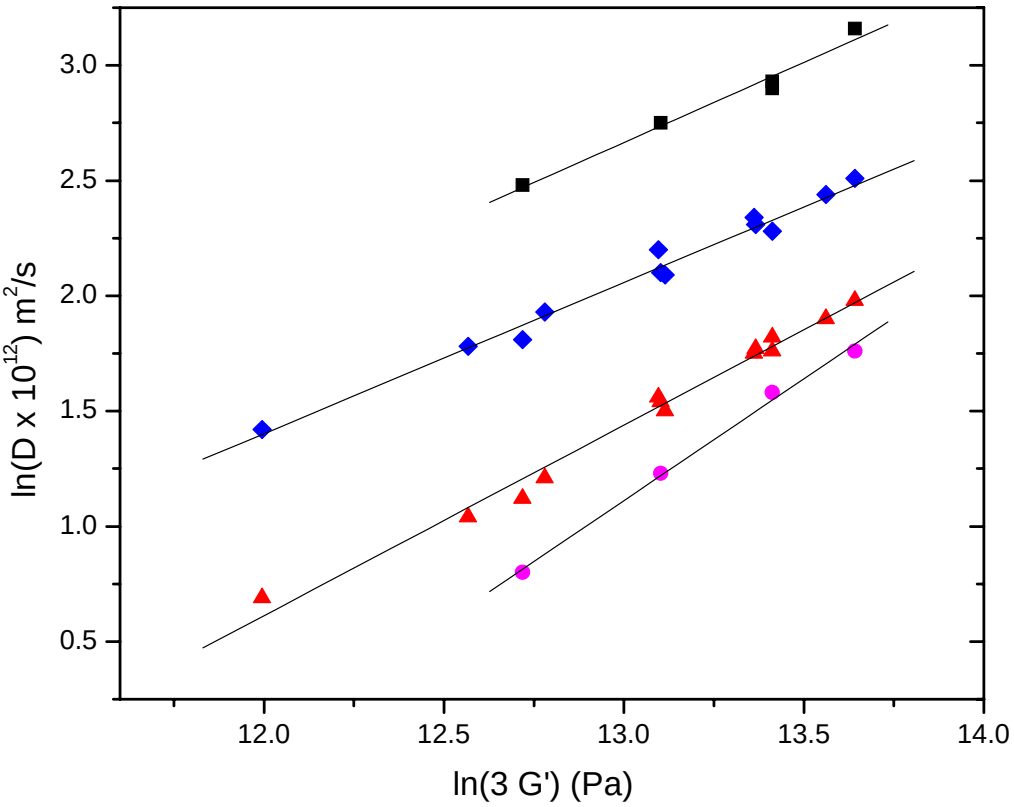

Figure 5.3. Log-log plot of macromer diffusivity with network modulus. ■ is M_n=500 g/mol, ◆ is M_n = 1000 g/mol, ▲ is M_n = 3000 g/mol, and ● is M_n = 5000 g/mol. Lines are linear least squares regressions to the data. Line slopes are 0.66 for M_n=500, 0.67 for M_n = 1000, 0.79 for M_n = 3000, and 1.01 for M_n = 5000. Increasing slopes with increasing molecular weight (and increasing PDI) suggest that molecular sieving is taking place.

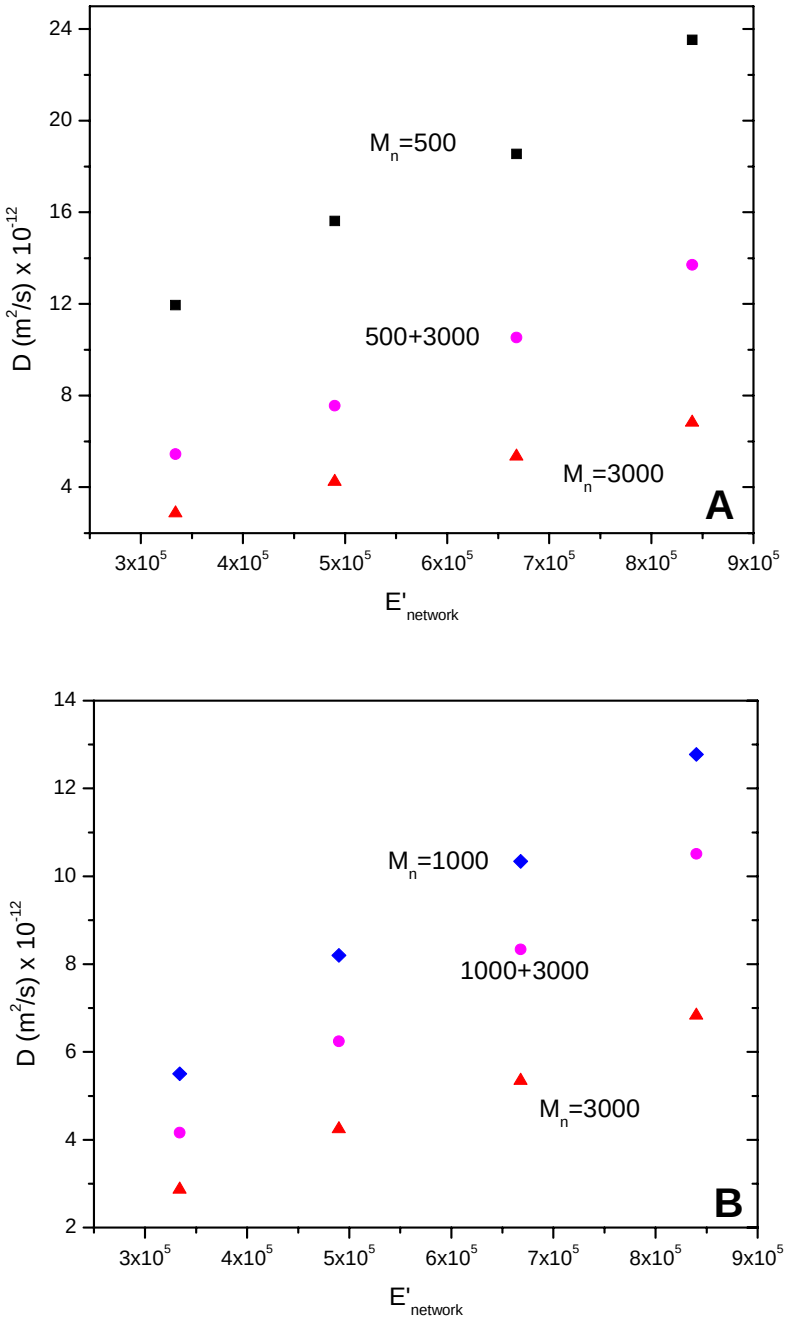

Figure 5.4. Diffusivity changes due to different network moduli. Plot A shows ■ M_n=500, ▲ M_n=3000 and a ● 50/50 mixture. Plot B shows ◆ M_n=1000, ▲ M_n=3000 and a ● 50/50 mixture. As network crosslink density increases, mixture diffusivities diverge further from the diffusivity of M_n = 3000 g/mol and more closely approach that of the lower molecular weight.

5.7. References

1. Gent, A. N., Diffusion of Linear Polyisoprene Molecules into Polyisoprene Networks. *Journal of Polymer Science: Part B: Polymer Physics,* 1989. **27**: p. 893-911.
2. Gent, A. N., Diffusion of Polymer Molecules into Polymer Networks: Effect of Stresses and Constraints. *Journal of Polymer Science: Part B: Polymer Physics,* 1991. **29**: p. 1313-1319.
3. Tanner, J. E., Diffusion in a polymer Matrix. *Macromolecules,* 1971. **4**: p. 748-750.
4. Mazan, J., Diffusion of Free polydimethylsiloxane chains in polydimethylsiloxane elastomer networks. *European Polymer Journal,* 1995. **31**(8): p. 803-807.
5. Gent, A. N., Diffusion and Equilibrium swelling of macromolecular networks by their linear homologs. *Journal of Polymer Science : Polymer Physics Edition,* 1982. **20**: p. 2317-2327.
6. Garrido, L., J. E. Mark, S. J. Clarson, and J. A. Semlyen, Studies of Cyclic and Linear Poly(Dimethylsiloxanes) .15. Diffusion-Coefficients from Network Sorption Measurements. *Polymer Communications,* 1984. **25**(7): p. 218-220.
7. Cosgrove, T., C. Roberts, G. V. Gordon, and R. G. Schmidt, Diffusion of polydimethylsiloxane mixtures with silicate nanoparticles. *Abstracts of Papers of the American Chemical Society,* 2001. **221**: p. U323-U323.
8. Pryor, T., E. vonMeerwall, and V. Galiatsatos, Diffusion of siloxane oligomers in the melt and in PDMS networks: Host effects. *Abstracts of Papers of the American Chemical Society,* 1996. **211**: p. 200-PMSE.
9. Garrido, L., Studies of Self-diffusion of Poly(dimethylsiloxane) Chains in PDMS Model Networks by Pulsed Field Gradient NMR. *Journal of Polymer Science, Part B: Polymer Physics,* 1988. **26**: p. 2367-2377.

10. Kubo, T., Diffusion of Single Chains in Polymer Matrices as Measured by Pulsed-Field-Gradient NMR: Crossover from Zimm to Rouse-Type Diffusion. *Polymer Journal,* 1992. **24**(12): p. 1351-1361.

11. Matsukawa, S. and I. Ando, A study of self-diffusion of molecules in polymer gel by pulsed-gradient spin-echo H-1 NMR. *Macromolecules,* 1996. **29**(22): p. 7136-7140.

12. Cosgrove, T., M. J. Turner, P. C. Griffiths, J. Hollingshurst, M. J. Shenton, and J. A. Semlyen, Self-diffusion and spin-spin relaxation in blends of linear and cyclic polydimethylsiloxane melts. *Polymer,* 1996. **37**(9): p. 1535-1540.

13. Griffiths, M. C., J. Strauch, M. J. Monteiro, and R. G. Gilbert, Measurement of diffusion coefficients of oligomeric penetrants in rubbery polymer matrixes. *Macromolecules,* 1998. **31**(22): p. 7835-7844.

14. Huang, W. J., Tracer Diffusion Measurements in Polymer Solutions Near the Glass Transition by Forced Rayleigh Scattering. *AIChE Journal,* 1987. **33**(4): p. 573-581.

15. Kohler, W., Polymer Analysis by Thermal-Diffusion Forced Rayleigh Scattering. *Advances in Polymer Science,* 2000. **151**: p. 1-59.

16. Lodge, T., Applications of Forced Rayleigh Scattering to Diffusion in Polymeric Liquids. *Trends in Polymer Science,* 1997. **5**(4): p. 122-128.

17. Park, H. S., Forced Rayleigh Scattering studies of mixtures of amplitude and phase gratings in methyl yellow/alcohol solutions. *Journal of Chemical Physics,* 2000. **112**(21): p. 9518-9523.

18. Veniaminov, A. V., Forced Rayleigh Scattering from non-harmonic gratings applied to complex diffusion processes in glass-forming liquids. *Chemical Physics Letters,* 1999. **303**: p. 499-504.

19. Wesson, J. A., H. Takezoe, H. Yu, and S. P. Chen, Dye Diffusion in Swollen Gels by

Forced Rayleigh-Scattering. *Journal of Applied Physics,* 1982. **53**(10): p. 6513-6519.

20. Sung, J. M. and T. Y. Chang, Temperature-Dependence of Probe Diffusion in Polymer Matrix. *Polymer,* 1993. **34**(17): p. 3741-3743.

21. Milhaupt, J. M., T. P. Lodge, S. D. Smith, and M. W. Hamersky, Composition and temperature dependence of monomer friction in polystyrene/poly(methyl methacrylate) matrices. *Macromolecules,* 2001. **34**(16): p. 5561-5570.

22. Krongauz, V. V., Photopolymerization kinetics and monomer diffusion in polymer matrix. *Polymer,* 1990. **31**: p. 1130-1136.

23. Composto, R. J., E. J. Kramer, and D. M. White, Matrix Effects on Diffusion in Polymer Blends. *Macromolecules,* 1992. **25**(16): p. 4167-4174.

24. de Gennes, P. G., *Scaling Concepts in Polymer Physics*. 1979. Ithaca: Cornell University Press.

25. Klein, J., Effect of Matrix Molecular-Weight on Diffusion of a Labeled Molecule in a Polymer Melt. *Macromolecules,* 1981. **14**(2): p. 460-461.

26. Klein, J., Onset of Entangled Behavior in Semidilute and Concentrated Polymer-Solutions. *Macromolecules,* 1978. **11**(5): p. 852-858.

27. Garrido, L., Extraction and sorption studies using linear polymer chains and model networks. *Journal of Polymer Science: Polymer Physics Edition,* 1985. **23**: p. 1933-1940.

28. Crank, J. a. G. S. P., *Diffusion in Polymers*. 1968. New York: Academic Press Inc. Ltd.

Chapter VI: **Reaction Kinetics of Photopolymerized Macromer-matrix PDMS Systems**

6.1. Introduction

Polymerization kinetics of photoreactive macromer species in crosslinked host networks are tremendously important for understanding system dynamics in interpenetrating networks (IPNs). The addition of a second percolated network can change mechanical, thermodynamic, and optical properties of a host network. To fine tune the structure that forms during photopolymerization, reactions can be carried out under a wide variety of conditions; irradiation intensity and duration, concentration of initiator species, molecular weight and concentration of macromer, and matrix composition and crosslink density may all be altered. For all of these parameters, their effect on kinetic behavior must be understood as part of the foundation for rational control of IPN characteristics.

Reactions of multifunctional methacrylate monomer species have been extensively studied due to their broad use in coatings, lenses, dental materials, and stereolithography.[1-4] These polymerizations reveal several striking features over the course of the reaction. At early times, an increase in reaction rate, termed autoacceleration, occurs as radical chain sizes increase. Since reaction termination is controlled by radical diffusion rates, increased radical size also increases

radical lifetimes and allows more propagating radicals to accumulate in the system.[5-7] This results in an increased reaction rate. As conversion continues to increase, reaction rate typically decreases because of sample vitrification. Since reaction propagation is controlled by monomer and radical species diffusing together, increased viscosity drastically reduces reaction rates. In many systems, sample vitrification quenches the reaction between 40 and 60% reactive group conversion.[3, 8-11] This is undesirable for most applications since unreacted species have the potential to leach out or cause material property changes at long times. Another important phenomenon in monomer reaction systems is the decreased likelihood of bimolecular termination as radicals grow in size and their diffusivity decreases. Ultimately, propagating radicals in vitrified samples are unable to translate and therefore terminate by growing together through monomer addition. This process, termed reaction diffusion, is manifested by a region where termination and propagation rates are proportional.

Contrary to methacrylate monomer systems, kinetics of multifunctional methacrylates with a midblock spacer, or “macromers,” have not been well studied. If the midblock is of a material, such as siloxane, that is well above the glass transition temperature, material effects such as vitrification will not play an important role in polymerization kinetics and the polymerized network will remain rubbery. Unlike monomer systems, mobility is retained and the reaction may reach complete conversion. Using similar logic, it is also expected that termination kinetics should occur only through radical diffusion and not by reaction diffusion. However, several studies with 600 g/mol methacrylate endcapped polyethyleneglycol (PEG) indicate that reaction diffusion does play an important role in termination above 20% reactive group conversion.[5, 11, 12]

In this chapter, we examine the reaction kinetics of four different molecular weights of bifunctional macromer with flexible siloxane midblocks. The polymerization of each macromer is

examined as a function of initiator concentration, irradiation intensity, macromer concentration, and host network structure using a photo differential scanning calorimeter to measure the reaction rate as a function of time and reactive endgroup conversion. To elucidate termination kinetics, irradiation is stopped at partial conversion and the decay of the reaction rate is observed. Analysis of the propagation and termination rates allows us to compare overall polymerization kinetics of methacrylate endcapped macromers to those of methacrylate monomers used in the literature. Several striking features, such as full macromer conversion and chain length dependent termination processes, are found for these materials.

6.2. Experimental section

6.2.1. Preparation of photopolymerizable PDMS systems

Model PDMS networks are synthesized using the procedure in Chapter II. A single molecular weight precursor is used (15200 g/mol) with 0% and 50% dilution in a theta solvent during cure. Precursor α–ω vinyl chains are catalytically crosslinked at 35 °C with tetrakis(dimethylsiloxy)silane at a ratio of crosslinker silane functionality to vinyl endgroup functionality, *R*, that results in the highest modulus. The catalyst used was cis-dichlorobis(diethylsulfide)platinum(II).

Macromer as synthesized in chapter III is mixed with 2,2-dimethoxy-1,2,-diphenylethan-1-one (DMPO), a radical photonitiator with a strong absorbance band in the UV spectrum. DMPO is dissolved from 0.1% to 2% w/w DMPO / macromer in macromer with minimal exposure to UV radiation sources.

Dry networks are polymerized either in 40 µl stainless steel differential scanning calorimetry pans or 1 mm x 8 mm quartz molds and are swollen with 10-30% by total weight

macromer and DMPO at 35 °C by exposing one surface of a PDMS network to macromer. After short times (< 6 hours for DSC pans, < 24 hours for 1 mm x 8 mm samples), no macromer is visible on the polymer surface for any macromer molecular weights. Samples are allowed to equilibrate for 2 days before use in experiments.

Reaction rate experiments were also performed using macromer-swollen PDMS melts. Three different molecular weight (approximately 1, 50, and 500 kg/mol) melts are mixed with 10-30% macromer. For melts of 1 and 50 kg/mol, mixing could be accomplished with mechanical stirring. Macromer was incorporated into the 500 kg/mol melt by iterative “kneading” followed by time for diffusion. This mixed sol is then placed in 40 μl stainless steel calorimetry pans and allowed to sit for 1 hour before photocalorimatric polymerization.

6.2.2. Photopolymerization of macromer swollen networks and melts

Macromer swollen in model networks is cured using controlled exposure times and intensities at 365 nm. A 500W Oriel Hg-Xe arc lamp is equipped with an interference filter (5 nm HWHM with maximum transmittence at 365 ± 0.5 nm) and is used as a collimated emission source. Samples 1 mm thick x 8 mm in diameter are placed on a quartz disc and loaded into a quartz-windowed chamber. The chamber can either be open to normal atmospheric conditions or can be purged with argon.

6.2.3. Photo differential scanning calorimetry (DSC)

Reaction rates were measured using a Perkin Elmer DSC-7 with photocalorimeter attachment. The light source was a mercury arc lamp and a narrow band of wavelengths centered at 365 nm was obtained with a monochrometer. Light intensity was adjusted using appropriate neutral density filters. Experiments were performed isothermally at 35 °C. Samples were placed

in an uncovered large volume stainless steel pan and cured using intensities ranging from 0.19 mW/cm^2 to 6.2 mW/cm^2. Several series of samples were run: pure macromer, macromer swollen in a cured PDMS network, and macromer well-mixed with PDMS melts of different molecular. Total reactive macromer mass was between 10 and 20 mg; larger volumes were used for higher macromer molecular weight. All experiments were performed under an inert nitrogen atmosphere.

6.3. Results and discussion

6.3.1. Effects of oxygen inhibition in radical macromer polymerization

Since oxygen is a potent radical reaction inhibitor,[13] even low concentrations strongly affect methacrylate photopolymerization. Host networks with 30% dissolved macromer were photopolymerized under normal atmospheric concentrations of oxygen and in either argon or nitrogen. 1 mm thick samples were placed with one side contacting a quartz plate (side A) and one open to either air or inert gas (side B). After irradiation at 4 mW/cm^2 for 1 hour, samples in an inert atmosphere had 0% extractables. Samples polymerized in the presence of oxygen, however, still had over 40% extractables. In addition, macroscopic shape change was exhibited by samples cured under oxygen; the specimen edges curve toward side B, corresponding to a relative expansion of area on the A face. Although oxygen is initially at equilibrium within the sample, as photopolymerization progresses it is depleted by reaction with active radicals to form peroxy radicals. It is simultaneously replenished by diffusion into the sample from only one surface, creating a gradient in oxygen concentration. Thus, polymerization of macromer proceeds more rapidly near side A. The resulting concentration gradient drives macromer from side B towards side A. Macromer then macroscopically redistributes and induces shape change. Thus, the presence of oxygen leads to incomplete reactive group conversion and contributes to shape

changes during and after photopolymerization.

All further experiments in this chapter will be performed under an inert atmosphere. For photocalorimetry experiments, the DSC chamber is purged with nitrogen for a series of times (5, 10, 15, and 30 minutes). Increasing purge time from 5 to 10 minutes increases maximum reaction rates and decreases initial delays in reaction due to oxygen inhibition. For 15 and 30 minute purges, no initial lag time was observed, maximum reaction rates were equivalent, and overall reaction rate profiles were equivalent.

6.3.2. Salient characteristics of macromer photopolymerization

Effective application of photopolymerizable macromer-matrix systems requires control of reaction kinetics. However, macromers endcapped with photoreactive groups have considerably different reaction kinetics than reactive monomers. It is therefore necessary to map out the reaction space for irradiation dose and material parameters. One of the most distinct features exhibited by silicone macromer systems is the ability to attain complete reactive endgroup conversion. Even bulk macromer, which has the greatest potential to exhibit vitrification with polymerization, reaches complete conversion at ambient temperature in minutes using low irradiation intensities. For 1000 g/mol macromer with 0.75% by weight DMPO, conversion reaches > 99% in less than 7 minutes for an irradiation intensity of 6 mw/cm^2. In comparison, maximum conversion in mono- or multi-functional methacrylate monomers is limited to less than 60% at ambient temperatures.[3, 8-11]

When macromer is diluted into either a covalent network or polymer melt, the reaction rate trajectory slows because of reactive endgroup dilution. Although peak polymerization rates decrease, full endgroup conversion is attained in comparable time to that of bulk macromer (figure 6.2). When macromer is diluted to 30% wt in an unentangled PDMS melt with 0.25%

DMPO per total weight and 6.2 mW/cm^2 irradiation dosage, 99% conversion is attained at 8 minutes for 500 g/mol, 10 minutes for 1000 g/mol, 13 minutes for 3000 g/mol, and 24 minutes for 5000 g/mol macromer. For 1000 g/mol macromer, this is roughly 1.4x the time required for macromer to reach 99% conversion in bulk.

The time and irradiation dosage required to reach a desired conversion are of central importance to photopolymer applications. Prior literature on photopolymerization shows that light intensity can be used to adjust reaction rate, all other parameters held constant.[3, 12, 14, 15] However, 0th order dependence on irradiation intensity is seen over three orders of magnitude for polymerization of 30% wt 1000 g/mol macromer with 1% DMPO by total wt in a covalently crosslinked network figure 6.3). Although 0th order dependence on intensity is uncommon, it is known to occur for radical polymerizations in which photoinitiator radicals play a dominant role in terminating growing polymer chains.[13] Contrarily, when photoiniator concentration is decreased by one order of magnitude to 0.08% total wt, polymerization kinetics become moderately dependent on incident intensity (figure 6.4). A thirty-fold increase in irradiation intensity from 0.19 mW/cm^2 to 6.2 mW/cm^2 reduces the time taken to reach 50% conversion by approximately half. Similarly, if irradiation intensity is kept low (0.28 mW/cm^2), polymerization kinetics vary with photoinitiator concentration when all other parameters are held fixed; endgroup conversion progresses more quickly with higher photoiniator concentrations (figure 6.5). Thus, judicious choice of photoinitiator concentration and irradiation intensity allows alteration in the time to attain a specific endgroup conversion. For the purpose of determining rate constant for polymerization and termination, photo-calorimetry studies are performed in the low-intensity, low photoinitiator regime.

6.3.3. Reaction rate schemata

The previous plots have all been calculated using photo DSC where heat flow is measured during polymerization for a known amount of reactive macromer. From heat flow and macromer sample weight, we calculate that the heat evolved per double bond conversion is approximately 13.2 kcal/mol. This value is quite close to the theoretical value of ΔH = 13.1 kcal/mol,[16, 17] so we use the theoretical value for all further calculations. The reaction rate can therefore be directly obtained by normalizing total heat flow with the amount of sample reacted. As we noted above, photoinitiator concentration, irradiation intensity, and macromer concentration all have an effect on reaction rates. In order to quantify the extent of these changes, it is necessary to determine a theoretical rate equation. The rate of reaction, or rate at which monomer is consumed, is given by:

$$-\frac{d[M]}{dt} = R_i + R_p \tag{6.1}$$

where [M] is monomer concentration, t is time, R_i is the initiation rate, and R_p is the propagation rate. For most polymerizing systems, the rate of initiation is much lower than the rate of propagation. Also, initiator radical concentrations are generally several orders of magnitude lower than propagating species radical concentrations.[13] As such, neglecting R_i, the rate of reaction is:

$$-\frac{d[M]}{dt} = R_p \tag{6.2}$$

The propagation rate is a superposition of all lengths of reactive radical chains ($[M\cdot] = \sum_{n=1}^{\infty} [M_n\cdot]$); assuming equivalent reactivity for all [M_n•], we obtain:

$$R_p = k_p[M][M\cdot] \tag{6.3}$$

where k_p is the propagation rate constant and [M•] is the propagating radical concentration. It is important to note that, although k_p is referred to as a constant, it is inherently dependent on macromer and reactive radical diffusivity. For highly reactive systems, such as methacrylate radical polymerization, a radical and an unreacted macromer in close proximity will react quickly. If macromer concentrations are not extraordinarily high, a macromer molecule and radical will have to diffuse towards each other before reacting. If the diffusion rate of either species changes throughout the reaction, k_p will also change.

For photopolymerization, the initiation rate can be expressed by

$$R_i = 2\phi I_{abs} \tag{6.4}$$

where I_{abs} is the molar intensity of light absorbed and ϕ is the fractional number of radicals that initiate propagating chains as compared to the number of absorbed photons. The number 2 in this equation involves the assumption that two equally reactive radicals are produced when a photon is absorbed. Assuming only a small fraction of incident light is absorbed by the sample,

$$I_{abs} = \varepsilon I_0 [A] b \tag{6.5}$$

where ε is molar absorptivity, I_0 is incident light intensity, [A] is photoinitiator concentration, and b is the thickness of the irradiated sample. UV spectrometry measurements show that less than 5% of photoinitiator is consumed for complete macromer conversion for photoinitiator concentrations ranging from 0.03 to 0.25%. Combining equations 6.4 and 6.5, we obtain:

$$R_i = 2\phi\varepsilon I_0 [A] b \tag{6.6}$$

There are, however, several problems with the assumptions made for the reaction rate in equation 6.6. First, the photonitiator, DMPO, does not dissociate into two equally reactive primary radicals.[18, 19] Instead, a highly reactive benzoyl and less reactive benzoyl ketal radical are produced. The second issue is that we are not only unable to measure ϕ, but it changes with

sample viscosity due to a solvent cage effect. If the primary radicals are unable to diffuse away from each other, they may recombine to produce ineffective molecules.[20] Fortunately, as discussed in chapter III, sample viscosity should not change excessively even at complete conversion of macromer. Kurdikar and Peppas have derived a viscosity based value of ϕ for DMPO; this value is expected to be between 0.3 and 0.5 for our systems.[18] Because of the combined uncertainty of the theoretical prediction for ϕ and reactivity of the two primary radicals, we use a combined value of 1 for these two parameters.

In the absence of direct measurements of radical concentrations, it is commonly assumed that radical concentration initially increases rapidly and then attains a steady state concentration at small conversions. The rate of radical initiation would then equal the rate of radical termination. By directly measuring radical concentrations with electron paramagnetic resonance (EPR), it has been shown that this assumption does not precisely hold true.[5] Radical concentrations increase with time as radical size increases and termination rates decrease. However, comparing photopolymerization results between Fourier transform infrared (FTIR) experiments and EPR experiments, Berchtold et al., showed that absolute reaction rates and kinetic constants were not severely under or over predicted when using a pseudo steady state assumption.

There are two possible species that propagating radicals can terminate with: other propagating radicals or initiator radicals. For high monomer concentrations or low initiation rates, termination occurs mainly between two propagating radicals ($R_{t:m,n}=k_{t:m,n}[M_m\bullet][M_n\bullet]$); for low monomer concentrations or very high initiation rates, propagating radicals may terminate with initiator, or primary, radicals ($R_{t:A,n}=k_{t:A,n}[A\bullet][M_n\bullet]$). We will first discuss the rate law obtained by assuming that termination is only between two propagating radicals. In this case,

$$R_i = R_t = 2k_t[M\cdot]^2 \tag{6.7}$$

where R_t is the termination rate and k_t is the termination constant. The factor of 2 in this equation is because two radicals recombine during termination. It is important to note that this k_t is the average value for all propagating radicals. Since k_t depends on diffusion rate, radicals with degree of polymerization, N, >1 should have much smaller values for the termination constant. The validity of this assumption will be addressed in further detail later in the chapter. Rearranging equation 6.7 to obtain [M•] and substituting into equation 6.3, we obtain

$$R_p = k_p[M]\left(\frac{R_i}{2k_t}\right)^{1/2} \tag{6.8}$$

for the polymerization rate. Thus, although the reaction rate is linear in macromer concentration, it is only increases with the 1/2 power for initiation rate. Replacing R_i in equation 6.5 with this formulation results in:

$$R_p = k_p[M]\left(\frac{2\phi\varepsilon I_0[A]b}{2k_t}\right)^{1/2} \tag{6.9}$$

As such, if termination proceeds solely through a bimolecular reaction of propagating radicals, the reaction rate will be linear in macromer concentration but only to the ½ power in both irradiation intensity and photoinitiator concentration.

For systems with either very low macromer concentration or very high initiation rates, we no longer expect the radical termination rate to be as described in Equation 6.4. Instead of two propagating radicals reacting, a primary initiator radical would terminate a propagating radical. Using the steady state assumption,

$$R_i = R_t = k_{tp}[A\cdot][M\cdot] \tag{6.10}$$

where k_{tp} is the rate constant for primary radical termination and [A•] is primary radical concentration. Since many of the primary initiator radicals are no longer initiating polymer propagation, we rewrite R_i as

$$R_i = k_i[A\cdot][M] \tag{6.11}$$

where k_i is the initiation rate constant. Combining Equations 6.3, 6.9, and 6.10, the reaction rate is

$$R_p = \frac{k_p k_i}{k_t}[M]^2 \tag{6.12}$$

Thus, if primary radical termination occurs in our system, we expect the reaction rate to scale with $[M]^2$ instead of [M].

As mentioned previously, apparent k_t values used in the pseudo steady state assumption are dependent on diffusion and are averaged over all lengths of radical chains ($k_t = \sum_{n=1}^{\infty} k_{t,N}$, N= degree of polymerization). Since macromers have two reactive reactive endgroups, they will begin to form networks or clusters even at low degree of polymerization. We postulate two distinct species of propagating radicals: single macromers that can diffuse quickly and immobile clusters ($k_t = k'_t + k''_t$), where k_t' is for single macromers and k_t'' is for clusters. At early times, the majority of propagating radicals will be single macromers with high diffusivity. As time progresses, an increased population of radicals will be immobile clusters. Thus, as reaction time and conversion progress, apparent k_t will decrease significantly.

6.3.4. Comparison of photopolymerization rates in gel and melt

In Chapter III, we learned that the structure of microphase separation depends on host

network modulus. In contrast, here we find minimal differences between macromer reaction rates when swollen in a highly crosslinked network, a well-entangled melt, and a non-entangled melt. Using identical photoinitiator concentration and irradiation intensity, polymerization of 1000 g/mol macromer at 30 wt % concentration has very similar reaction trajectory and very similar maximum R_p. However, there is a small successive shift of maximum reaction rate towards higher conversion as one proceeds from a covalent host network to an entangled melt to an unentangled melt. Higher viscosity materials generally decrease macromer diffusion rates. Intuitively, R_p would be therefore be expected to be slower at any given conversion. However, the opposite occurs. The concentration of methacrylate groups is sufficiently high so that the propagation reaction is not limited by diffusion of macromer to a propagating radical. Propagating radicals, however, are moderately dilute and must diffuse together for bimolecular termination to occur. As matrix mobility is reduced, the rate of reaction increases due to reduced termination relative to propagation. Additional comparison of networks and entangled melts at other reaction conditions and molecular weights reveals similar trends. Since the deviation between different hosts is minimal, we use non-entangled melts as the host for studies of reaction kinetics using DSC.

6.3.5. Macromer concentration and reaction rate

Although the quasi steady state approximation does not hold for our system if we assume k_t to be constant throughout reaction conversion, dependence of reaction rate on the initial concentration of reactive endgroups for a specific macromer molecular weight is relatively robust. For 500 to 5000 g/mol macromer molecular weight, we find that the effect of macromer concentration from 15 to 60 wt % is approximately linear while holding photoiniator concentration and irradiation intensity constant (figure 6.7). Several series of experiments were run using different photoinitiator content and irradiation intensity. The approximately linear [M]

dependence is seen even under reaction conditions that create the highest number of primary radicals (highest intensity permitted by DSC light source and highest photoinitiator concentration permitted by solubility). The high concentration primary radical regime is where there is the greatest chance that primary radical termination becomes dominant, which would result in R_p having $[M]^2$ dependence. Instead of $[M]^2$ dependence, the data show a strong linear relationship between R_p and $[M]$; maximum reaction rates and overall shapes of reaction curves match well with $[M]$ scaling. There are two important deviations, however. When using linear scaling from a lower macromer weight fraction, we do not capture a "shoulder" that is seen during autoacceleration for higher concentration. The autoacceleration shoulder observed for ϕ=0.6 resembles that seen during photopolymerization in bulk macromer (figure 6.1) and is commonly seen in photopolymerization.[5, 9, 10, 16, 21] Long-time and high conversion deviations from linear scaling indicate that, as macomer concentration decreases to very low levels, some primary radical termination may occur. Thus, even though the majority of the reaction proceeds in the domain of propagating-propagating radical termination, at times near complete conversion propagating radicals may have negligible diffusivity.

6.3.6. Effects of irradiation intensity and photoinitiator content

Radical initiation rates are a function of total light absorbance and, therefore, photoinitiator content and irradiation intensity. Increasing intensity or photoinitiator concentration will also increase the rate of generation of $[A\bullet]$. An increase in primary radical concentration may not, however, translate into increased production of $[M\bullet]$ since the concentration of both $[A\bullet]$ and $[M\bullet]$ are governed by competition between generation and consumption rates. For the pseudo-state assumption given in section 6.3.2, the effect of $X=(\varepsilon\phi I_0[A])$ is $X^{1/2}$. Experimentally, we find behavior ranging from X^0 to $X^{0.5}$. This is rather

surprising considering that the system reaction rate remains linear with [*M*] for all values of *X*.

To characterize intermediate *X* behavior, we estimate the value of the exponent, α, that best describes the experimentally observed changes in R_p with I_0 and [*A*] where

$$R_p \propto [M](I_o[A])^{\alpha} \tag{6.13}$$

Evaluation is empirical and the best fit is determined by varying α in increments of 0.05 and choosing the value that produces the best match for both maximum reaction rates and reaction profiles. For example, as DMPO concentration is increased from 0.08 wt % to 0.25 wt %, rescaling R_p values from 0.08 wt % DMPO ([*A*]=(0.25 / 0.08)$^{\alpha}$ where a=0.3) gives good accord with experimental R_p values for 0.25 wt % DMPO (figure 6.8). It is important to note that, even when α is not equal to 1/2 as suggested in equation 6.8, the reaction rate is still linear in [*M*].

A similar analysis is performed by altering irradiation intensities while holding macromer weight percent, photoinitiator concentration, and macromer molecular weight constant. Higher irradiation intensity leads to an increase in maximum reaction rates (figure 6.9). Using 2.1 mW /cm^2 irradiation intensity as a basis, we calculate α = 0.2 for 6.2 mW/cm^2 and α = 0.5 for both 0.56 mW/cm^2 and 0.19 mW/cm^2. In Table 1, α is shown for a wide array of different irradiation intensities and photoinitiator concentrations. For high values of irradiation intensity and photoinitiator content, α is 0.1; as we decrease both of these variables, α increases to a steady value of 0.5 as predicted by equation 6.8. It is unexpected that, even though we increase initiation rates enough to change scaling behavior, we never enter a region where the reaction rate has quadratic dependence on monomer concentration, which would indicate primary radical termination.

6.3.7. Reaction rate comparison for different molecular weight macromer

In section 6.3.4., we established that for a given macromer molecular weight the reaction rate is linearly related to macromer concentration, i.e., it is proportional to the concentration of reactive methacrylate endgroups. This section examines the qualitatively different reaction trajectories that result from changing PDMS midblock chain length. These differences cannot be captured by linear rescaling to account for differences in end-group concentration (figures 6.10 and 6.11). The analysis methods used in section 6.3.5 for variable power law dependence are also ineffective because the reaction trajectories have altogether different shapes. For example, differences in maximum R_p with conversion and time for 500, 1000, and 3000 or 5000 g/mol occur at very different values and cannot be superimposed.

However, linear scaling behavior for reactive endgroup concentrations between 3000 and 5000 g/mol macromers does show excellent correlation (figures 6.9 and 6.10). Therefore, R_p decreases proportionally to [M] indicating that, for these macromer molecular weights, the pseudo-steady state approximation is valid for the majority of the reaction. The initial increase in reaction rate during the first 30 seconds is a combination of an initial increase in primary radical concentration and decrease in apparent k_t. It is quite surprising that the less mobile macromer species exhibit agreement with pseudo-steady state assumptions and the more mobile 500 g/mol and 1000 g/mol macromer do not.

Since termination only occurs between two propagating radicals, they will have one of three ways of recombining: segmental diffusion, center of mass diffusion, or reaction diffusion. Segmental diffusion is merely diffusion on the length scale of a Kuhn monomer; this is only important if reactive groups functionally overlap. Since we use only 30% macromer and the macromer has long unreactive midblocks, segmental diffusion is unlikely to be an important process. Center of mass diffusion occurs in dilute to semi-dilute systems, and is the expected process for termination at small conversions in these macromer systems. Reaction diffusion

occurs when propagating radicals are completely trapped; monomer species react with two propagating radicals until the two radicals grow together. In most monomers, reaction diffusion is the primary termination process at large conversions. If reaction termination is mainly due to center of mass diffusion, termination rates will decrease if the propagating radical species becomes relatively immobile. Since these macromer have two endcaps, they have the potential to quickly form large non-linear networks with slow diffusion rates. However, if reaction termination occurs by means of reaction diffusion, the termination rate should be proportional to the propagation rate, where

$$k_t = \beta k_p [M] \tag{6.14}$$

and β is a reaction diffusion proportionality constant. Replacing k_t in Equation 6.5 and simplifying,

$$R_p = [M]^{1/2} \left(\frac{k_p}{\beta} \right)^{1/2} \left(\frac{R_i}{2} \right)^{1/2} \tag{6.15}$$

Thus, if termination is diffusion controlled, $R_p^2/[M]$ should remain constant if plotted against reaction conversion. Figure 6.12 shows a plot of $R_p^2/[M]$ against fractional conversion for all four molecular weights of macromer. A plateau region indicates that k_p and k_t are proportional and, therefore, that termination is diffusion controlled. All molecular weights show no sign of a plateau region. This complete lack of reaction diffusion controlled termination makes sense in light of the relatively low reactive endgroup concentrations.

6.3.8. Determination of propagation and termination constants

Additional insight into propagation and termination mechanisms may be obtained if we are able to calculate time dependent kinetic constants. Since both k_t and k_p are dependent on

diffusivities of reactants, they will change over the course of the reaction. In particular, if the reactive medium increases in viscosity or vitrifies, all species' diffusion rates will be retarded. This would decrease both the propagation and diffusion kinetic constants. If the solution viscosity remains nearly the same throughout the reaction, we would expect macromer diffusion rates to stay the same and propagating radical diffusion to decrease with conversion as the radicals increase in size. Thus, k_p would remain somewhat constant throughout the reaction; only k_t would constantly decline since termination is center of mass diffusion, not reaction diffusion, controlled. For these measurements, k_t is apparent k_t as described in Section 6.3.2 and is a superposition of all propagating radical chain length termination constants. Reexamining Equation 8,

$$R_p = k_p[M]\left(\frac{2\phi\varepsilon I_0[A]b}{2k_t}\right)^{1/2} \tag{6.8}$$

R_p can be directly measured using photo DSC, [M] is known, ε is measured with UV spectrometry, b is known, and [A] is known. As mentioned in section 6.3.1, we will set the quantity $2\phi = 1$. The only unknown is the value $k_p/k_t^{1/2}$, which can be evaluated from R_p and conversion at each point in the reaction trajectory. In order to separate these two reaction constants, we need an independent measure of termination kinetics. If we irradiate a sample for some specific time or conversion and then shut off the irradiation source, we can record the decay in R_p due to termination of propagating radicals (figure 6.13). Assuming all radical terminations are between two propagating radicals,

$$\frac{d[M\cdot]}{dt} = -2k_t[M\cdot]^2 \tag{6.16}$$

Rearranging this equation and integrating, we obtain

$$-\frac{1}{[M\cdot]}\Bigg|_{[M\cdot](t=0)}^{[M\cdot](t)} = -2k_t t\Big|_{t=0}^{t} \tag{6.17}$$

Combining Equations 6.16 and 6.3 and evaluating the result gives

$$k_t = k_p \frac{1}{2(t-t_0)} \frac{[M]_t}{R_{p_t}} - \frac{[M]_{t=0}}{R_{p_{t=0}}} \tag{6.18}$$

In particular, $t = 0$ is when irradiation is terminated and time t is some short time (5 seconds) afterwards. This method of analysis assumes that k_t and k_p are constant over the time period t-t_0. For long times, k_t will decrease as smaller propagating radicals are consumed and non-mobile cluster radicals become the dominant radical concentration. For macromer molecular weights of 500 g/mol, 1000 g/mol, and 3000 g/mol, k_t is significantly larger at early times than it is as reaction conversion increases (figure 6.14) as is expected for chain length dependent termination. At short times, since propagating radicals will still be either monomeric or dimeric, diffusion rates should still be very high. As conversion progresses and radicals increase in size, the termination rate is drastically reduced.

The propagation rate shows two regimes. At short times, we see an increase which can potentially be attributed to initial unsteady state kinetics as primary radicals are being formed. After this initial increase, we see a slow but steady decline due to decreasing macromer diffusion rates. Diffusion rates decrease as material modulus increases from formation of IPNs. In figure 6.15, we plot the relative value k_p/k_t against fractional conversion for all three macromer molecular weights. The concurrence of data indicates that the methacrylate endgroups have equivalent reactivity for all three molecular weights of macromer. Unlike multifunctional methacrylate monomers or species with a one or two atom spacer between two reactive endgroups, the state of one endgroup (unpolymerized, radical, or polymerized) does not affect the

reactivity of the other endgroup.

6.4. Conclusions

In this chapter, we have examined the kinetics of polymerization for methacrylate endcapped monomers. Unlike polymerization in multifunctional methacrylate or acrylate monomers, we are able to attain complete endgroup conversion even in neat macromer. We also find that, for a specific macromer molecular weight, the reaction rate scales linearly with macromer concentration. Surprisingly, we find that the scaling behavior for irradiation intensity and photoinitiator concentration are strongly dependent on reaction conditions. As irradiation intensity and photoinitiator concentration increase, reaction rate eventually reaches 0th order. This result indicates that, no matter how high photoinitiator concentrations and irradiation intensities are, there is some minimum reaction time required to attain a specific conversion.

Even though macromer polymerization follows a first order rate law in endgroup concentration within a single molecular weight, scaling analysis is not adequate to describe reaction trajectories for different macromer molecular weights. Not only are maximum reaction rates not well quantified, but the extent of reaction at which they occur is also poorly predicted. It is also very surprising that, although 500 g/mol and 1000 g/mol macromers do not support a pseudo-steady state assumption, 3000 and 5000 g/mol are well described. Finally, we have shown effect of chain length dependent termination in describing reaction rate trajectories. It is highly suggested that EPR experiments be performed to attain actual radical concentrations for these systems. These values would allow direct calculation of kinetic constants using a simple first order rate equation that we have shown to hold for these systems. Dark reaction radical concentration measurements would also allow us to more fully explore the effects of chain length termination dependence.

6.5. Tables

Table 6.1. Values for the scaling exponent α, where $R_p=[M](2\phi I\varepsilon[A])^{\alpha}$. Systems are polymerized with 30% 1000 g/mol macromer, contain a variable amount of photoinitiator and are irradiated with different light intensities.

	0.03% DMPO	0.08% DMPO	0.25% DMPO
6.2 mW/cm^2	0.2	0.2	0.1
2.1 mW/cm^2	0.5	0.3	0.3
0.56 mW/cm^2	0.5	0.3	0.3
0.19 mW/cm^2	0.5	0.3	0.3

6.6. Figures

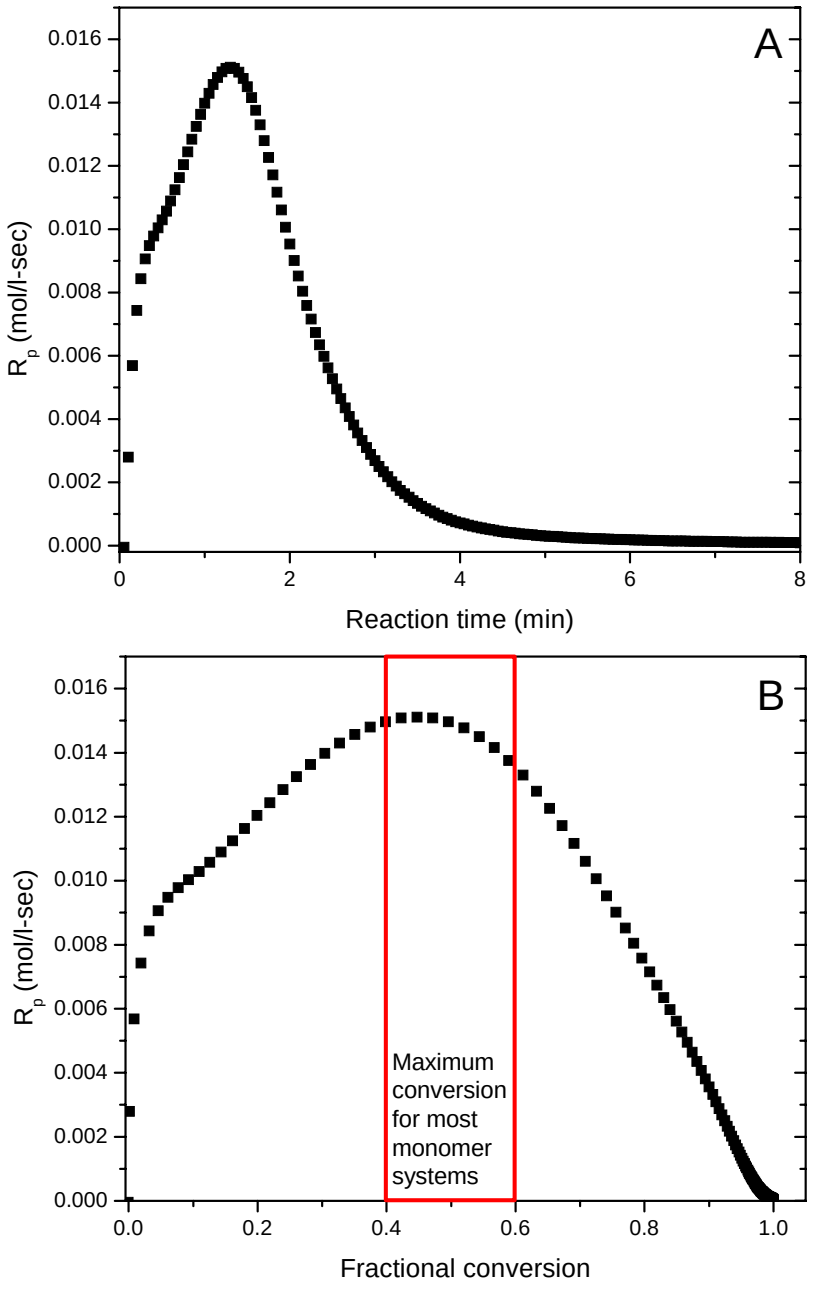

Figure 6.1. Reaction rate plotted against time (Plot A) and fractional conversion (Plot B) for pure 1000 g/mol macromer. Similar reaction profiles sith complete conversion are seen from 500 to 5000 g/mol macromer. Samples are polymerized at 6 mW/cm^2 with 0.75% by weight photoinitiator. Conversion for most monomer systems is quenched between 40 and 60% due to vitrification.

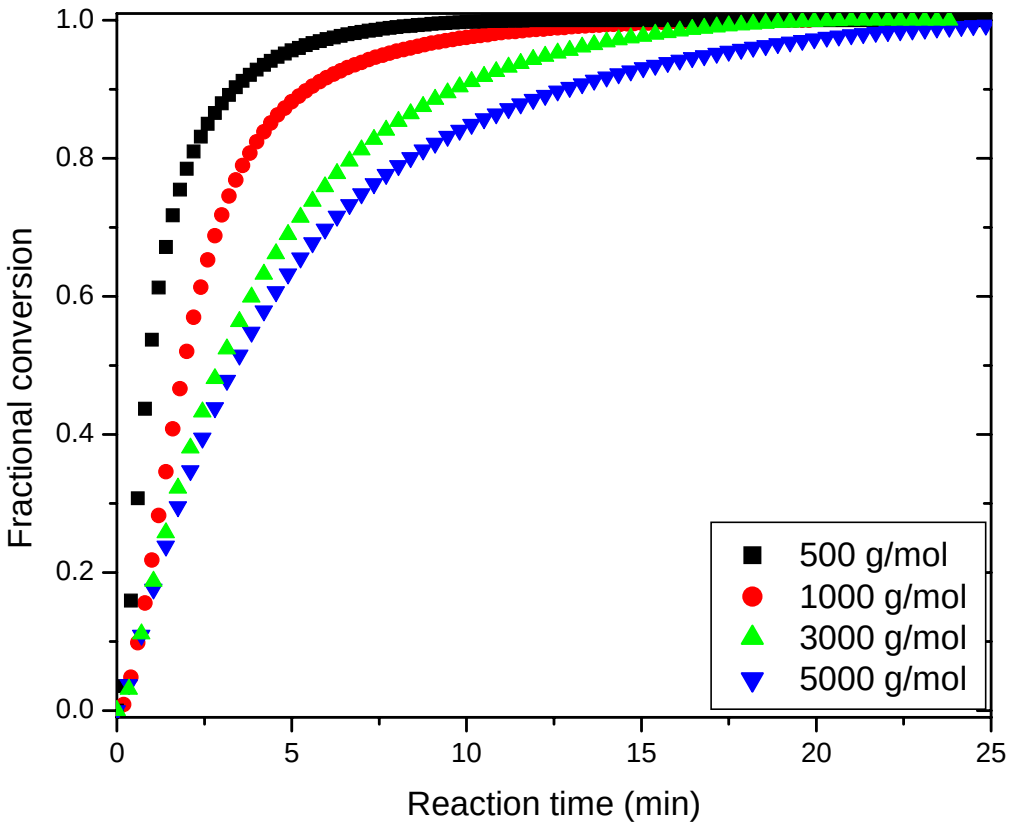

Figure 6.2. Fractional conversion plotted against reaction time for different macromer molecular weights. All samples are 30% macromer in a short chain PDMS melt, are irradiated at an intensity of 6.2 mW/cm^2, and have 0.25 % photoinitiator by total sample weight.

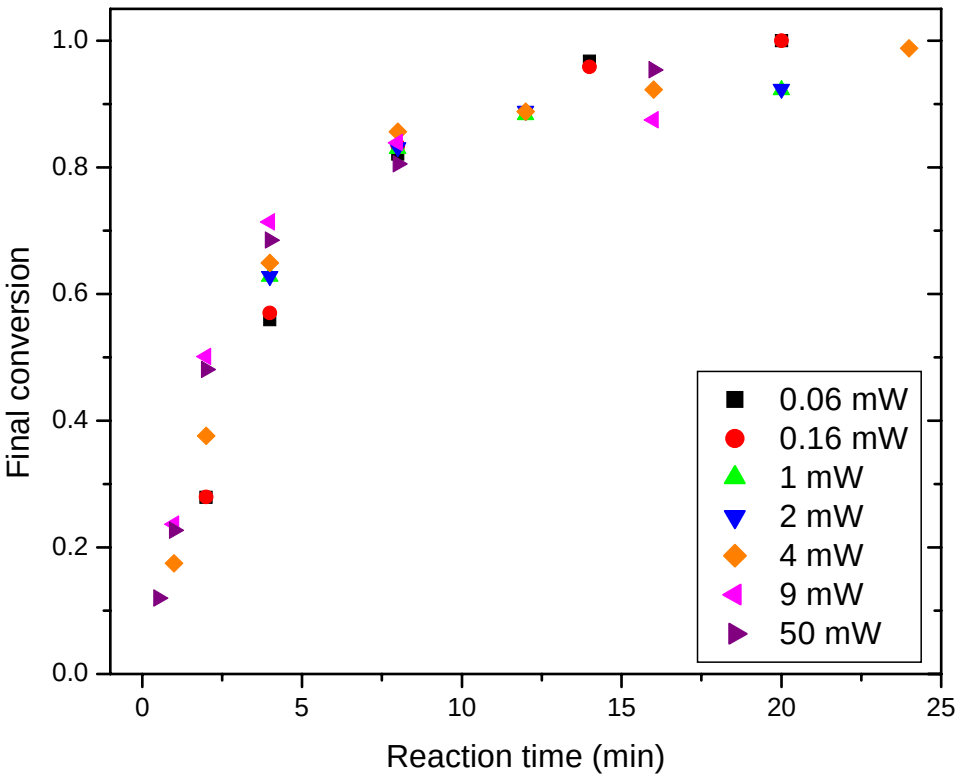

Figure 6.3. Fractional conversion plotted against reaction time for multiple irradiation intensities as determined by extraction experiments. Irradiation intensities are altered by three orders of magnitude while macromer (30% by weight, 1000 g/mol) and photoinitiator content (1% by total weight) are held constant.

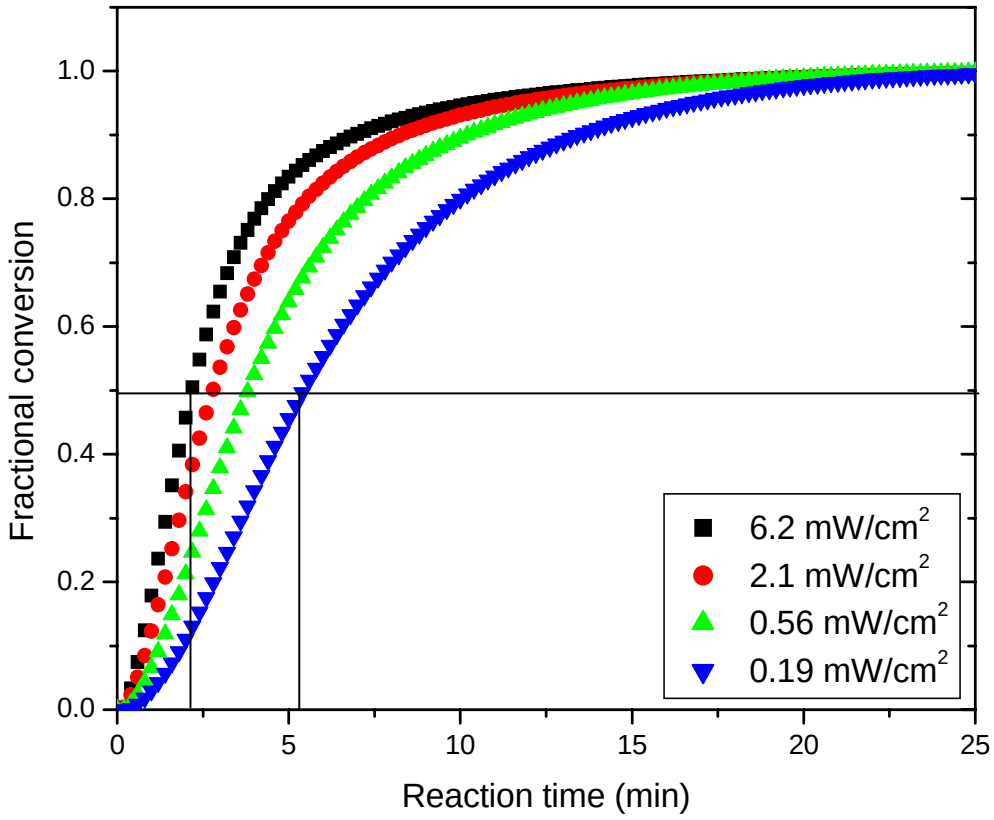

Figure 6.4. Fractional conversion plotted against reaction time for different irradiation intensities. All samples are 30% 1000 g/mol macromer in a short chain PDMS melt with 0.08% by weight photoinitiator. Lines are drawn to indicate the difference in reaction time to obtain a specific conversion.

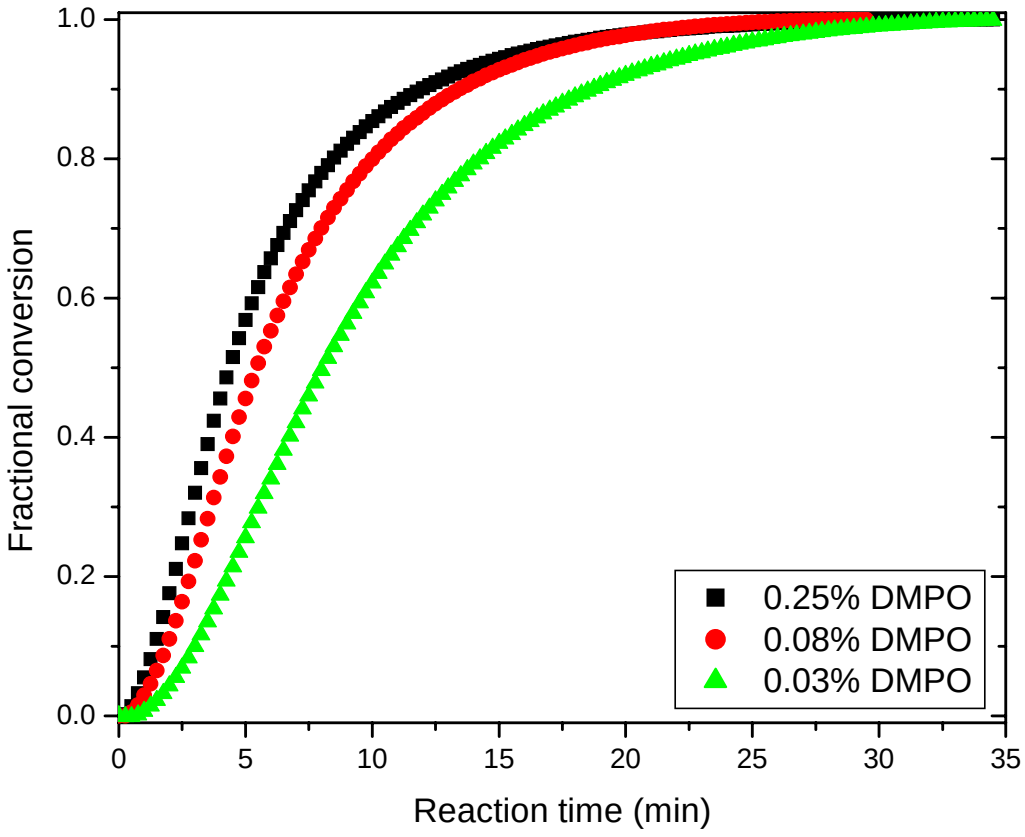

Figure 6.5. Fractional conversion plotted against reaction time for different photoinitiator (DMPO) content. All samples are 30% 1000 g/mol macromer in a short chain PDMS melt and are irradiated at an intensity of 0.28 mW/cm^2.

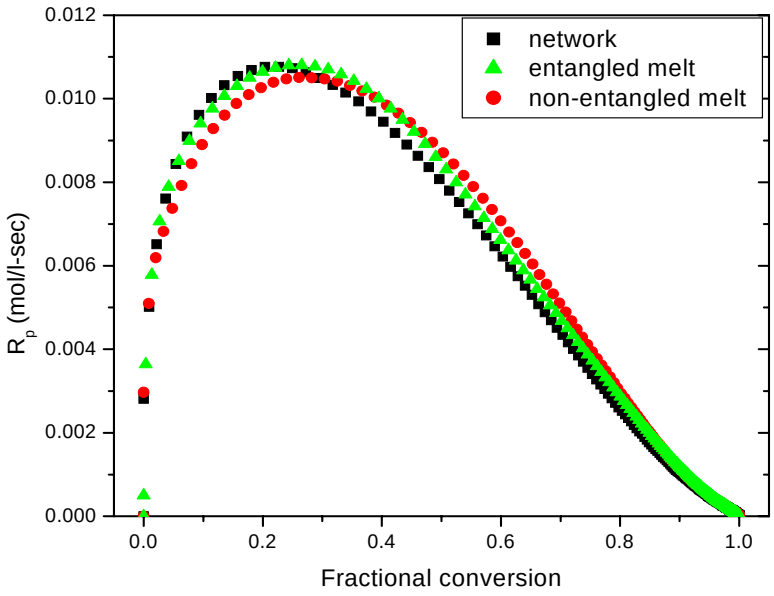

Figure 6.6. Reaction rate plotted against fractional conversion for 30 wt % 1000 g/mol macromer in one of three PDMS hosts: a cross-linked network, highly entangled melt, or non-entangled melt. An irradiation intensity of 6.2 mW/cm^2 and photoinitiator concentration of 0.25% by total sample weight is used for all three hosts.

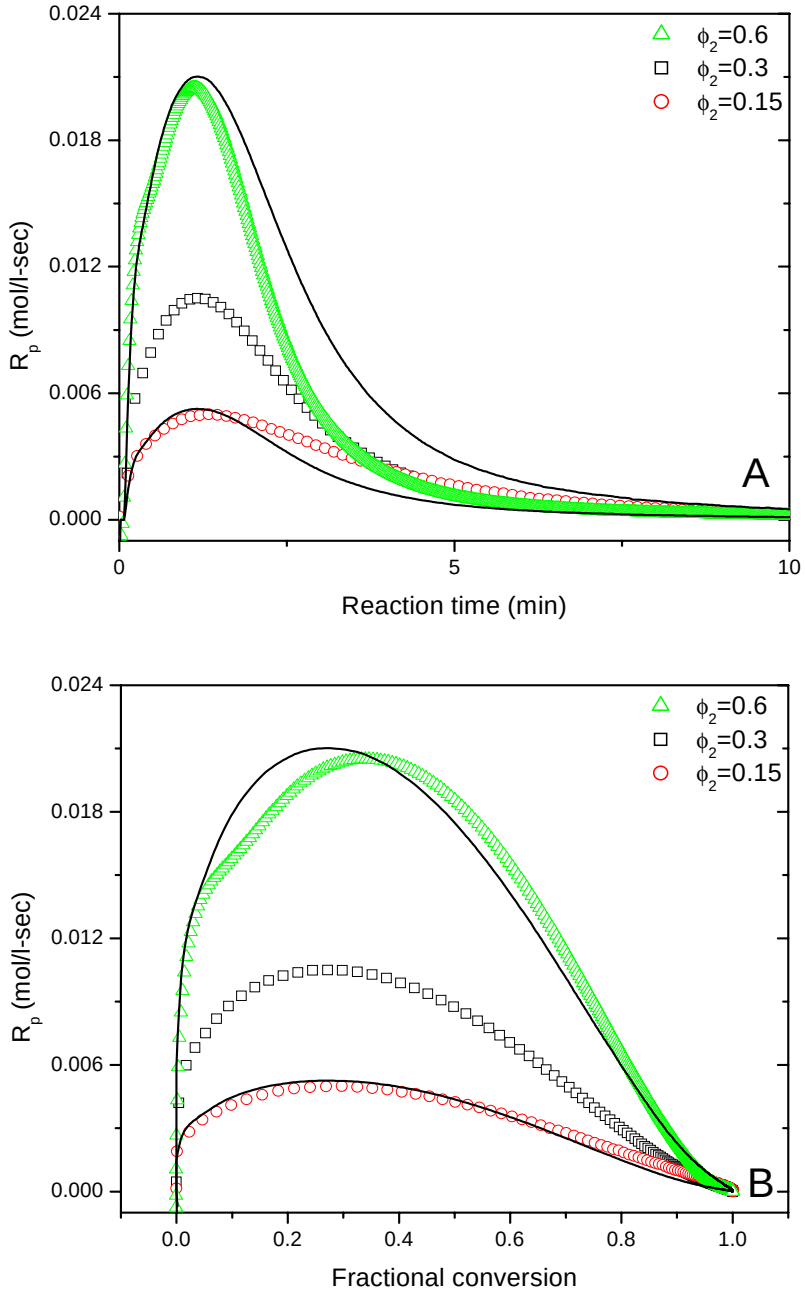

Figure 6.7. Reaction rate plotted against time (Plot A) and fractional conversion (Plot B) for different macromer weight fraction (ϕ_2). Macromer of 1000 g/mol molecular weight is polymerized at 6 mW/cm^2 with 0.25% by total weight photoinitiator. Lines show the reaction trajectory for ϕ_2 = 0.3 re-scaled linearly with concentration.

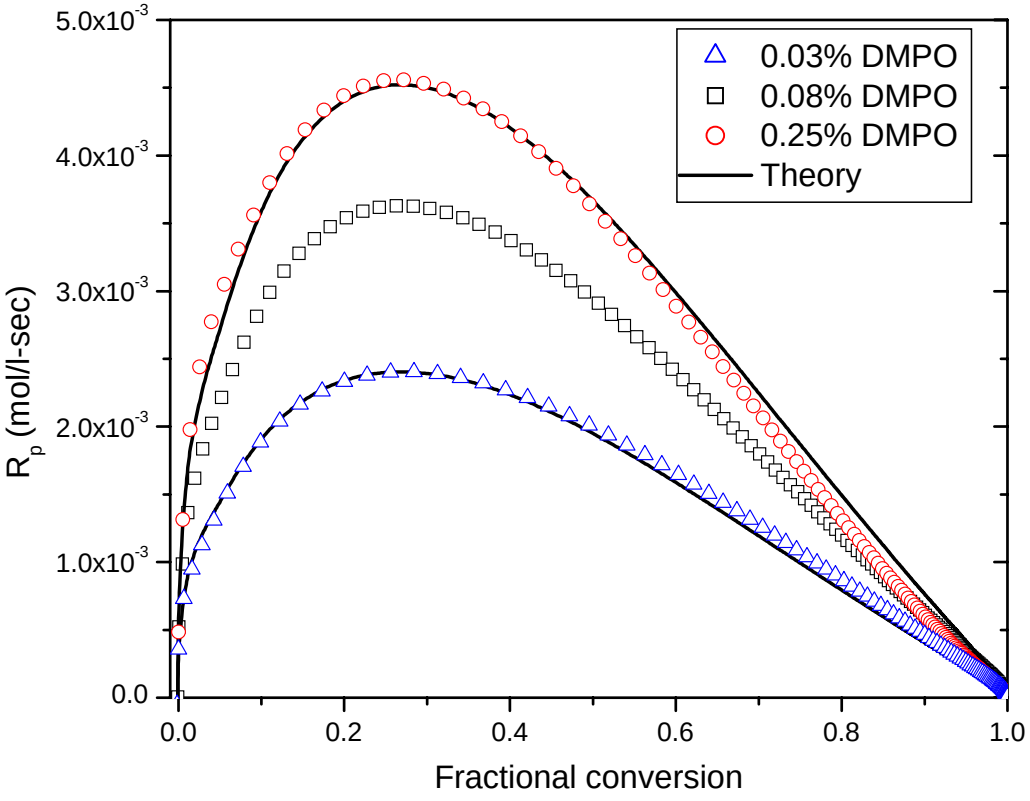

Figure 6.8. Reaction rate plotted against fractional conversion for different concentrations of photoinitiator. Systems are polymerized at 2.1 mW/cm^2 for 30% 1000 g/mol macromer. Lines are reaction rate profiles calculated using a variable α, where $R_p=[M](2\phi I\varepsilon[A])^{\alpha}$. The upper line has α = 0.3 and the lower has α = 0.5.

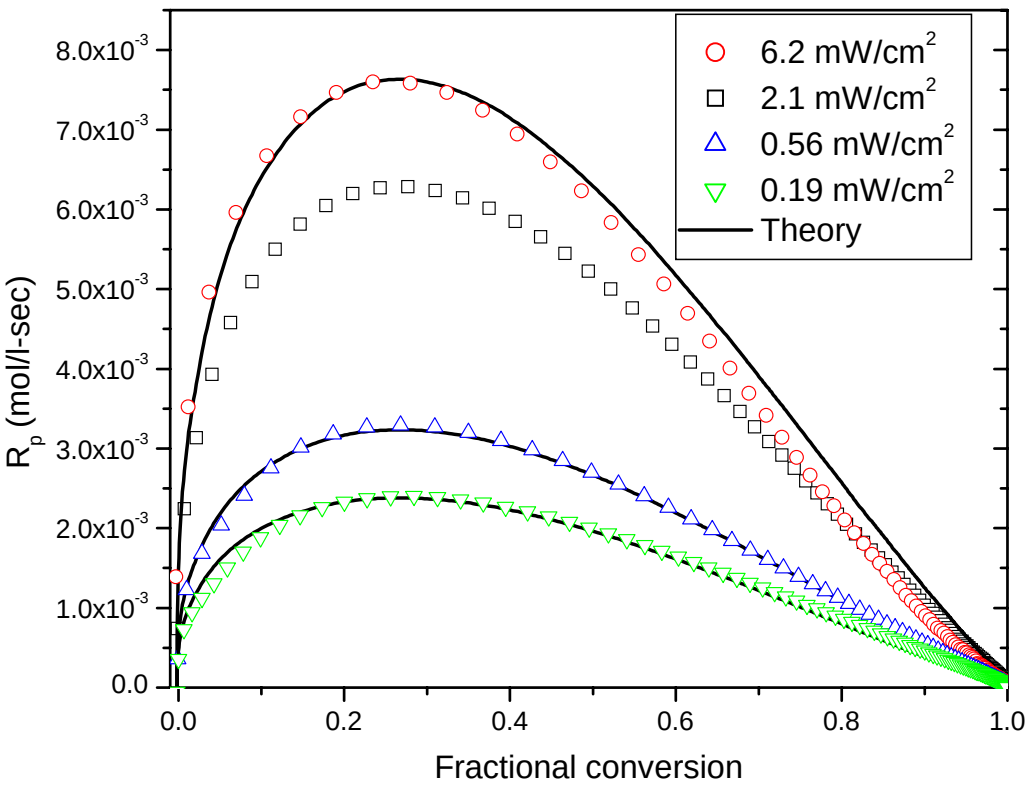

Figure 6.9. Reaction rate plotted against fractional conversion for different irradiation intensities. Systems are polymerized with 30% macromer and contain 0.03% by weight photoinitiator. Lines are reaction trajectories calculated by rescaling the observed reaction rate profile for 2.1mW/cm^2. α, where $R_p=[M](2\phi I\varepsilon[A])^{\alpha}$ is 0.2 for the 6.2 mW/cm^2 and 0.5 for the 0.56 and 0.19 mW/cm^2.

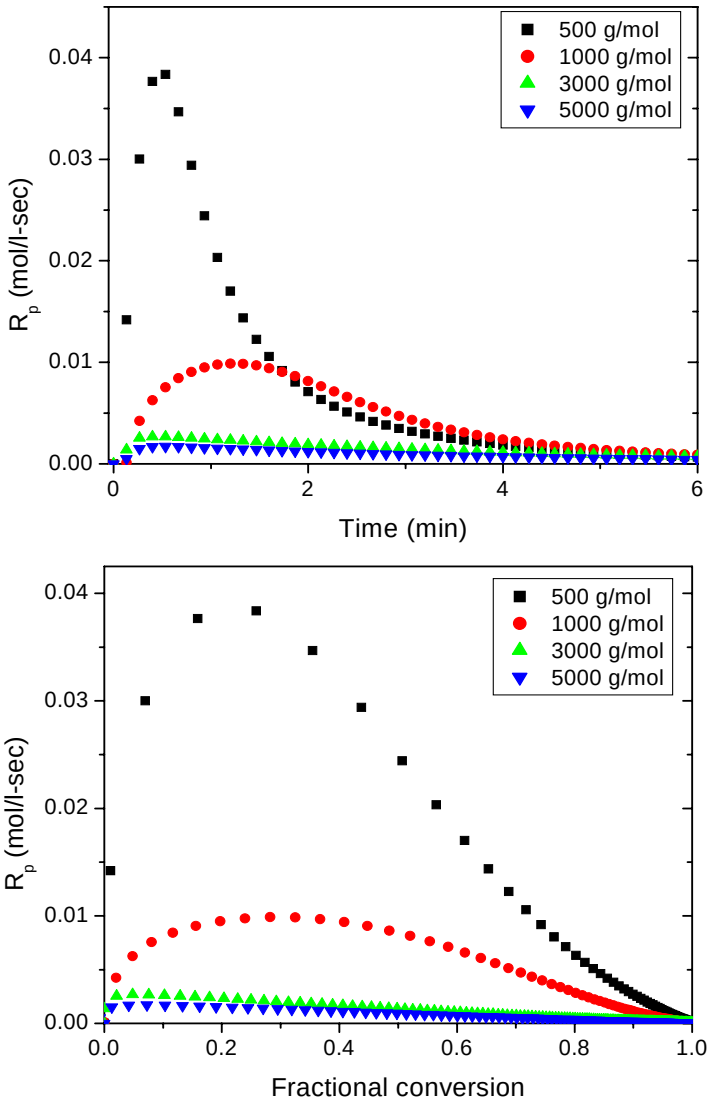

Figure 6.10. Reaction rate plotted against reaction time and fractional endgroup conversion for different macromer molecular weights.All samples are 30% macromer in a short chain PDMS melt, are irradiated at an intensity of 6.2 mW/cm^2, and have 0.25 % photoinitiator. Endgroup concentrations are 1.2 mol/l for 500 g/mol, 0.6 mol/l for 1k g/mol, 0.2 mol/l, and 0.12 mol/l for 5000 g/mol.

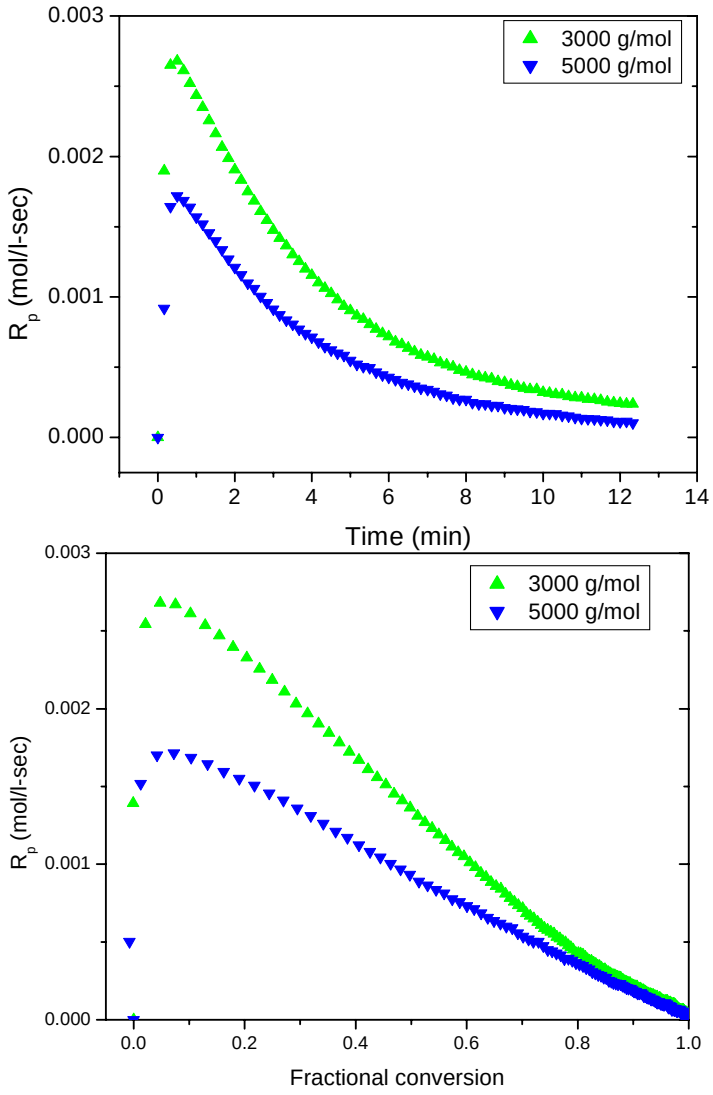

Figure 6.11. Reaction rate plotted against reaction time and fractional endgroup conversion for different macromer molecular weights.All samples are 30% macromer in a short chain PDMS melt, are irradiated at an intensity of 6.2 mW/cm^2, and have 0.25% photoinitiator. Endgroup concentrations are 0.2 mol/l, and 0.12 mol/l for 5000 g/mol.

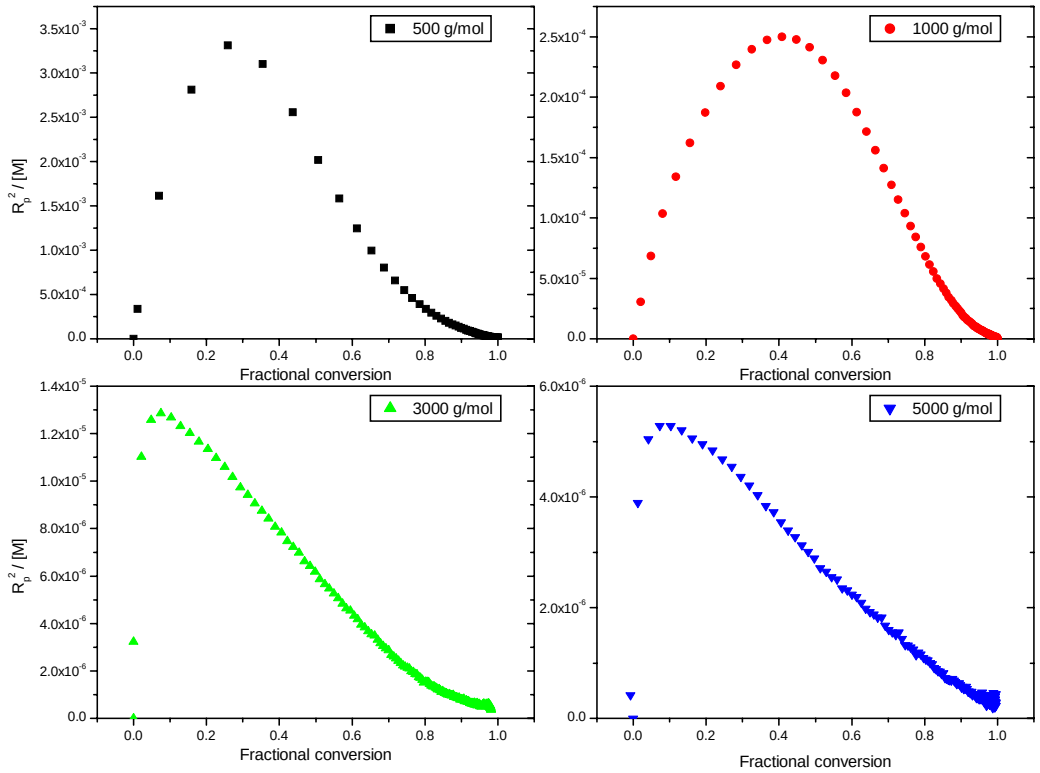

Figure 6.12. $R_p^2/[M]$ plotted against fractional conversion for different macromer molecular weights. All samples are 30% macromer in a short chain PDMS melt, are irradiated at an intensity of 6.2 mW/cm^2, and have 0.25% photoinitiator.

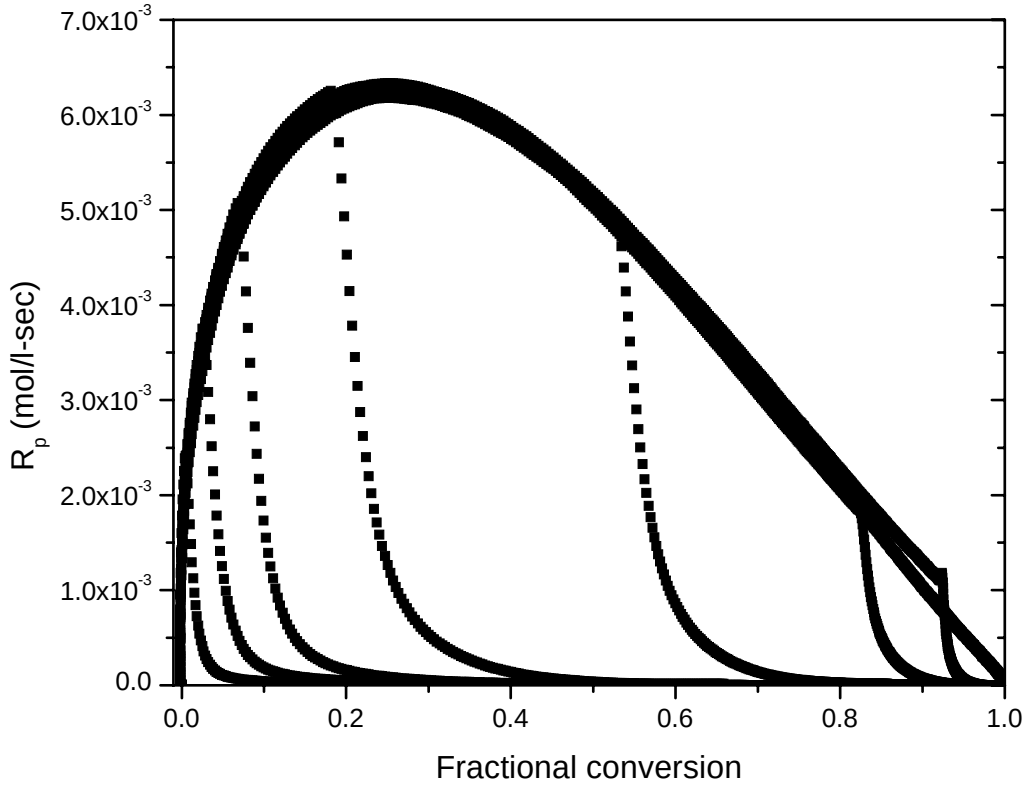

Figure 6.13. Reaction rate plotted against fractional conversion for 30% 1000 g/mol macromer in a short chain PDMS melt. Samples contained 0.03% photoinitiator and were irradiated at 2.1 mW/cm^2. The full curve in this plot is for a reaction taken to completion; partial curves are from reaction where irradiation is terminated at a specific time. Analysis of dark time reaction rates gives information on termination kinetics. Sparse data points are applied for visual purposes; a faster data acquisition rate of 1 Hz is used for experimental calculations.

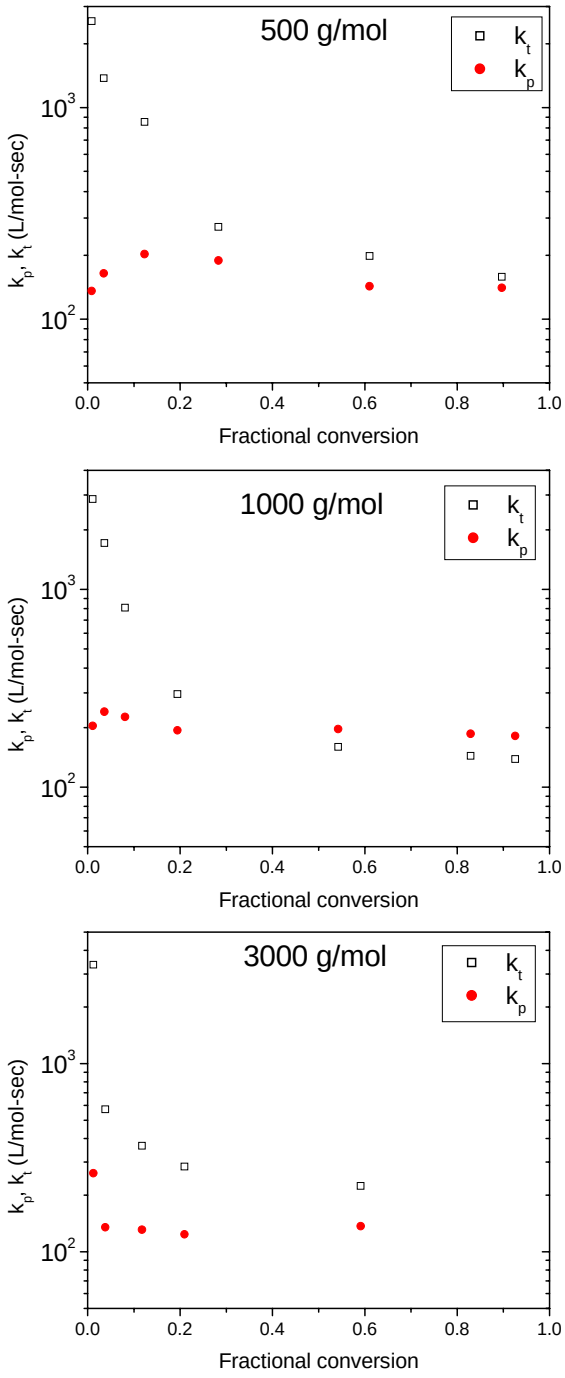

Figure 6.14. Propagation (k_p) and termination (k_t) reaction constants plotted against time for different molecular weight macromers. Samples were 30% macromer in a short-chain PDMS host, irradiation was at 2.1 mW/cm^2, and photoinitiator content was 0.03%.

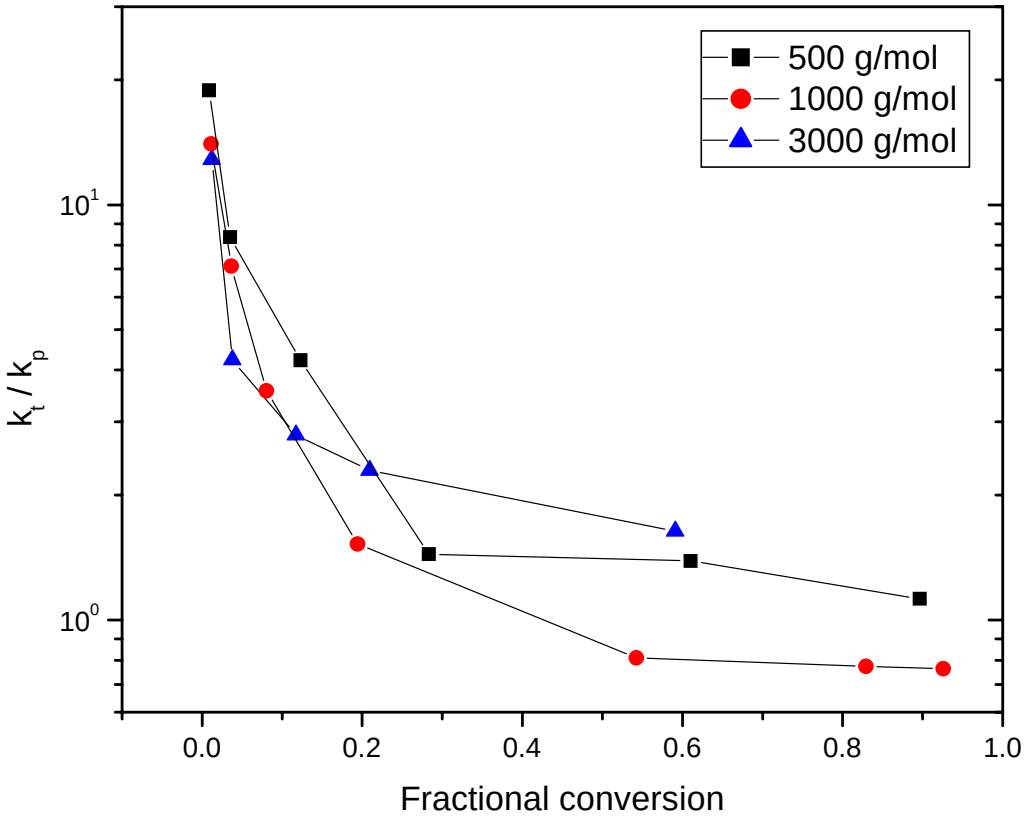

Figure 6.15. Propagation constant (k_p) divided by termination constant (k_t) plotted against fractional conversion. Reaction conditions are the same as those used in Figure 13.

6.7. References

1. Urabe, H., K. Wakasa, and M. Yamaki, Application of Multifunctional Base Monomer to Dental Composite Resins. *Journal of Materials Science-Materials in Medicine,* 1990. **1**(3): p. 163-170.
2. Kloosterboer, J. G., Network Formation by Chain crosslinking Photopolymerization and its Applications in Electronics. *Advances in Polymer Science,* 1988: p. 1-60.
3. Anseth, K. S., C. M. Wang, and C. N. Bowman, Reaction Behavior and Kinetic Constants for Photopolymerizations of Multi(Meth)Acrylate Monomers. *Polymer,* 1994. **35**(15): p. 3243-3250.
4. Lee, J. H., R. K. Prud'homme, and I. A. Aksay, Cure depth in photopolymerization: Experiments and theory. *Journal of Materials Research,* 2001. **16**(12): p. 3536-3544.
5. Berchtold, K. A., T. W. Randolph, and C. N. Bowman, Propagation and termination kinetics of cross-linking photopolymerizations studied using electron paramagnetic resonance spectroscopy in conjunction with near IR spectroscopy. *Macromolecules,* 2005. **38**(16): p. 6954-6964.
6. Zhu, S., Y. Tian, A. E. Hamielec, and D. R. Eaton, Termination of Trapped Radicals at Elevated-Temperatures During Copolymerization of Mma/Egdma. *Polymer,* 1990. **31**(9): p. 1726-1734.
7. Zhu, S., Y. Tian, A. E. Hamielec, and D. R. Eaton, Radical Concentrations in Free-Radical Copolymerization of Mma/Egdma. *Polymer,* 1990. **31**(1): p. 154-159.
8. Anseth, K. S., C. M. Wang, and C. N. Bowman, Kinetic Evidence of Reaction-Diffusion During the Polymerization of Multi(Meth)Acrylate Monomers. *Macromolecules,* 1994. **27**(3): p. 650-655.
9. Cook, W. D., Photopolymerization Kinetics of Oligo(Ethylene Oxide) and

Oligo(Methylene) Oxide Dimethacrylates. *Journal of Polymer Science Part A-Polymer Chemistry*, 1993. **31**(4): p. 1053-1067.

10. Bowman, C. N. and N. A. Peppas, Coupling of Kinetics and Volume Relaxation During Polymerizations of Multiacrylates and Multimethacrylates. *Macromolecules*, 1991. **24**(8): p. 1914-1920.
11. Lovestead, T. M., K. A. Berchtold, and C. N. Bowman, An investigation of chain length dependent termination and reaction diffusion controlled termination during the free radical photopolymerization of multivinyl monomers. *Macromolecules*, 2005. **38**(15): p. 6374-6381.
12. Anseth, K. S., L. M. Kline, T. A. Walker, K. J. Anderson, and C. N. Bowman, Reaction-Kinetics and Volume Relaxation During Polymerizations of Multiethylene Glycol Dimethacrylates. *Macromolecules*, 1995. **28**(7): p. 2491-2499.
13. Odian, G., *Principles of Polymerization*. 1991. New York: John Wiley and Sons.
14. Carre, C., D. J. Lougnot, and J. P. Fouassier, Holography as a Tool for Mechanistic and Kinetic-Studies of Photopolymerization Reactions - a Theoretical and Experimental Approach. *Macromolecules*, 1989. **22**(2): p. 791-799.
15. Sillescu, H. and D. Ehlich, *Application of holographic grating techniques to the study of diffusion processes in polymers*, in *Lasers in Polymer Science and Technology: Applications*, J.-P. Fouassier and J. F. Rabek, Editors. 1990, CRC Press: Boca Raton, Fl. p. 211-226.
16. Horie, K., A. Otagawa, M. Muraoka, and I. Mita, Calorimetric Investigation of Polymerization Reactions .5. Crosslinked Copolymerization of Methyl-Methacrylate with Ethylene Dimethacrylate. *Journal of Polymer Science Part A-Polymer Chemistry*, 1975. **13**(2): p. 445-454.

17. Miyazaki, K. and T. Horibe, Polymerization of Multifunctional Methacrylates and Acrylates. *Journal of Biomedical Materials Research,* 1988. **22**(11): p. 1011-1022.

18. Kurdikar, D. L. and N. A. Peppas, Method of Determination of Initiator Efficiency - Application to Uv Polymerizations Using 2,2-Dimethoxy-2-Phenylacetophenone. *Macromolecules,* 1994. **27**(3): p. 733-738.

19. Groenenboom, C. J., H. J. Hageman, T. Overeem, and A. J. M. Weber, Photoinitiators and Photoinitiation .3. Comparison of the Photo-Decompositions of Alpha-Methoxy-Deoxybenzoin and Alpha, Alpha-Dimethoxydeoxybenzoin in 1,1-Diphenylethylene as Model Substrate. *Makromolekulare Chemie-Macromolecular Chemistry and Physics,* 1982. **183**(2): p. 281-292.

20. Pryor, W. A., H. T. Bickley, and E. H. Morkved, Homolysis of Some Radical Initiators - Viscosity Dependence and Cage Return. *Journal of Organic Chemistry,* 1972. **37**(12): p. 1999.

21. Anseth, K. S. and C. N. Bowman, Kinetic Gelation Model Predictions of Cross-Linked Polymer Network Microstructure. *Chemical Engineering Science,* 1994. **49**(14): p. 2207-2217.